UNDERSTANDING THE MECHANISM OF ANDROGEN BIOSYNTHESIS

BY

MICHAEL CARLTON GREGORY

DISSERTATION

Submitted in partial fulfillment of the requirements
for the degree of Doctor of Philosophy in Biochemistry
in the Graduate College of the
University of Illinois at Urbana-Champaign, 2016

Urbana, Illinois

Doctoral Committee:

Professor Stephen Sligar, Chair
Professor James Morrissey
Professor Robert Gennis
Assistant Professor Aditi Das

Abstract

Cytochrome P45017A1 (CYP17A1) is a multifunctional steroidogenic enzyme responsible for the 17α-hydroxylation of pregnenolone and progesterone as well as the subsequent 17,20 carbon-carbon bond scission of its hydroxylated products in a reaction that constitutes the first committed step of androgen formation. Though over 40 years have passed since discovery of this enzyme, key questions regarding the nature of the reactive intermediate responsible for androgen formation have heretofore remained unanswered. Specifically, while the hydroxylase activity of CYP17A1 is expected to proceed through standard P450 ferryl-oxene intermediate, identity of the iron-oxygen species involved in carbon-carbon bond scission has until now remained elusive. This dissertation documents the steady state kinetics of CYP17A1 catalysis as well as detailed characterization of its heme environment in the ferric, oxy-ferrous, and peroxo- states by resonance Raman spectroscopy in order to answer this essential question. Presence of an inverse solvent isotope effect during dehydroepiandrosterone formation, as well as functional lyase catalysis by a CYP17A1 mutant possessing an impaired proton-delivery network, strongly support the hypothesis that a ferric peroxoanion is responsible for androgen formation. Additionally, resonance Raman spectroscopy of the oxy-ferrous form of this enzyme revealed that identity of the carbon-3 substituent on the pregnene- nucleus directs the 17α-OH group to hydrogen bond with the Fe-O-O ligand in a manner that alternately promotes or impedes efficient lyase catalysis via this nucleophilic pathway. Finally, resonance Raman of the during stepwise thermal annealing of the cryotrapped peroxo- state permitted identification of a new peroxo

hemiacetal intermediate species initiated by nuclophilic attack on the substrate molecule by the peroxoanion. As a whole, this work details the structural and functional properties of CYP17A1 active in human androgen biosynthesis.

Table of Contents

Chapter 1: Introduction

1.1 P450 Discovery

In 1954 Martin Klingenberg was a post-doctoral researcher at the University of Pennsylvania studying redox kinetics of cytochrome b_5, a 12-15 kDa hemeprotein discovered fifteen years prior. While working with rat liver homogenates, he discovered a novel and unknown pigment displaying a strong absorption band at 450 nm after dithionite reduction and addition of carbon monoxide.[1] However, the origin of this novel pigment remained elusive: attempts at solubilization with cholate resulted in what was then a confounding shift in absorbance to a peak at 420 nm, and the absence of readily apparent α and β bands which led to dispute over its hemeprotein nature.[2] Klingenberg subsequently abandoned his investigations of this new pigment and returned to his home in Germany to study mitochondrial electron transport, delaying publication of his discovery until 1958.[3]

Studies of the P450s were thus destined to begin in earnest some five years later in the laboratory of Ryo Sato at Osaka University. As an early career scientist, Sato's decision to study this curious microsomal pigment was largely defined by friendly conversations he enjoyed with Klingenberg and another pioneer, Ronald Estabrook during a visit to the University of Pennsylvania as well as the crowdedness of the field of microsomal electron transport.[4] He recruited a young assistant professor, Tsuneo Omura to drive the work on this exciting new project. Omura characterized the phospholipase C mediated conversion of the

absorption band at 450 nm to 420 nm, and was able to perform detailed investigations on partially solubilized preparations of what appeared to be a *b*-type cytochrome. In 1964 this work culminated in publication of Omura and Sato's seminal texts defining the pigment-450 nm (P450) and pigment 420 nm (P420) as originating from a new microsomal hemeprotein, which they named cytochrome P450.[5]

The intervening 60 years have witnessed maturation of the P450 field and discovery of more than 17,000 members of this superfamily responsible for oxidation reactions operating on a rich tapestry of substrates.[6] The list of brilliant contributors to this vast field is far too exhaustive to catalog in this dissertation, however any author's discussion of the history of P450s would be remiss without mention the discovery of the soluble bacterial P450cam by I.C. Gunsalus.[7] The ease of purification and stability in solution exhibited by this enzyme has resulted in solidification of its role as a mechanistic exemplar of the P450s, providing the foundational knowledge upon which the following studies are based.

1.2 Structure and Function of P450s and Associated Redox Partners

The ubiquity of the cytochromes P450 throughout the "tree of life" is a testament to the value of the complex chemistry catalyzed by this key class of enzymes. The most common perception of P450 enzymes is that of a vehicle for the oxidation of unactivated alkanes via a hydroxylase activity, however these enzymes are also known to catalyze dealkylation, epoxidation, dehydrogenation, heteroatom oxidation, and carbon-carbon bond scission reactions.[8] These diverse reactivities are employed in xenobiotic metabolism, steroid hormone biosynthesis as well as the formation of eicosanoids and fatty acids in humans.

Despite the broad range of substrate specificities exhibited by members of the P450 superfamily, these enzymes share a conserved protein fold and the key to their reactivity is an absolutely conserved protoporphyrin IX cofactor with a proximally ligated cysteine residue. Despite a conserved fold, there exists remarkable diversity in detailed structural aspects and sequence identity among P450s; as low as 16% in some cases. Diversity in sequence is the basis for nomenclature identifying specific P450 proteins, with phylogenetic criteria and gene organization being additional criteria. A CYP prefix identifies the enzyme as a P450, with the following number used to identify a family with greater than 40% sequence identity. The subsequent letter and number denote a subfamily with greater than 55% protein sequence identity and a specific gene, respectively.[9]

There are, however, several canonical sequences within the core of the P450 protein involved in heme binding and proton delivery. The sequence (Phe-X-X-Gly-X-Arg-X-Cys-X-Gly) contains the absolutely conserved cysteine residue that acts as a fifth ligand to the heme iron on the heme binding loop. Additionally, on the K-helix a conserved (Glu-X-X-Arg) is thought to be essential for stabilizing the protein core.[10] Finally, (A/G-G-X-Asp/Glu-T-T/S) on the I-helix contains the essential acid/alcohol pair necessary for proton delivery to activated iron-oxygen intermediates in the distal active site pocket.[11] Predictably, a high degree of sequence variability is generally observed in regions involved in substrate binding, notably in the B, B', F, F' and G helices which are thought to possess conformational flexibility involved in substrate binding.[12]

A key distinguishing feature between eukaryotic and prokaryotic P450s is the presence of an N-terminal membrane anchor on the latter. Unlike soluble prokaryotic P450s, those in eukaryotes are typically bound to the membrane of the endoplasmic reticulum or

mitochondrial inner membrane via a hydrophobic 20-50 amino helix. In P450s associated to the mitochondrial membrane, this membrane anchor is expressed with a targeting sequence that is subsequently cleaved during import into the mitochondrion, whereas microsomal P450s are inserted co-translationally without processing.[13] Membrane association is also enhanced in these proteins via a longer peptide chain spanning the region between the F and G helices that form a hydrophobic patch thought to be in close proximity to, or buried in the membrane.[14,15]

Despite catalytic activity observed in some membrane associated P450s following solubilization via truncation of their hydrophobic tail, proper *in vivo* function is highly dependent on their insertion into the membrane. A large number of substrates are highly hydrophobic and partition preferentially into lipid bilayers. Juxtaposition of the active site near the membrane is expected to facilitate delivery of hydrophobic substrates to P450 systems operating on such molecules, such as in the CYP11A1 mediated cleavage of isocaproic acid from cholesterol.[16] Additionally, N-terminal membrane anchoring is an essential orienting factor in generation of functional electron transfer complexes involving P450s and their various redox partners in the protein milieu of the bilayer[17] and close association to the membrane is thought to be an important modulator of redox potential in these complexes.[18,19]

P450 mediated oxidation is dependent on not only the presence of substrate and enzyme, but also input of atmospheric dioxygen and reducing equivalents, the delivery of which is generally mediated by accessory proteins. In the case of human microsomal P450s, cytochrome P450 oxidoreductase (CPR) orchestrates sequential delivery of electrons derived from NADPH to the heme cofactor.[20] CPR is a multidomain 78,000 Da protein

containing flavin adenine dinucleotide (FAD) and flavin mononucleotide (FMN) cofactors anchored to the membrane via a hydrophobic tail that facilitates efficient orientation with the P450 in conjunction with additional electrostatic interactions. In this system, the FAD cofactor accepts two reducing equivalents from NADPH and sequentially transfers these to the FMN domain, which act as an adapter between the two-electron transfer from NADPH and the requisite one-electron reduction needed for proper P450 function.[21,22]

In mitochondrial P450 systems, another redox shuttle is operating, composed of a three-protein system constituting a P450, ferredoxin reductase and ferredoxin adrenoxodin. In such systems a FAD cofactor in ferredoxin reductase accepts electrons from NADPH and subsequently reduces the 2Fe-2S cluster of adrenoxodin that acts as a one-electron shuttle to the P450.[23]

1.3 The P450 Reaction Cycle

After nearly 60 years of intensive study, a general consensus has emerged regarding the nature of reactive intermediates involved in P450 function (Figure 1.1). Worthy of mention at this juncture is the depth in which this field has been studied, therefore this section is intended as merely an overview of the mechanics of P450 mediated oxygen activation—more substantive discussion of the intricacies of the complex chemistries operating in this cycle will follow in later chapters.

In the resting P450 state [1] the ferric heme iron possesses a molecule of water as a sixth ligand and is the (S=1/2) low spin state. Substrate binding generally displaces water as a ligand resulting in a rearrangement of d-orbital electrons, shifting the equilibrium to the

S=5/2 high spin state [2] with a concomitant ~100mV increase in redox potential.[24] Increased redox potential enhances electron transfer from an associated redox partner, which once delivered results in formation of ferrous heme [3] that readily binds a molecule of dioxygen forming the oxy-ferrous complex [4].[25] This adduct represents the first unstable intermediate and may either decompose via the autoxidation route with release of superoxide and a return to the ferric state, or proceed productively via a second one-electron reduction and formation of the peroxoanion species.

Delivery of a single proton to the distal oxygen of the peroxoanion [5a] results in formation of the hydroperoxoanion [5b], another uncoupling point at which the peroxide ligand may be non-productively released as a hydrogen peroxide. Alternatively, a second protonation of the distal oxygen and subsequent heterolytic O-O bond scission may release a molecule of water and form the high-valent iron-oxo Compound I (CpdI) [6] with a cation radical delocalized on the porphyrin.[26] This adduct has been the focus of considerable study and is generally regarded as the active intermediate responsible for the overwhelming majority of P450 mediated reactions. In the "Groves Rebound" mechanism, CpdI abstracts a hydrogen atom from the substrate, forming an iron (IV) hydroxide transient that rapidly recombines to the substrate radical to yield the final hydroxylated product and ferric iron.[27,28] As with other unstable intermediates, though, CpdI abortive reactions involving this adduct are possible via further 2-electron reduction and release of a water molecule.

1.4 Human Steroid Hormone Biosynthesis

Steroid hormone biosynthesis is a tightly regulated process essential for development and maintenance of the normal human phenotype. Primarily occurring in the adrenal and gonadal tissues, the steroid precursor cholesterol is subjected to a bevy of chemical transformations responsible for the formation of mineralocorticoids, glucocorticoids, androgens, and estrogens. Production and systemic delivery of these steroid molecules is essential in maintenance of salt and water balance, carbohydrate metabolism, catecholamine response, and sexual development.[29] The overall process, shown in Figure 1.2, is dependent upon the actions of six cytochrome P450 enzymes and several steroid dehydrogenases distributed throughout the mitochondrial inner membrane and endoplasmic reticulum.[30]

All steroids are derived from cholesterol, primarily originating from dietary sources, and delivered to steroidogenic tissues incorporated in high-density lipoprotein particles.[31] Cellular cholesterol uptake is primarily mediated by endocytosis of lipoprotein particles, followed by transport to the outer mitochondrial membrane. In the subsequent step that is rate limiting for overall steroid synthesis, cholesterol is transported into the inner mitochondrial membrane by steroidogenic acute regulatory protein (StAR)[32], a 37,000 Da phosphoprotein. In the first enzymatic step of steroid hormone biosynthesis, cholesterol is subjected to three processive reactions by a single enzyme, CYP11A1, ultimately resulting in formation of pregnenolone and release of isocaproaldehyde.[33]

The multiple reactivities of Cytochrome P45017A1 (CYP17A1) lie here, at the heart of this pathway, and define a key branch point at which steroid hormone precursors are directed towards corticoid production or committed to formation of androgens and estrogens.[34] Pregnenolone (PREG) may be subjected to hydroxylation by CYP17A1 to form

17α-hydroxyprenenolone (17-OH PREG) or conversion of the alcohol on carbon-3 and isomerization of the B-ring double bond to form progesterone (PROG) in a reversible process dependent on the activity of 3β-hydroxysteroid dehydrogenase and NAD^+ input.[35]

CYP17A1 catalyzes an analogous hydroxylation on carbon-17 of progesterone, forming the 17α-hydroxyprogesterone product (17-OH PROG). It is at this key point at which the CYP17A1 products may be subjected to a round of 17,20 carbon-carbon scission forming the 19 carbon androgens dehydroepiandrosterone (DHEA) and androstenedione (AD).

Alternatively, both progesterone and hydroxyprogesterone may be further processed by P450c21 which introduces an alcohol functionality to carbon-21, directing these products towards formation of mineralcorticoids and glucocorticoids, respectively.[36] The deoxycorticosterone and 11-deoxycortisol products of the former process are further processed, once more, in the mitochondria by CYP11B2 in a straightforward 11β-hydroxylase reaction forming corticosterone and cortisol.[37] An isozyme sharing a 93% sequence identity, CYP11B1, is expressed only in tissues producing aldosterone and is able to catalyze the sequential C-18 hydroxylation of deoxycoricosterone as well as the 18-methyl oxidase activity responsible for formation of aldosterone.[38]

Focusing on the steroid production directed towards androgen formation, both AD and DHEA are subjected to additional downstream processing as they are directed toward the production of testosterone, dihidrotestosterone and the 18 carbon estrogens. The complexity of this latter pathway precludes a detailed description in this text, as there are multiple isoforms of the various enzymes and "backdoor" pathways operating.[29] However, the process can be reduced to the statement that flux through this pathway in humans occurs

via DHEA isomerization via the action of 3β-HSD forming AD, which is either directed towards estrogen production by CYP19 mediated A-ring aromatization and 10,19 C-C cleavage or towards testosterone production via reduction of the C-20 keto group to an alcohol by 17β-hydroxysteroid dehydrogenase.[39]

1.5 CYP17A1

As described above and shown in Figure 1.2, the multifunctional human CYP17A1 plays a central role in the steroidogenic pathway, catalyzing the 17α-hydroxylation of pregnenolone and progesterone as well as the subsequent 17,20 carbon-carbon lyase of its hydroxylated products to form dehydroepiandrosterone and androstenedione.[36,40] The various activities of CYP17A1 represent crucial branch points in human steroidogenesis and are absolutely essential for both glucocorticoid and androgen production. Consistent with its functional significance, polymorphisms affecting the activity of CYP17A1 are deleterious to normal human physiology. Congenital adrenal hyperplasia secondary to CYP17A1 deficiency has been known to manifest as symptoms of hypertension and abnormal sexual development in afflicted individuals. Additionally, owing to its key role in the generation of sex hormones this enzyme has become a front-line target for inhibition in the treatment of androgen receptor positive prostate cancer, reinvigorating the half-century old practice of androgen deprivation therapy for the treatment of this malady.[41,42]

Human CYP17A1 is a ~57,000 Da protein localized in the endoplasmic reticulum membrane of tissues of the adrenals, testes, and ovaries. As a microsomal P450, CYP17A1 activity is dependent on cytochrome P450 oxidoreductase (CPR) for electron input, but has

an additional requirement of the presence of cytochrome b_5 (cyt b5) to catalyze carbon-carbon bond scission.[43–45] Maximal velocity of this latter chemistry is enhanced up to 10-fold in the presence of cyt b5, whereas the hydroxylase activity is largely unaffected by the presence of this effector.[17] Additional studies suggest that phosphorylation at several key positions can similarly enhance C-C bond scission.[46–48] Both expression of cyt b5 and activation of CYP17A1 phosphorylation in the adrenal *Zona reticularis* coincides with andrenarche and initiation of androgen production in adrenal tissues, suggesting these processes are key regulatory elements in controlling sex hormone production.[49] This represents an important method of temporal control over sex hormone production, delaying this process until andrenarche while maintaining 17α-hydroxylase activity which is required throughout the entire lifespan of an individual.

A central question regarding CYP17A1 mediated catalysis has long remained the nature of the reactive intermediate responsible for cleavage of the 17,20 carbon-carbon bond on the steroid, resulting in the release of acetic acid and androgen product. Whereas it is clear that the hydroxylase activity of CYP17A1 proceeds via a straightforward CpdI mediated "Groves rebound" mechanism, a role for a nucelophilic peroxoanion in initiation of C-C scission in the formation of androgens has been suggested.[50–53] In such an event, attack of the electrophilic center of the C-20 carbonyl by a peroxoanion would result in formation of an peroxo hemiacetal intermediate that could then decompose via either heterolytic or homolytic scission of the dioxygen bond to yield androgen product and acetic acid. Alternatively, radical mechanisms utilizing CpdI as the active oxidant have been proposed that could decompose to the androgen product as shown in in Figure 1.3.[34,54]

1.6: Tables and Figures

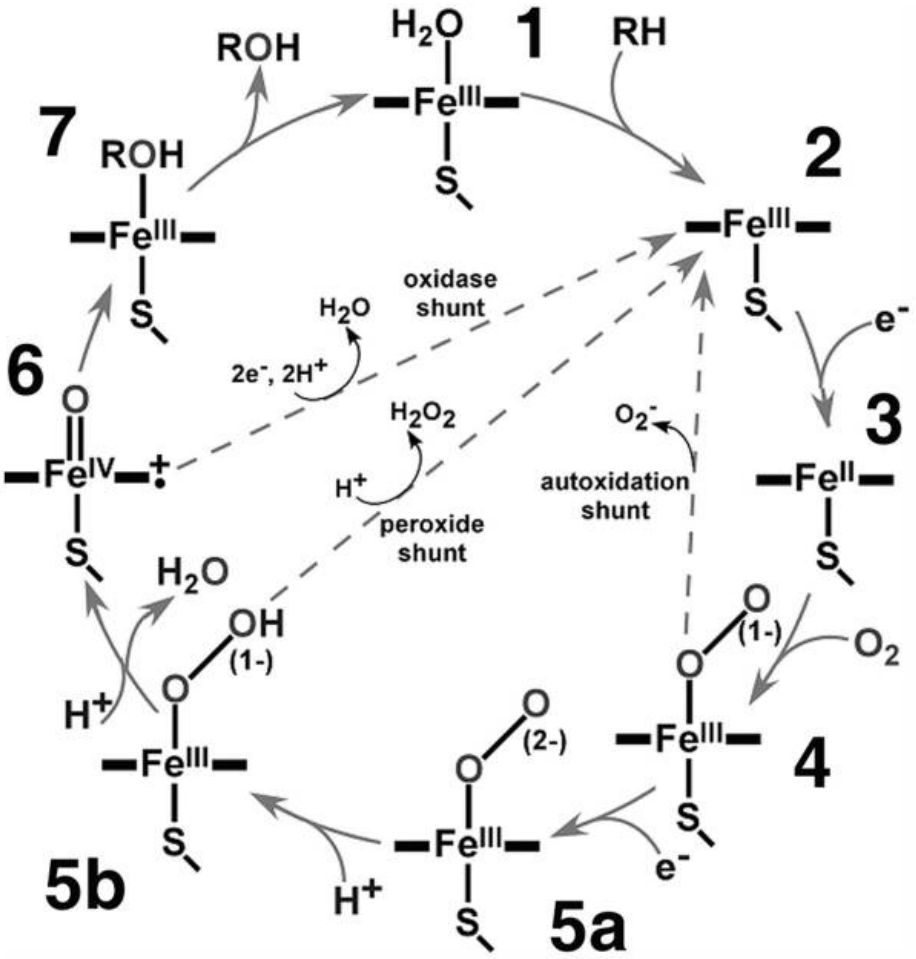

Figure 1.1: The P450 Catalytic Cycle

The canonical P450 catalytic cycle.

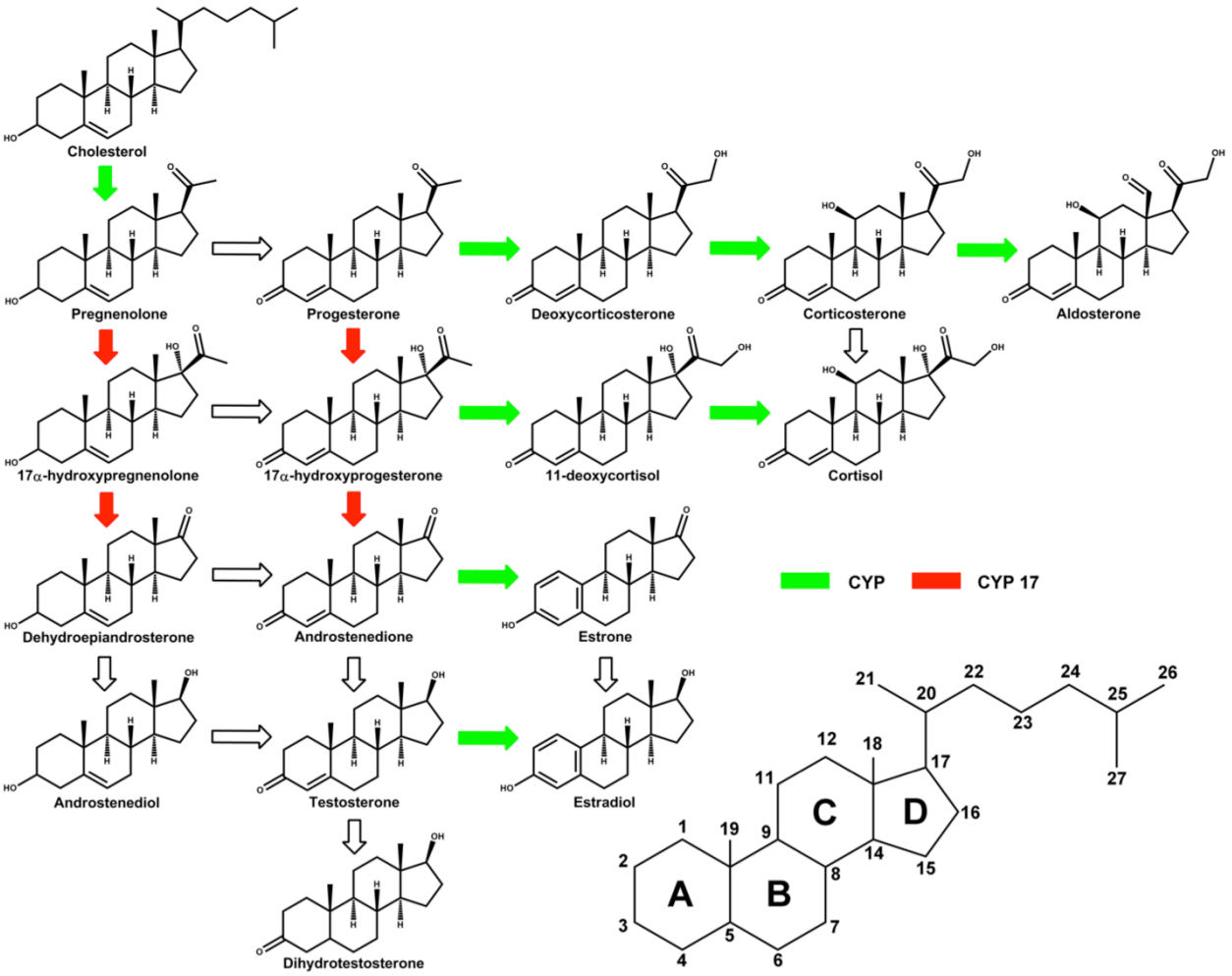

Figure 1.2: Human Steroid Biosynthetic Pathway

The human steroid hormone biosynthetic pathway, beginning with cholesterol, and ending with corticoids, androgens, and estrogens. The inset on the lower right indicates numbering of the carbon atoms on the cholesterol molecule.

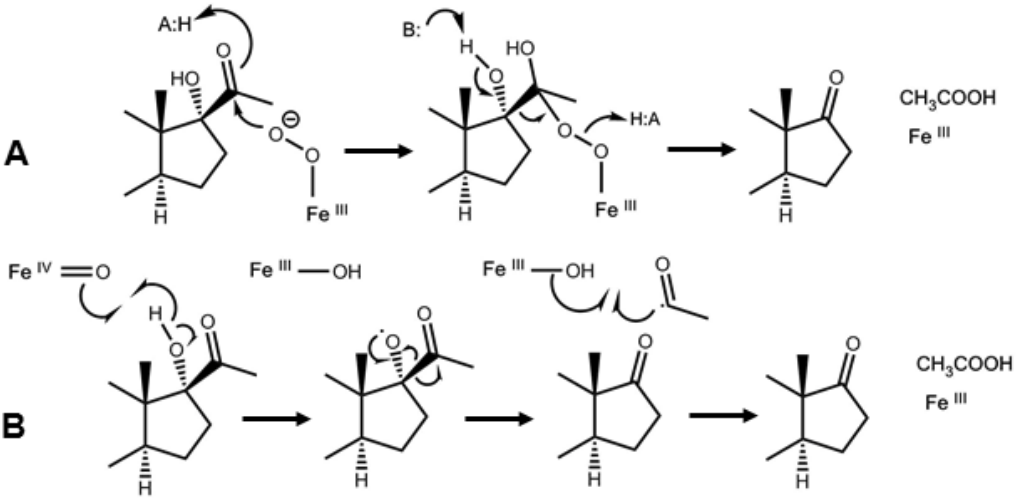

Figure 1.3: Proposed Mechanisms of Androgen Biosynthesis

Proposed mechanisms involving a reactive peroxo intermediate (A) beginning with a nucleophilic attack on the C20 carbonyl and CpdI (B), initiated by abstraction of the hydrogen atom on the 17-OH group.

Chapter 2: Methods for Reconstitution of CYP17A1 in Nanodiscs with Associated Redox Partners

2.1 Introduction

Groundbreaking work by the Waterman laboratory in the late 1980's identified 5' sequence modifications to native bovine and human CYP17A1 cDNA permitting heterologous expression of milligram quantities of this enzyme in *E. coli*, making this the first mammalian P450 to be expressed in high yield.[55–57] However, despite development of expression systems in *E. coli*, Yeast, and SF9 cells, the detergent solubilized preparations yielded by these early methods represent a suboptimal platform for characterization by many commonly used *in vitro* methods in the biochemist's toolbox. Though such treatment was demonstrated to provide soluble and highly purified protein, these targets exist in a decidedly non-native environment hampering the efforts of investigators. Oligeromeric states are difficult to control, substrate molecules may partition preferentially into the detergent micelles, and in the absence of stabilizing protein-membrane interactions targets of interest may adopt non-native functional properties or fail to form functional protein-protein interactions in which membrane association is an important orienting factor.[58,59]

These impediments are overcome via incorporation of target proteins into Nanodiscs. These nanoscale particles are monodisperse, discoidal lipid bilayers solubilized by an encircling amphipathic scaffold protein. These nanoscale particles are formed through a self-assembly process in which detergent is removed from a solution containing precise

ratios of target membrane protein, lipid, and scaffold protein.[60,61] The end product of this process is a stable and soluble platform that renders membrane proteins amenable to the rigorous interrogation previously reserved for soluble proteins.

2.2 Expression and Purification of CYP17A1

2.2.1 Design of a synthetic human CYP17A1 gene

A full length gene was designed including a C-terminal penta-histidine tag for purification based on the CYP17A1 cDNA sequence available from GenBank, accession number NM_000102, version NM_000102.3. The first twenty-four 5' bases were modified as reported by Imai et al.[57] to improve heterologous expression and include an NdeI restriction endonuclease site in the start codon, resulting in a total of five amino acid substitutions in the hydrophobic tail of CYP17A1, such that 5'- GAG GTA AAA CAT ATG GCT CTG TTA TTA GCA GTT TTC – 3'. The remaining codons were optimized for *E. coli* expression by a proprietary process of DNA 2.0, and an XbaI restriction site was added immediately following the stop codon. A full sequence is included in Appendix A. The resultant gene was ligated into a pCWori^{+} plasmid conferring ampicillin resistance. Competent DH5α F'IQ cells (Invitrogen) were co-transformed with the ligation product and the pGro7 vector (Takara Bio), containing GroEL/ES and conferring chloramphenicol resistance. Glycerol stocks were prepared from 50 mL cultures of transformed cells and were stored at -80°C for future use.

2.2.2 Expression of P45017A1

Each expression session was initiated by the plating of DH5α containing pCW_CYP17A1 and pGro7 vectors from glycerol stock onto LB-agar plates containing 20

μg/mL chloramphenicol and 100 μg/mL ampicillin. Plates incubated overnight at 37°C and a single isolated colony was selected to inoculate 50 mL LB containing 20 μg/mL and 100 μg/mL ampicillin. This starter culture generally incubated at 37°C for 6-8 hours while rotating at 250 RPM. 1 mL of starter culture was used to inoculate each 1 L volume of Terrific Broth containing 1X Bracken's Trace Metals Solution, 33.7 mg/mL thiamine, 100 μg/mL ampicillin and 20 μg/mL chloramphenicol contained in a 2.8L Fernbach flask. Cultures incubated at 37°C while rotating at 250 RPM until OD_{600} reached 0.4-0.6. At this time cultures were transferred to a 27°C incubator programmed to rotate at 220RPM and δ-aminolevulinic acid was added to a final concentration of 1 mM. When OD_{600} reached 0.8, expression of CYP17A1 and GroEL/ES was induced by the addition of isopropyl β-D-1-thiogalactopyranoside and powdered L-Arabinose to final concentrations of 1 mM and 4 mg/mL, respectively. Cultures incubated at 27°C while rotating at 250 RPM for 40-48 hours, at which point cells were pelleted by centrifugation at 11,000 x g for 10 minutes. Cell pellets were stored at -80°C until purification.

2.2.3 Purification of P45017A1

Frozen cell pellets, typically 25-30 g/L, from 6 L culture were resuspended in 270mL lysis buffer (0.1M KPi pH 7.4, 0.05 M NaCl, 20% glycerol, 50 μM Progesterone, 10 mM B-Me, 0.5 mM PMSF, 0.1mg/mL lysozyme, 0.1 mg/mL DNase, 0.1 mg/mL RNase). Lysis solution stirred at 4°C for 45 minutes. Resultant spheroplasts were lysed by sonication using a Branson Sonifier 450 attached to a 0.5 cm probe. Lysis solutions were subjected to six, two minute cycles at 0.6 output and 70% duty cycle with five minute incubations on ice between cycles.

The lysate was subsequently centrifuged at 100,000 x g for 30 minutes at 4°C and the supernatant was discarded and membrane pellets resuspended in 270 mL membrane solubilization buffer (0.1M KPi pH 7.4, 0.5 M NaCl, 20% glycerol, 50 μM Progesterone, 10 mM B-Me, 0.5 mM PMSF) by stirring for 1 hour at 4°C. To solubilize membrane associated proteins, 20% Triton X-100 was added dropwise until the final detergent concentration reached 1.5%. This solution incubated at 4°C while stirring for 1 hour, and was then centrifuged at 100,000 x g for 30 minutes at 4°C. Supernatant containing solubilized membrane proteins was collected and the insoluble membrane fraction discarded.

The solubilized fraction was immediately purified by Ni^{2+} affinity chromatography utilizing a 2.5x12cm column containing a 20 mL bed of nitrilotriacetic acid agarose resin (Qiagen) attached to a peristaltic pump and fraction collector at a flow rate of approximately 3.0 mL/min. The column was charged with 0.1M $NiSO_4$, washed extensively with water, and equilibrated with 4 column volumes of membrane solubilization buffer containing 1.5% Triton X-100. The entire volume of solubilized membrane fraction was then loaded onto the column. The column was washed first with 5 column volumes of Wash Buffer A (0.05 M Tris, pH 7.4, 0.3 M NaCl, 20% Glycerol, 50 μM Progesterone, 0.02% Emulgen 913, 10 mM B-Me), and then 10 column volumes of Wash Buffer B (Wash Buffer A with 50mM Imidazole, 5 mM adenosine triphosphate, and 20 mM $MgCl_2$. Bound protein was eluted with 2 column volumes of Elution Buffer (0.05 M Tris pH 7.4, 0.05 M NaCl, 20% Glycerol, 0.02% Emulgen 913, 50 μM progesterone, 10 mM β-Me, 300 mM imidazole) and collected in 4mL fractions.

Colored fractions were pooled and dialyzed once overnight against 1 L of 0.1M KPi pH 7.4, 20% Glycerol, 0.05 M NaCl, 50 μM Progesterone, 10 mM B-Me, 2 mM EDTA at 4°C in a 10,000 MWCO membrane, and twice against the same buffer without EDTA. Finally,

protein was and concentrated to ~100 μM in a 15mL centrifugal concentrator with a 10,000 MWCO (Millipore), flash frozen in liquid N_2 and stored at -80°C. P450 concentration was determined by the method of Omura and Sato.

2.3 CYP17A1 Nanodisc Self-Assembly

Generally, 32 μmol POPC in choloform was delivered to borosilicate tubes in triplicate, dried under a stream of nitrogen, and dessicated under vacuum overnight. Dried POPC was hydrated in a 1.73 mL solution of 0.1M KPi pH 7.4 and 0.05M NaCl with three sequential steps of vortexing, freezing in liquid N_2, and thawing at room temperature. Triton X-100 was added in a 1.15:1 molar ratio to lipid and solution was sonicated for 30 minutes at 60°C in order to assist complete solubilization of the dried lipid. The final reconstitution solution contained 10mM POPC, 0.3M NaCl, 0.1M KPi pH 7.4, 40mM Triton X-100, 154μM MSP1D1$^-$, 7.7μM P45017A1, 50μM progesterone, and 10mM B-Me. This mixture incubated on ice for 30 minutes, at which point 8 grams of wet Amberlite XAD-2 (Supelco) was added, and the solution was incubated at 4°C on a shaker for 6 hours. Amberlite was removed and washed with buffer C (0.1 M KPi, pH 7.4, 300mM NaCl), and the resultant solution was pooled with the extracted reconstitution mixture and loaded onto a 7 mL Ni-NTA column to separate empty Nanodiscs from those with embedded CYP17A1. The column was washed with 5 volumes of buffer C containing 30 mM imidazole, and eluted with buffer C supplemented with 300 mM imidazole. The eluate was loaded onto a Superdex 200 10/300GL column (GE Life Sciences) using a 0.1 M KPi, pH 7.4, mobile phase at a flow rate of 0.5 mL/min. 10 nm fractions corresponding to properly formed Nanodiscs were pooled and concentrated, and

stored in 15% (v/v) glycerol at -80°C until required. The concentration of Nanodiscs was determined by the difference spectrum of substrate free and pregnenolone bound protein using the peak to trough extinction coefficient of $\varepsilon_{390} - \varepsilon_{420} = 100\ mM^{-1}\ cm^{-1}$.[62]

2.4 Expression and Purification of Redox Partners and Cyt *b5*

2.4.1 Expression of Cytochrome P450 Oxidoreductase

Cytochrome P450 oxidoreductase was expressed and purified by a modified method of Shen et. al.[63] CD41 cells transformed with plasmid pOR262 containing full-length wild type rat liver CPR was a generous gift from Todd Porter.[63] Each growth was initiated by streaking, from glycerol stock, an agar plate containing 100 μg/mL ampicillin which was subsequently grown overnight at 37°C. Starter culture was grown in 50 mL flasks of LB media containing 100 μg/mL ampicillin while shaking at 220 RPM at 37°C until OD_{600} reached 0.4. CPR was typically expressed in 12 L batches, consisting of 12 x 2.8 L Fernbach flasks containing Luria-Bertan Media supplemented with 100 μg/mL ampicillin and 1 μg/mL riboflavin, inoculated with 8 mL of starter culture. Flasks were maintained at 33°C while shaking at 220 RPM, and were induced with 1 mM IPTG at OD_{600} = 1.0. After ~20 hours of growth cells were harvested by centrifugation at 11,000 x g for 10 minutes and stored at -80°C until purification.

2.4.2 Purification of Cytochrome P450 Oxidoreductase

Cells from 6 L culture were thawed and resuspended in 2.4 L lysozyme buffer (0.75 M Tris pH 8.0, 0.25 M sucrose, 250 μM EDTA, 0.02 mg/mL lysozyme) while stirring at 4°C for 2 hours, and the resultant spheroplasts harvested by centrifugation at 11,000 x g for 30

minutes. Cells were then resuspended in lysis buffer (0.05 M Tris pH 8.0, 1 mM PMSF) and lysed on ice by sonication using a Branson Sonifier with a 0.5 cm probe and 80% duty cycle, with the output set to 4 using 5 x 30 second pulses. The membrane fraction was then isolated by centrifugation at 100,000 x g for 30 minutes.

After complete resuspension of membrane pellet in 260 mL MQ H_2O, the remaining solubilization buffer components were added such that the concentrations of each were: 0.05 M Tris pH 7.7, 0.1 mM EDTA, 0.1 mM DTT, 20 % v/v glycerol, 0.5 M NaCl, 0.2% Triton X-100. The resultant suspension stirred at 4°C for 2 hours and the insoluble fraction was pelleted at 185,000 x g for 1 hour. The supernatant was loaded on a 25 mL bed of 2'5' adenosine diphosphate agarose column equilibrated with ADP column buffer (0.05 M Tris pH 7.7, 0.1 mM EDTA, 0.1 mM DTT, 20 % v/v glycerol, 0.1% Triton X-100). The column was then washed with 200 mL ADP wash buffer (ADP column buffer supplemented with 2 mM adenosine). Bound protein was eluted with ADP elution buffer (ADP column buffer containing 2 mM NADPH). Detergent was removed by immobilization on a 1.5 x 10 cm DE-52 DEAE column equilibrated and washed with DEAE column buffer (0.05 M Tris pH 7.7, 0.1 mM EDTA, 0.1 mM DTT, 20 % v/v glycerol) until absorbance of the eluting buffer was less than 0.1 at 280 nm. Purified CPR was eluted with DEAE column buffer containing 0.4 M NaCl, and was dialyzed against 3 L DEAE column buffer with three buffer exchanges. Concentration of purified CPR was determined spectrophotometrically after complete oxidation with potassium ferricyanide using ε_{455} = 21.4 mM^{-1} cm^{-1}.

2.4.3 Expression of Cytochrome b_5

Cytochrome b_5 from *Rattus norvegicus* was expressed and purified in a modified method as described by the Waskel laboratory[64] using a pET15b plasmid containing full

length cyt b5 with an N-terminal membrane anchor. Transformed BL-21gold(DE3) cells were plated from glycerol stock on agar plates containing 100 μg/mL ampicillin and grown overnight at 37°C. Starting culture was then prepared by delivery of a single colony to a 50 mL volume of LB media containg 100 μg/mL ampicillin which rotated at 220 RPM at 37°C for 8 hours. Fernbach flasks containing 500 mL terrific broth supplemented with 100 μg/mL ampicillin and 1X Bracken's Trace Metal Solution were inoculated with 5 mL starting culture and incubated at 37°C while rotating at 200 RPM. At OD_{600} = 0.8, δ-ALA and IPTG were added to a final concentration of 0.5 mM and 1 mM, respectively. Cultures continued to incubate for 20 hours and cells were then harvested via centrifugation at 11,000 x g for 15 minutes and stored at -80°C until purification.

2.4.4 Purification of Cytochrome b_5

Purification began with resuspension of cell pellet from 12 L of culture in 2.4 L lysozyme buffer (0.075 M Tris pH 8.0, 0.25 M sucrose, 0.25 mM EDTA, 0.02 mg/mL lysozyme) for 30 minutes while stirring at 4°C. Spheroplasts were harvested by centrifugation at 11,000 x g for 30 minutes and the pellet was then resuspended in lysis buffer 360 mL lysis buffer (20 mM KPi pH 7.0, 1 mM EDTA, 2.5 mM PMSF) and lysed via five rounds of sonication on ice with a 0.5 cm probe attached to a Branson Sonifier set to an 80% duty cycle, output setting 4, 30 second duration. Membranes were harvested by ultracentrifugation at 100,000 x g for 30 minutes at 4°C. Supernatant was then discarded and the pellet resuspended in 1.2 L MQ H_2O, to which the following buffer components were added: 20 mM KPi pH 7.0, 1 mM EDTA, 2.5 mM PMSF, 1% tergitol) and stirred for 2 hours at 4°C.

In order to ensure purification of holo-cyt b5, the quantity of apo-cyt b5 was determined and a 10% molar excess of hemin solution (relative to apoprotein) was added to the lyase and stirred for 10 minutes at 4°C. The insoluble fraction was removed by ultracentrifugation at 185,000 x g for 1 hour at 4°C and the supernatant loaded on a 2.5 x 17 cm DEAE (DE-52) column equilibrated with DEAE buffer A (25 mM Tris pH 8.0, 1 mM EDTA, 10 mM sodium cholate) and eluted with a linear gradient from 0-100% DEAE buffer B (DEAE buffer A supplemented with 0.4 M NaCl). Fractions with an Rz greater than 1.6 were pooled and purified on a Protein-Pak DEAE 15HR (Waters) column and DEAE buffers described previously at a flow rate of 1.2 mL/min. A segmented linear gradient was employed in which % buffer B increased from 0 to 40% at 35 minutes, then to 100% at 45 minutes. Fractions with an Rz greater than 2.8 were pooled and rigorously dialyzed against 50 mM potassium phosphate, pH 7.4. The final Rz was generally greater than 3.5 and concentration was determined using ε_{412} = 117 mM^{-1} cm^{-1}.

2.4.5 Expression and Purification and TEV cleavage of MSP1D1

Membrane scaffold protein was expressed and purified using the standard protocol described in detail elsewhere.[65] Following purification, the poly-histidine tag was removed by tobacco etch virus protease (TEV) by addition of 1 mg protease to 100 mg MSP1D1 in the presence of 1 mM DTT. The resultant solution incubated at 30°C until complete cleavage of the histidine tag was verified by either MALDI-MS or SDS-PAGE. The excised peptide and protease were subsequently removed from the $MSP1D1^{-}$ on a Ni-NTA column. Scaffold protein was collected as flow-through and wash using buffer containing 50 mM TRIS pH 7.2, 300 mM NaCl, 50mM Imidazole. These fractions were pooled, concentrated, and dialyzed rigorously against buffer containing 100 mM KPi, pH 7.4 and 50 mM NaCl.

2.5 Results

In the initial phases of this dissertation, a major goal involved leveraging of past advances by combining established expression and purification methodologies with optimization of codon usage for *E. coli* throughout the remainder of a synthetic gene, and incorporation of the final purified product in Nanodiscs. We obtained a synthetic gene from DNA 2.0 including the N-terminal amino acid sequence modifications identified by Barnes *et al*. with the remainder of the DNA sequence "optimized for *E. coli* expression" by a proprietary process intended primarily to reduce usage of rare codons in *E. coli*. Interestingly, when this gene was subcloned into a pCWori^{+} construct and expressed and purified as described by Waterman[57], final yields of CYP17A1 were disappointingly low, at roughly 0.5 mg P450/L. Ultimately co-transformation with the bacterial GroEL/ES chaperone system was found to rescue expression levels to the values reported in the literature, suggesting a misfolding pathway was operating with our synthetic construct, though no efforts were made to experimentally confirm this hypothesis.

Overexpression of chaperones had the unexpected consequence of the co-purification of GroEL subunits with CYP17A1. GroEL is a tetradecamer composed of identical 57 kD subunits which form a structure resembling two opposing cups joined at the base. Misfolded proteins are targeted for refolding through association with hydrophobic patches on the interior of the chaperone.[66] Presumably, hydrophobic regions of CYP17A1 normally associated with the membrane bilayer interact with GroEL in an analogous manner as misfolded peptides. This interaction was resistant to disruption by typical purification methods such as use of detergents and high salt concentrations and has been observed by others during co-expression of chaperones and GST-tagged proteins. Fortuitously, the

ATP/Mg^{2+} dependent conformational changes utilized by the GroEL/ES chaperones can be triggered while CYP17A1 is immobilized on a Ni-NTA column by inclusion of these constituents in wash buffer.[67–69] As the chaperone cycles through high and low affinity states, GroEL may be washed off of the immobilized CYP17A1, yielding electrophoretically homogeneous enzyme.

The last decade has witnessed incorporation of myriad membrane proteins into Nanodiscs and evolution of a generalized protocol for this task.[60,61] A hallmark of these established methods is use of sodium cholate in the reconstitution mixture, a detergent compatible with most membrane proteins that readily solubilizes lipids and adsorbs to hydrophobic beads. Cholate, though, was found to be incompatible with CYP17A1. CYP17A1:Nanodiscs prepared with this detergent exhibited a peculiar Soret maximum at 410 nm and were found to exist primarily in the P420 state. It is unclear whether these effects were the result of denaturation or if cholate, as a cholesterol derivative with similar structure to CYP17A1's native substrates, was present in the active site of the enzyme.

After exhaustive screening Triton X-100 was identified as an alternative to sodium cholate despite its slightly inferior ability to solubilize 1-palmitoyl-2-oleoyl-*sn*-glycero-3-phosphocholine (POPC) and adsorb to Amberlite beads. These qualities are overcome by carefully controlling the ratio of POPC to Triton X-100 and the method described in the following section is competent to produce stable, properly formed Nanodiscs containing POPC and a single CYP17A1 in high yield (~20% of starting CYP17A1 is successfully incorporated).

Chapter 3: Characterizing the Functional Properties of Wild Type and T306A CYP17A1[1]

3.1 Introduction

In the human adrenal gland, the chemical transformations catalyzed by CYP17A1 are highly compartmentalized within the various regions of this organ. In the *adrenal zona fasciculata,* PREG and PROG are converted into their respective 17α-hydroxy products via a CpdI mediated addition of an alcohol to C17 of the steroid. In the *adrenal zona reticularis*, each of these hydroxylated products are converted to the estrogen and testosterone precursors dehydroepiandrosterone (DHEA) and androstenedione (AD) via 17,20-carbon-carbon bond scission in which the 21-carbon 17α-hydroxysteroids are cleaved to 19-carbon, 17-ketosteroids, and acetic acid (Figure 3.1).[30] Notably, while the hydroxylase activity of CYP17A1 is present throughout the entire lifespan of an individual, adrenal production of androgens is initiated only at andrenarche, a point that coincides with expression of cyt b5 in the *adrenal zona reticularis*.[70] Both *in vivo* and *in vitro* experimental methods have confirmed a substantial stimulatory effect on androgen production by CYP17A1 when cyt b5 is present, with some laboratories reporting as much as a 10-fold increase in DHEA production.[49,43,45,71] A significant limitation, however, in previous studies has been lack of a well-defined reconstitution system as other researchers have relied upon microsomal,

[1] Portions of this chapter are reprinted with permission from Khatri, Y., Gregory, M. C., Grinkova, Y. V, Denisov, I. G. & Sligar, S. G. Active site proton delivery and the lyase activity of human CYP17A1. *Biochem. Biophys. Res. Commun.* **443,** 179–184 (2014).

detergent solubilized, or soluble experimental modalities. This chapter reports in detail the stimulatory effects of cyt b5 in a Nanodisc system containing a POPC membrane and controlled stoichiometric ratios of both CPR and cyt b5 to CYP17A1.

Additionally, although many laboratories have characterized the catalytic properties of human CYP17A1, in addition to reliance on sub-optimal reconstitution systems, these reports have generally failed to evaluate the complete set of substrates (PREG, PROG, 17-OH PREG, 17-OH PROG) under identical conditions. Given the dramatic inconsistencies in V_{max} reported by various groups[47,56,72], the problematic partitioning of these hydrophobic substrates into detergent micelles, and the absence of any characterization of NADPH oxidation during catalysis, these limitations have heretofore represented a severe impairment in the ability to assess the influence of substrate structure on catalysis and coupling efficiency. In order to address these deficiencies methods were developed to quantitate NADPH oxidation and product forming rates in the presence of all substrates with precisely controlled stoichiometric ratios of CPR, cyt b5, and CYP17A1 assembled into Nanodiscs.

These baseline data are subsequently used to evaluate the properties of the T306A mutant of CYP17A1 possessing an impaired acid/alcohol pair on the I-helix. The analogous T252 residue in P450cam is known to play an essential role in proton transfer essential for O-O bond scission required for CpdI formation and dioxygen activation during catalytic turnover.[73–75] This residue forms part of the essential "proton shuttle" that delivers two protons in rapid succession to the peroxo-ferric, and hydroperoxo-ferric intermediates, respectively, resulting in release of H_2O and formation of CpdI. Impairment of the proton delivery pathway via introduction of a hydrophobic residue in this position has been shown

to result in a dramatic inhibition of hydroxylation of camphor despite comparable NADPH consumption comparable to wild-type enzyme.[76] In such an impaired system electron consumption is nearly completely uncoupled from substrate hydroxylation, and reducing equivalents instead appear in released hydrogen peroxide. Similar results are reported in other P450 systems as well, including P450BM3, CYP2E1, CYP2D6, and CYP1A2.[77–81]

The hydroxylase activity of CYP17A1 is expected to proceed through the CpdI initiated hydrogen abstraction observed in other members of the P450 superfamily, and thus the T306A mutant was expected to show a straightforward decrease in product formation and increase in uncoupling, as documented in other P450 systems. The latter C-C scission reactivity, however, is more circumspect and analysis of the product forming rate and coupling of the T306A mutant offers the ability to differentiate between a CpdI or peroxoanion mediated mechanism.

3.2 Materials and Methods

3.2.1 Design, Expression, and Purification of Proteins

In order to obtain the conserved I-helix variant of human CYP17A1 T306A, the wild-type pCWori_CYP17A1 construct was mutated using primers 5'-ggt gcc ggt gtg gaa gcc acc acc agc gtc gtc-3' (forward) and 5'- gac gac gct ggt ggt ggc ttc cac acc ggc acc-3' (Reverse). The sequence of the mutant was verified by automated DNA sequencing (ACGT, Inc.). T306A CYP17A1 was purified in an identical manner as described for wild type protein. All other proteins were prepared as described in Chapter 2.

3.2.2 Spectral Characteristics

Spectral dissociation constants were determined by the sequential addition of substrate dissolved in methanol to a cuvette containing 1.5 μM CYP17A1. Electronic absorption spectra were recorded from 350-800 nm in a Cary 300 spectrophotometer at 25°C. Spectral dissociation constants were estimated by plotting the change in the peak to trough A_{390} – A_{420} difference spectrum versus substrate concentration and fitting the resultant binding isotherm to the quadratic tight binding equation. Spin state change was estimated using a singular value decomposition routine in MATLAB to compare spectra obtained during the titration relative to reference spectra representing 100% high and low spin P450 forms.

3.2.3 Reconstitution System and Analysis of NADPH Oxidation Kinetics

Incorporation of CPR into preformed and purified CYP17A1 (or T306A)-Nanodiscs was made by direct addition of CPR at 1:4 CYP17A1 (or T306A)/CPR molar ratio, as described in detail by Grinkova *et al*. Briefly, 1 ml of CYP17A1 (or T306A) and CPR solution, in presence or absence of cyt b5 (1:4:4 molar ratio), in 100 mM potassium phosphate buffer, pH 7.4, containing 50 mM NaCl and 50 μM substrate (PROG, 17-OH PROG, PREG or 17-OH PREG) was brought to 37°C in a stirred quartz cuvette. The solution incubated for 5 min and the reaction initiated by addition of NADPH to a concentration of 100 μM (for PREG and PROG) or 300 μM (17-OH PREG and 17-OH PROG) from a 20 mM stock in reaction buffer. The rate of NADPH consumption was determined by monitoring the decrease in absorbance at 340 nm using an extinction coefficient of 6.22 $cm^{-1}mM^{-1}$. Each reaction was quenched by addition of 50 μl of 9 M sulfuric acid to bring the pH below 4.0. The sample was removed

from the cuvette, flash frozen in liquid nitrogen, and stored at -80°C until product analysis. Optical measurements were performed on a Hitachi U-3300 or Cary 300 spectrophotometer equipped with a temperature controller and magnetic stirrer.

3.2.4 Analysis of 17-OH PREG Formation

Conversion of PREG to 17-OH PREG was determined by a thin layer chromatographic method. Radiolabeled [7-^{3}H] pregnenolone (8.5 nmol, 0.8 μCi) was incubated with CYP17A1 or T306A (62 pmol) incorporated in POPC Nanodiscs, CPR (248 pmol) and, when present, cyt b5 (235 pmol) in 0.25 ml of 0.1 M potassium phosphate buffer, pH 7.4, containing 50 mM NaCl for 10 min before the reaction was initiated by addition of NADPH (120 nmol). The reaction proceeded for 15 min and was terminated by addition of 2 mL methylene chloride. The mixture was vigorously mixed for 20 seconds and after phase separation the organic layer was transferred into new tube and the solvent evaporated under stream of nitrogen gas. The sample was dissolved in 30 μl of methanol and loaded onto TLC plate (EMD TLC Silica gel 60 F254, 20X20 cm), which was then run once in the mixture of chloroform: ethyl acetate: water (80:20:1). Five-point calibration with known amounts of radioactivity was performed for each plate. The plate was imaged using BAS-IP TR 2025 imaging plate and Storm 840 imaging system. The data were processed using Image J software to obtain percent conversion.

3.2.5 Analysis of 17-OH PROG Formation

Conversion of PROG to 17-OH PROG was determined by reversed phase HPLC. Briefly, 1 μl of a 27 mM cortexolone internal standard in methanol was added to 500 μl of each reaction sample and vortexed for 10 sec. 2 mL of chloroform was added to each sample

and vortexed for 30 seconds. The organic phase was removed and dried under a stream of nitrogen. The dried sample was dissolved in 100 μl of methanol and 40 μl was injected onto C_{18}-HPLC column, using a 150 x 2.1 mm, 3μm (ACE-111-1502) with a mobile phase of 45% each of methanol and acetonitrile in water and a flow rate of 0.2 mL/min. The 17-hydroxy product of PROG was separated in a linear gradient of methanol and acetonitrile from 20% to 80% in 28 min. Peak integration was performed with GRAM/32 software (Thermo Fischer Scientific).

3.2.6 Analysis of Androgen Formation

DHEA and AD were analyzed using a flame ionization discharge detector following gas chromatographic separation. Each frozen reaction solution was thawed and 800 μL was delivered to a test tube and steroid product separated via double extraction with 2 mL of dichloromethane after addition of a progesterone internal standard. The organic layer was dried under a stream of nitrogen and the extract reconstituted in 1.5 ml of 80% methanol. The resultant lipemic mixture was further purified via a second separation with 750 μl pentane, wherein lipids partition preferentially into the pentane layer. The methanol/steroid solution was evaporated to dryness under vacuum. Steroids were reconstituted in cyclohexane and analyzed on an Agilent 6890 GC-FID equipped with a 15 m DB-1 column, 530 μm I.D., 1.5 μm film thickness (J & W Scientific). Injector temperature and volume were 250°C and 3 μl. Nitrogen carrier gas was set to 2.2 ml/min and the oven temperature was held at 100°C for 1.5 min and ramped to 275°C at 30°C/min and held for 13 min. Data analysis was performed using GRAM/32 AI software.

3.3 Results

3.3.1 Spectral Properties of CYP17A1

Both prenenolone and progesterone were found to bind Nanodisc incorporated CYP17A1 quite tightly, with spectral dissociation constants (K_s) of 65 nM and 90 nM, respectively. At saturating concentrations both substrates caused a complete conversion to the high spin state. Hydroxylated substrates had substantially higher K_s values and failed to completely convert the enzyme to the high spin state. 17-OH PREG was found to bind to CYP17A1 with a K_s of 0.77 μM with a corresponding value of 0.98 μM for 17-OH PROG. At saturation, both substrates resulted in a mixed population of spin states, calculated to be ~60% high spin for both 17-OH PREG and 17-OH PROG. The Soret maximum for low spin ferric CYP17A1 was 417 nm. All substrates bound in a straightforward Type I manner increasing the high spin population with a Soret at 393 nm. In the presence of substrate, the enzyme is readily reduced to the ferrous state (408 nm) by sodium dithionite, and addition of carbon monoxide saturated buffer results in the immediate formation of nearly 100% of the P450 Fe^{II}:CO state at 447 nm (Figure 3.2).

Despite spectra reflective of the "canonical" P450s in the ferric state, the oxy-ferrous spectrum of CYP17A1 exhibits considerable substrate dependent variability. In the case of PROG and PREG, Soret maxima were consistent with other P450 enzymes at 421 nm and 422 nm, respectively. However, formation of this transient species in the presence of hydroxylated substrates results in a red-shift to 426 nm with 17-OH PROG and 431 nm in the presence of 17-OH PREG.

The T306A mutant of this protein exhibited identical behavior to the WT protein in the ferric, ferrous, and ferrous-CO states. Although substrate titrations were not performed, percent conversion to the high spin state was similar to wild-type enzyme and saturation occurred at < 10 μM in the presence of all substrates.

3.3.2 NADPH Oxidation and Product Forming Rates of WT and T306A CYP17A1

Rates of pyridine nucleotide oxidation and product formation were measured for both wild type CYP17A1 and the T306A mutant in the absence and presence of a 4-fold molar excess of cyt b5. All CYP17A1 mediated reactions were evaluated using PREG, PROG, 17-OH PREG, and 17-OH PROG as substrates. For the hydroxylation reaction the yield of 17α-hydroxy product was quantitated. Due to the slow product forming rate and lack of processivity owing to substantially higher K_d for lyase substrates, androgen formation does not occur under the experimental conditions described above, permitting straightforward analysis of product forming rates for this first step. In another set of experiments use of 17-OH PREG and 17-OH PROG allowed specific examination of the 17,20-carbon-carbon lyase reaction of the corresponding substrates by monitoring production of DHEA and AD, respectively.

When PREG was used as a substrate, the wild type enzyme formed 17-OH PREG at a rate of 5.6 min^{-1} in the absence of cyt b5 while consuming pyridine nucleotide at 5.8 min^{-1}. In the presence of cyt b5 product forming rates increase marginally to 6.2 min^{-1} (NADPH oxidation was not measured). As expected, in the case of the T306A mutant, 17-OH PREG formation was substantially diminished, with rates of 0.23 min^{-1} and 0.35 min^{-1} in the absence and presence of cyt b5, respectively. NADPH consumption increased dramatically, to 38 min^{-1} in reactions containing T306A without cyt b5. In the presence of PROG, the wild

type enzyme formed product at 4.8 min^{-1} consuming NADPH at a rate of 23 min^{-1}. The mutant CYP17A1 showed a similar expected catalytic impairment, forming 17-OH PROG at 0.38 min^{-1} while consuming NADPH at a rate of 54 min^{-1}. These results are summarized in Figure 3.3.

In a separate set of experiments, the lyase activities of wild type and mutant CYP17A1 in the absence and presence of a 4-fold molar excess of cyt b5 were evaluated. For both 17-OH PREG and 17-OH PROG, the presence of cyt b5 significantly enhanced the rate of product formation, from 0.15 min^{-1} to 0.76 min^{-1} for 17-OH PREG and from a barely detectable 0.05 min^{-1} to 0.34 min^{-1} for 17-OH PROG. Despite the large changes in product forming rates, only minor differences in NADPH consumption were observed upon addition of cyt b5. Unlike the hydroxylase activity, T306A CYP17A1 was competent to catalyze androgen formation, turning over 17-OH PREG at 0.07 min^{-1} and 0.37 min^{-1} in the absence and presence of cyt b5, respectively. Its behavior was similar when given 17-OH PROG as a substrate, generating AD with rates of 0.03 min-1 and 0.12 min-1 with and without cyt b5, respectively. In another departure from its behavior when given hydroxylase substrates, NADPH oxidation rates were essentially unchanged during lyase catalysis relative to those observed in wild type protein. These results are reported in Figure 3.4.

3.4 Conclusions

It is well documented that cyt b5 augments the 17,20-carbon–carbon bond scission of mammalian CYP17A1, although detailed studies as a function of the P450:CPR:cyt b5 ratio in their full length forms in a controlled membrane environment have not been reported.[34]

Therefore, we explored the effect of cyt b5 during lyase activity on our well defined assay system consisting of CYP17A1 Nanodiscs and co-incorporated CPR and cyt b5. We unambiguously observed the preference of 17-OH PREG (>2-fold higher compared to 17-OH PROG) during 17,20-lyase activity for both the WT and T306A in presence of cyt b5. In this study, we also observed that the presence of cyt b5 enhanced the lyase activity by ~ 5- and 7-fold in the WT and ~ 5- and 4-fold in the T306A mutant for 17-OH PREG and 17-OH PROG, respectively.

We observed that T306A consumed NADPH at 15% and 43% faster rates than WT during the conversion of PREG and PROG to their corresponding 17α-OH product. However, the product formation rates were dramatically reduced by ~94% and 92% respectively. As a result, the coupling efficiency of T306A was less than 1% during the hydroxylation of PREG and PROG, compared to 97% and 22%, respectively, for the wild type enzyme. These two conversions were highly uncoupled in which reducing equivalents and protons likely funneled into formation of superoxide and hydrogen peroxide without O-O bond cleavage rather than productive hydroxylation of the substrates. This is consistent with disruption of proton delivery to the distal oxygen atom of the peroxoanion required to initiate O-O bond scission and formation of the CpdI reactive intermediate. These results are comparable with previous investigations of P450cam, in which mutation of this critical residue severely impairs formation of CpdI with a concomitant decoupling of product formation from NADPH oxidation.[73,82]

Notably, catalysis of carbon-carbon bond scission by the T306A mutant was largely unimpeded by disruption of the CYP17A1 acid/alcohol pair. During carbon-carbon bond scission reaction monitored by the conversion of 17-OH PREG to DHEA, the rate of NADPH

oxidation was similar (21 vs 17 nmol/min/nmol P450) for WT and T306A, respectively, and did not show the dramatic difference in coupling 4% vs 2% for WT and mutant. Likewise, the lyase reaction of 17-OH PROG to AD also showed similar rates of NADPH oxidation of (26 vs 36 nmol/min/nmol P450) corresponding to coupling of 1.3% vs 0.3% for WT and T306A, respectively (Figure 3.5). In both lyase reactions, we did not observe the dramatic changes as during hydroxylase activity. Absence of significant ablation of catalytic activity and constant rates of NADPH oxidation in this experiment are inconsistent with results observed in other P450s, where a functional "proton shuttle" is required for formation of the active oxidant CpdI. These data support the hypothesis that C-C lyase chemistry conducted by CYP17A1 proceeds independently of O-O bond scission and CpdI formation, and are consistent with expected behavior of a peroxoanion intitiated catalysis.

3.5 Tables and Figures

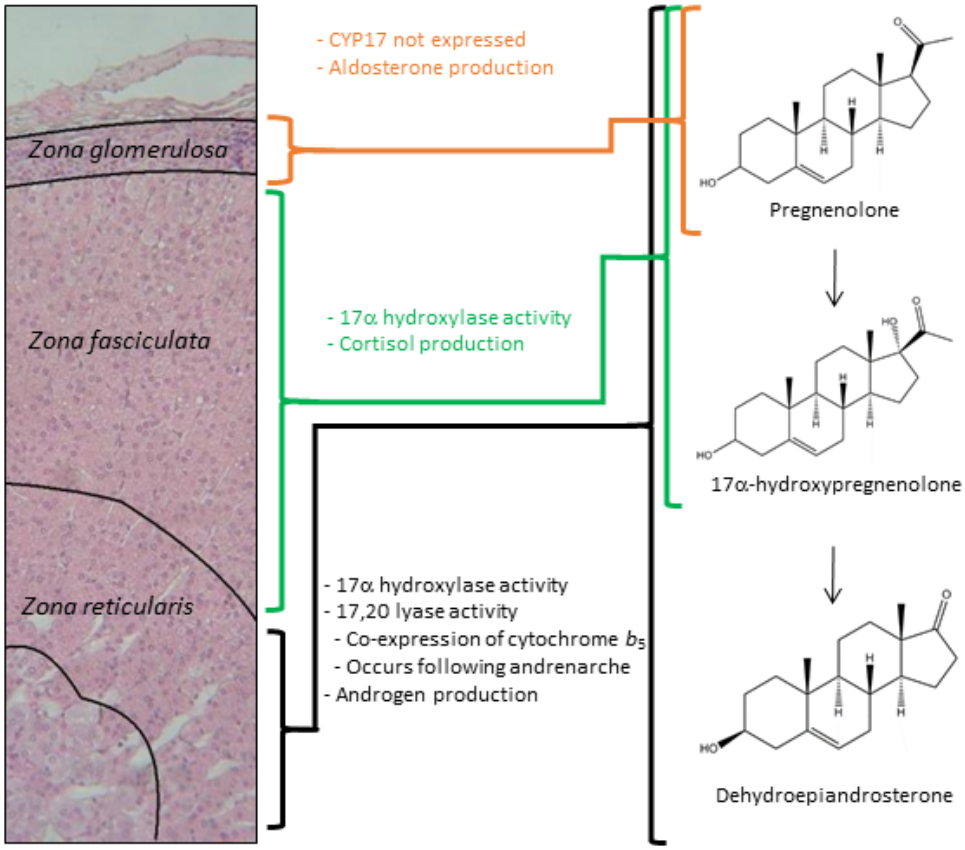

Figure 3.1: Compartmentalized Steroid Formation in the Adrenal Gland.

The histological slice on the left labeled with the various regions of the adrenal gland with the corresponding biological transformations performed by CYP17A1 on the right.

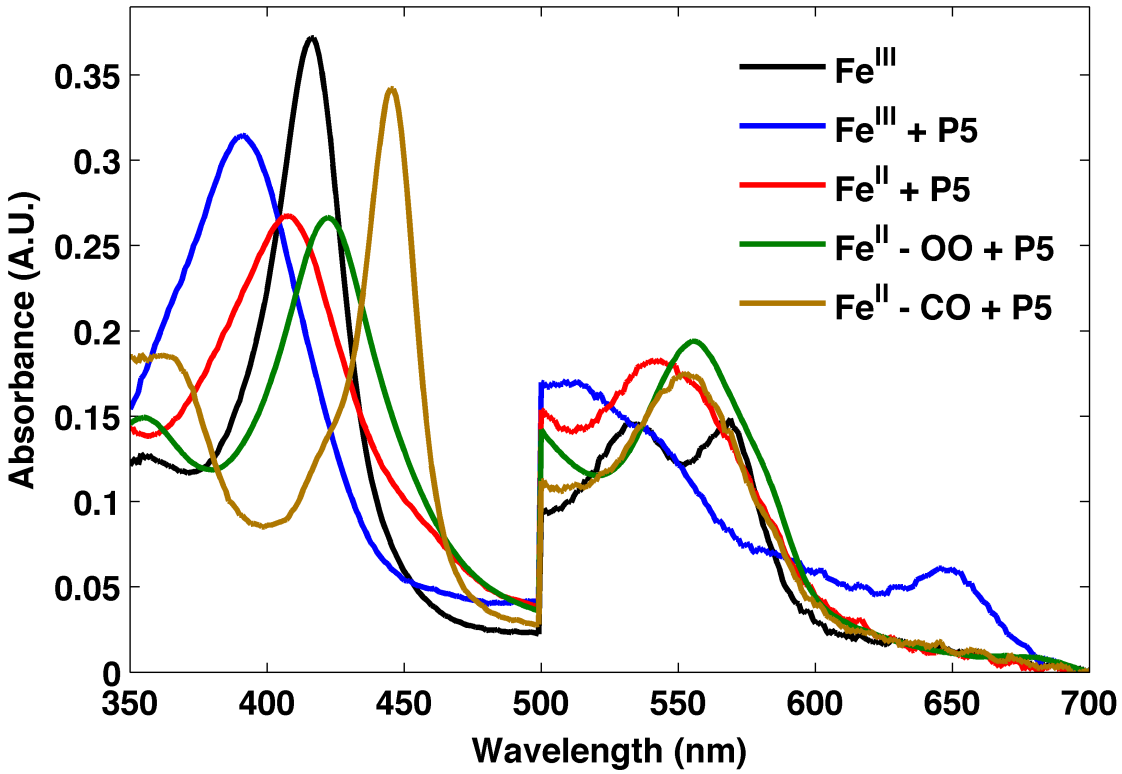

Figure 3.2: Spectra of Pregnenolone (P5) Bound CYP17A1 Nanodiscs.

Optical spectra of CYP17A1 in Nanodiscs obtained in the substrate free and PREG bound states. Ferric, ferrous, ferrous-CO, and oxy-ferrous spectra are shown.

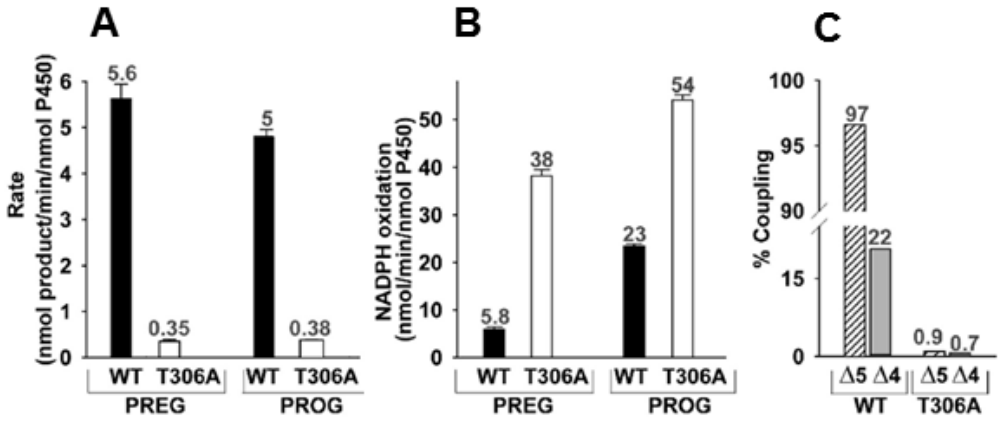

Figure 3.3: Product Formation, NADPH Oxidation, and Coupling Efficiency for Pregnenolone and Progesterone Substrates.

Determination of steady state product formation (A), and NADPH consumption (B) rate of PREG and PROG catalyzed by WT CYP17A1 and the T306A mutant are shown. Panel C indicates coupling efficiency for PREG (Δ5) and PROG (Δ4) for both the wild-type and mutant CYP17A1.

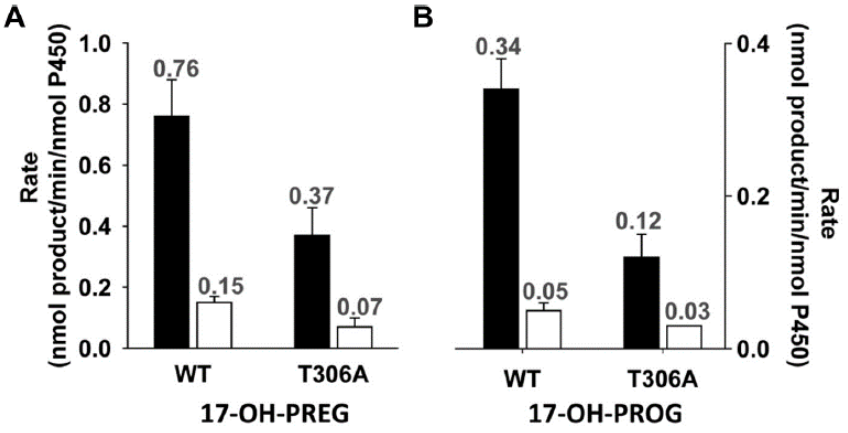

Figure 3.4: Product Forming Rates for 17-OH PREG and 17-OH PROG

Steady state product forming rates when 17-OH PREG (A) and 17-OH PROG (B) are used as substrates. Black bars indicate reactions in the presence of a 4-fold excess of cyt b5, white bars are turnover in the absence of cyt b5.

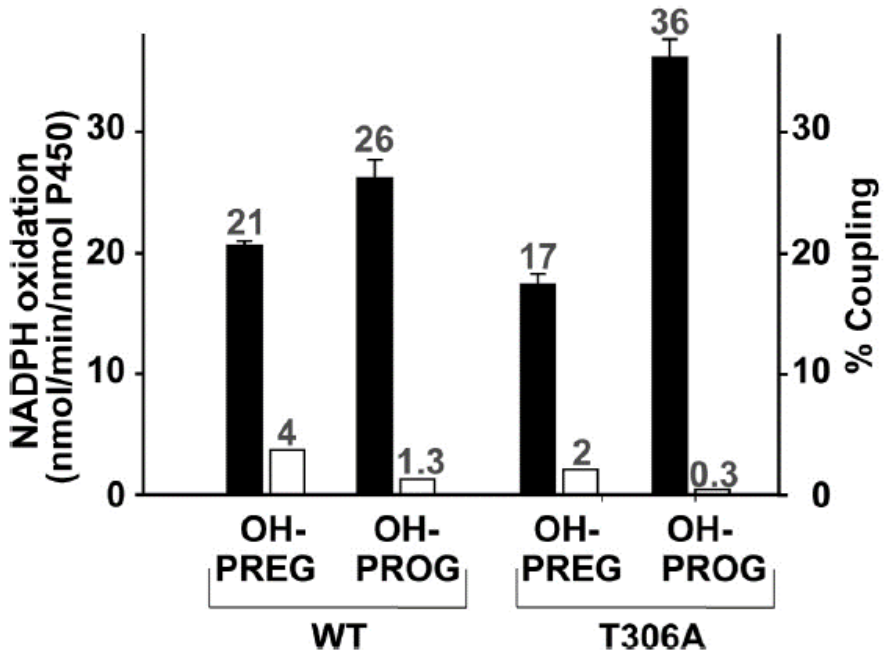

Figure 3.5: NADPH Oxidation and Coupling Efficiency for 17-OH PREG and 17-OH PROG

NADPH oxidation (left axis, black bar) and coupling efficiency (right axis, white bar) for lyase reactions when conducted in the presence of 4-fold excess of cyt b5.

Chapter 4: Kinetic Solvent Isotope Effect During Lyase Catalysis[2]

4.1 Introduction

As seen in Figure 1.1, a key distinguishing feature between CpdI and peroxoanion mediated P450 catalysis is the involvement of protons in scission of the iron ligated dioxygen bond and generation of the ferryl oxo species. The necessity of at least two protons in flight to generate the hydroperoxo and later CpdI species suggests that kinetic solvent isotope effects (KSIE) might be used to distinguish between a peroxoanion or CpdI active intermediate. Should a rate limiting step exist between formation of the peroxoanion and CpdI, monitoring steady state product forming rates as a function of buffer deuterium oxide content could exclude one of the two potential pathways. In the case of a CpdI intermediate, substitution of protium oxide with D_2O would be expected to result in a slowing of the steady state product forming rate, resulting in a $k_H/k_D > 1$. Alternatively, the proton independent peroxo- mediated catalysis should exhibit a kH/kD of ≤ 1.[83]

An additional concern in comparing these two pathways of androgen formation are uncoupling reactions which release hydrogen peroxide: the "peroxide shunt" in Figure 1.1. As described in Chapter 3, the hydroxylation of pregnenolone (PREG) at the 17-position is well coupled, however during the C-C lyase 17-OH PREG much of the pyridine nucleotide

[2] Portions of this chapter are reprinted with permission from Gregory, M. C., Denisov, I. G., Grinkova, Y. V, Khatri, Y. & Sligar, S. G. Kinetic Solvent Isotope Effect in Human P450 CYP17A1-Mediated Androgen Formation: Evidence for a Reactive Peroxoanion Intermediate. *J. Am. Chem. Soc.* **135,** 16245–16247 (2013). Copyright 2013 American Chemical Society.

reducing equivalents appear in free hydrogen peroxide rather than carbon product.[84] Uncoupling occurring from the iron-peroxide intermediates can also involve protons. We thus have the following branching pathways (Figure 4.1) where the addition of two protons to the ferric peroxoanion **[1]** results in formation of CpdI which is utilized in the hydroxylation of pregnenolone **[3]** to 17-OH PREG **[4]** in the first step of CYP17A1 catalysis. The second, uncoupled step responsible for androgen formation, either proceeds productively from **[1]** through an acyl-peroxo intermediate **[5]** to form DHEA **[6]**, or unproductively through proton dependent formation of **[2]** and ultimate release of peroxide.

4.2 Materials and Methods

4.2.1 Protein Expression and Purification

CYP17A1 in Nanodiscs, CPR, and cyt b5 were prepared as indicated in the relevant sections of Chapter 2.

4.2.2 Turnover Assays

Product formation and NADPH oxidation rates of human CYP17A1 incorporated into Nanodiscs in the presence of its redox partner cytochrome P450 oxidoreductase (CPR) and its effector cyt b5 were measured in the presence of saturating concentrations of PREG (50 μM) and 17-OH PREG (50μM) at 37°C and pH/pD 7.4. Deuterated samples were prepared by exhaustive exchange of the proteins in 100 mM KPi, pH 7.4 D_2O buffer, with the pH meter corrected using the method of Glascoe and Long.[85] The 17-OH PREG formation assay was performed as indicated in Chapter 3.2.. DHEA formation was quantitated in a reconstituted system containing 208 pmol CYP17A1 Nanodiscs and a four-fold molar excess of cyt b5 and

CPR in 1.0 mL of 100mM potassium phosphate, pH/pD 7.4 containing 50 mM NaCl and 50 μM 17-OH PREG. Reactions were carried out in a stirred cuvette in a temperature controlled Cary 300 spectrophotometer and monitored at 340 nm after initiation by addition of 600 nmol NADPH. Each reaction was quenched after 20 minutes by addition of 50 μL 8.9 N H_2SO_4. Product analysis was performed using the gas chromatographic method described in Chapter 3.2.6. PREG product formation was assayed as described in section 3.2.4.

4.3 Results

When PREG was used as a substrate, the rate of 17α-hydroxy product formation occurred at a rate of 22.6 ± 0.9 min^{-1}, while in deuterated buffer this rate slowed to 17.5 ± 0.8 min^{-1}. This corresponds to a kinetic solvent isotope effect (KSIE) for the hydroxylation reaction of k_H/k_D = 1.3, very similar to values reported for other P450 systems catalyzing hydroxylation chemistry.[11,86,87] When 17-OH PREG was used as a substrate, the rate of conversion of the α-hydroxy ketone to DHEA via C-C lyase activity was much slower, as previously described in Chapter 3. Unexpectedly, however, when D_2O was substituted for H_2O, the rate of product formation with this substrate was dramatically augmented, from 0.86 ± 0.1 min^{-1} to 2.2 ± 0.1 min^{-1}. This corresponds to an inverse KSIE of 0.39. (Figure 4.2)

In addition to product formation, the overall rate of NADPH oxidation also monitors the uncoupling pathway. In the case of the lyase activity when 17-OH PREG is a substrate, the majority of reducing equivalents appear as released hydrogen peroxide without substrate formation[84]. Despite the inverse KSIE seen in the product forming rate, the rate of NADPH oxidation decreased by 40%, from 27.5 ± 0.6 min^{-1} to 16.6 ± 0.3 min^{-1}. This difference is also

reflected in turnover experiments conducted in the absence of substrate, where rates of NADPH oxidation in H_2O and D_2O were 31.5 ± 0.7 min^{-1} and 18.1±1.0 min^{-1}, respectively. This normal slowing of rates in the presence of D_2O versus H_2O is another important indicator of the intermediates involved in lyase chemistry. The same rate decrease in D_2O as compared to H_2O in the substrate-free CYP17A1, reflecting NADPH oxidation in this system unrelated to product formation, suggests the same rate-limiting step for the overall steady-state NADPH consumption kinetics that is strongly dependent on protonation. This protonation step is likely to be the first protonation of peroxo-anion coordinated to the heme iron. An alternative suggestion of the second protonation event and formation of CpdI as the rate limiting step can be rejected as incompatible with the different signs of KSIE observed in hydroxylation of PREG and lyase reaction with 17-OH PREG as substrate. If formation of CpdI would be the rate-limiting step, the KSIE of lyase reaction would be higher or equal to one, depending on the masking by other steps in the catalytic cycle.

4.4 Conclusions

The hydroxylase activity of CYP17A1 is expected to proceed through the classical Groves rebound mechanism[28] with CpdI as the reactive intermediate. Results for this first reaction are entirely consistent with expectations of a partially masked, proton dependent, CpdI mediated mechanism, and are congruent with previous reports of solvent isotope effects in P450cam.[11,87,88] The large inverse isotope effect and decrease in NADPH oxidation rate for the latter lyase reaction where 17-OH PREG is subjected to 17,20 C-C bond cleavage to form DHEA, however, cannot be reconciled with a CpdI mediated reaction. Rather, these

observations are consistent with inhibition of protonation of the peroxo-ferric species in a manner that serves to facilitate productive, rather than unproductive oxidation. Formation of the peroxo-ferric intermediate and nucleophilic attack of C-20 carbonyl does not involve any protonation event and is expected to exhibit the same kinetics in H_2O and D_2O. Alternatively, two protonation steps with concomitant formation of the hydroperoxo-ferric complex and CpdI progress much slower in D_2O. Because of this difference in rates between productive and unproductive pathways at the peroxo- branching point (**[1]** and **[2]** in Figure 4.1) the steady-state concentration of this intermediate **[1]** increases and the apparent rate of product formation also increases in D_2O, although the microscopic catalytic rate of **[1]→ [5]** is the same in both solvents. Such mechanism is also confirmed by significant decrease of NADPH consumption rate in D_2O, indicating smaller fraction of reducing equivalents following proton-dependent pathways of hydrogen peroxide formation from hydroperoxo-ferric intermediate and oxidase reaction of CpdI.

Similar mechanistic studies in other enzymes also reported inverse solvent isotope effect as the result of slower uncoupling reaction that competed with the productive pathway. This was observed in tyrosine hydroxylase, where uncoupling pathway via the breakdown of peroxypterin intermediate with formation of H_2O_2 can be compared to the release of peroxide in cytochrome P450 catalytic cycle and to uncoupling in flavin monooxygenases.[89,90] Another example of improved product formation in steady-state is the reaction catalyzed by putidamonooxin caused by considerable inhibition of uncoupling channel in D_2O studied by Twilfer *et al*.[91] In this work, the uncoupling reaction resulted in peroxide release and thus required protonation. In D_2O this protonation was significantly slower and as a result, partitioning of the active intermediate between productive and

unproductive pathways was shifted in favor of the former. This example of directly observed competition between the productive (monooxygenase and dioxygenase reaction) and unproductive (protonation of active oxygen species and formation of H_2O_2 in uncoupling pathway) pathways of this enzyme was interpreted as indicating the iron-peroxo complex as an active intermediate in putidamonooxin.

The normal KSIE for hydroxylation reaction and strong inverse apparent KSIE for the lyase reaction catalyzed by CYP17A1 cannot be reconciled with the same rate-limiting protonation dependent step commonly observed in other cytochromes P450 when CpdI is the main catalytic intermediate. Rather, an inverse KSIE implies catalysis via a proton-independent intermediate and the presence of the branching proton-dependent uncoupling pathway, which is considerably slower in D_2O, thus providing higher yield of the product. Taken together, these results suggest two distinct mechanisms for the first and the second steps of CYP17A1 catalyzed reactions.

These results highlight a novel property of the CYP17A1 active site: the ability to select between use of multiple reactive intermediates based on presence of a 17α-hydroxy moiety on the substrate molecule. In the presence of pregnenolone, this enzyme preferentially catalyzes formation of 17-OH PREG in a straightforward CpdI mediated mechanism known to function in other P450s. However, when 17-OH PREG is used as a substrate, our observations strongly implicate the peroxoanion as the reactive intermediate.

4.5 Tables and Figures

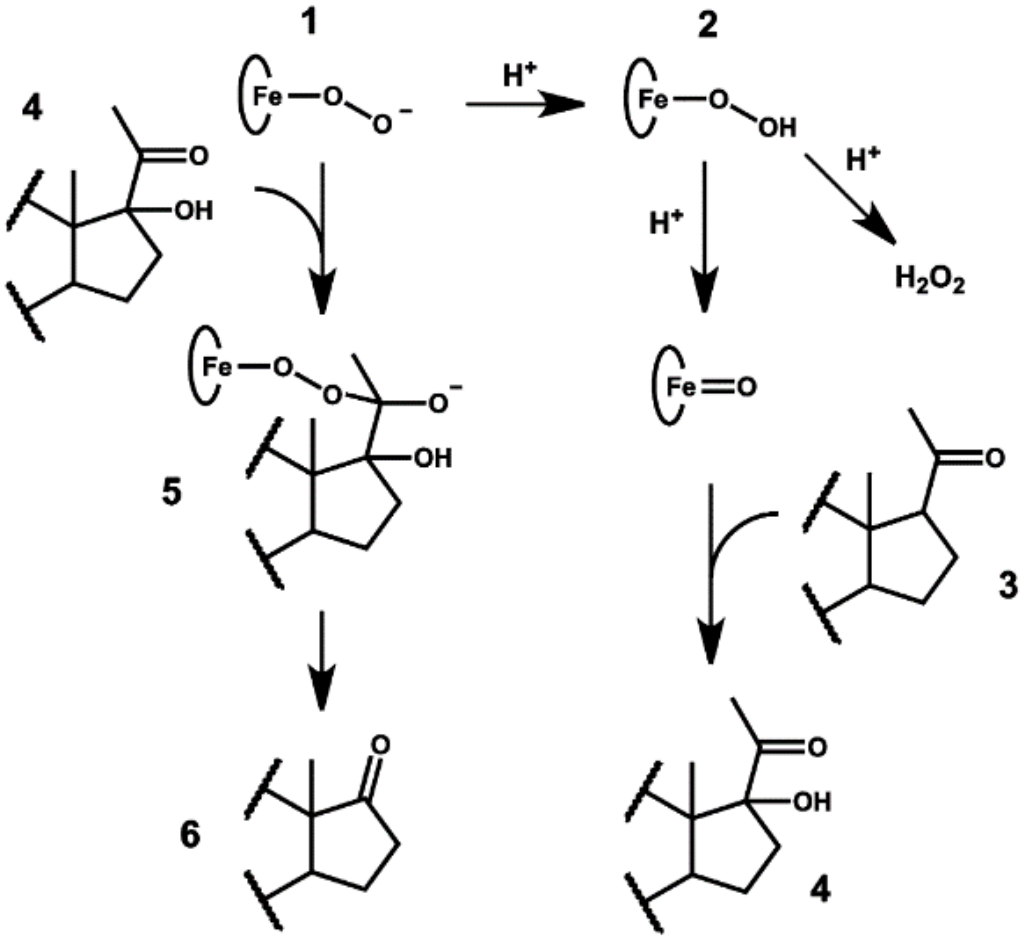

Figure 4.1: Branch Points in P450 Catalysis

17-OH PREG (4) can undergo a proton-independent reaction with the peroxoanion (1), forming a peroxo hemiacetal (5) and decomposing to androgen product (6). Alternatively, protonation of the peroxoanion forms the hydroperoxo species (2) that following the input of a second proton can be release non-productively as hydrogen peroxide, or form CpdI to hydroxylate PREG (3).

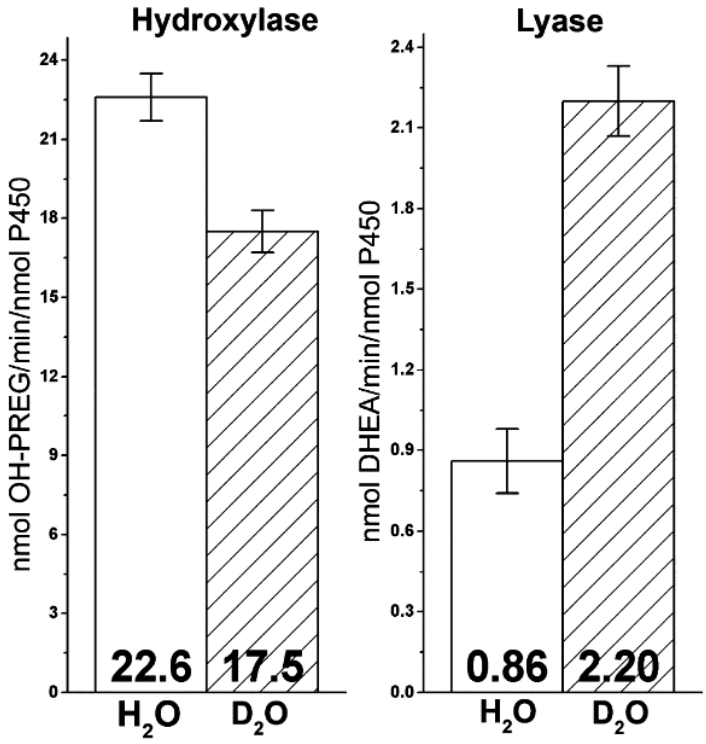

Figure 4.2: Product Forming Rates in H_2O and D_2O

Left panel shows the rate of 17-OH PREG formation when PREG is used as a substrate. Right panel shows rate of DHEA formation when 17-OH PREG is a substrate. Numbers at base of bars represents nmol product/min/nmol P450.

Chapter 5: Resonance Raman Spectroscopy of Ferric and Ferrous CYP17A1[3]

5.1 Introduction

As outlined in Figure 1.2, the first reactions catalyzed by CYP17A1 are 17α-hydroxylation of PREG to 17-OH PREG and PROG to 17-OH PROG. These hydroxylated products are then subjected to a second round of catalysis generating the DHEA and AD androgens.[34] It is particularly notable that the relatively minor structural differences in these substrates, such as the identity of the C-3 substituent, positioning of the C=C bond (Δ4 vs Δ5), and the presence of a 17α-OH exhibit structurally, kinetically, and mechanistically distinct interactions with this enzyme. As defined in two recent publications by the Scott laboratory in which the crystal structure of CYP17A1 was solved in the presence of the inhibitor Abiraterone acetate and native substrates, the presence of either an alcohol (PREG/17-OH PREG) or a keto fragment (PROG/17-OH PROG) can have profound impact on the positioning of these molecules in the active site.[92,93]

In this and the following chapters, the impressive power of resonance Raman (rR) spectroscopy is employed to probe the heme environment of Nanodisc incorporated CYP17A1. Here, rR is utilized to characterize the ferric and ferrous:CO states in the presence of the native substrates of this enzyme. Well established high frequency marker modes are

---

[3] Portions of this chapter were reprinted with permission from Mak, P. J., Gregory, M. C., Sligar, S. G. & Kincaid, J. R. Resonance Raman Spectroscopy Reveals That Substrate Structure Selectively Impacts the Heme-Bound Diatomic Ligands of CYP17A1. *Biochemistry* **53,** 90–100 (2014). Copyright 2014 American Chemical Society.

sensitive to changes in oxidation or spin state of the heme iron atom and low frequency modes report changes in protein interactions with the heme periphery.[94] Particularly important in these stable states are the various changes to propionic acid and vinyl heme substituents which have been suggested to be important structural determinants of heme reactivity.[95,96] Additionally, Fe-S and Fe-C-O modes may be selectively enhanced providing an especially sensitive probe of these key linkages.[97]

In this chapter a combination of Nanodisc and rR spectroscopic methods are utilized in the interrogation of the active site structure of CYP17A1 in its interaction with all four of its native substrates. Low and high frequency spectra were collected in the ferric and ferrous:CO states, the latter species being the accepted paradigm for probing distal and proximal effects on heme-bound exogenous ligands.

5.2 Materials and Methods

5.2.1 Preparation of Ferric Samples for rR Spectroscopy

Substrate stock solutions containing PROG, 17-OH PROG, PREG and 17-OH PREG in methanol were prepared at concentrations of 8-10 mM. CYP17A1 Nanodisc solutions in 100 mM KPi, pH 7.4 buffer containing 15% ultrapure glycerol were prepared as indicated in Chapter 2.2.3 and Chapter 2.3. Solutions were concentrated to ~100 μM and PROG and PREG bound samples were prepared by the addition of the appropriate substrate to a final concentration of 400 μM. The 17-OH PROG- and 17-OH PREG bound samples were similarly prepared by the addition of the appropriate substrate to 500 μM. Samples were subsequently flash frozen in liquid N_2 before further use.

5.2.2 Preparation of Ferrous:CO CYP17A1 Samples

A 100 μL volume of ~ 100 μM ferric ND:CYP17A1 sample in a septum-sealed 5 mm NMR tube (WG-5 Economy, Wilmad) was degassed by multiple rounds of application of vacuum and filling with argon gas. After the final gas evacuation, the CO gas was introduced to the NMR tube and the ferric sample was reduced by addition of ~2-5 molar equivalents (~2 μL) of sodium dithionite dissolved in freshly degassed 100 mM potassium phosphate buffer, pH 7.4. Formation of ferrous CO adducts was confirmed by electronic absorption spectroscopy in the Q band region. Reduction and CO saturation was deemed complete when the UV-Vis spectra of these samples exhibited a single Q band at around 552 nm. The samples contained no P420 impurities as judged by the lack of bands near 540 nm and 570 nm characteristic for ferrous CO adducts of P420.

5.2.3 Collection of rR Spectra

The samples of ferric CYP17A1 samples were measured using the 406.7 nm and 356.7 nm excitation lines from a Kr^+ laser (Coherent Innova Sabre Ion Laser) and the Fe(II)-CO adducts were excited by a 441.6 nm line provided by a He-Cd laser (IK Series He-Cd laser, Kimmon Koha CO., LTD.). The rR spectra of all samples were measured using a Spex 1269 spectrometer equipped with Spec-10 LN-cooled detector (Princeton Instruments). The slit width was set at 100 μm and the 1200 g/mm grating was used. With this grating, the resultant spectral dispersion is 0.46 cm^{-1}/pixel. The laser power at the ferric sample was adjusted to ~ 10 mW while for ferrous CO adducts it was kept at ~1 mW to minimize photodissociation. Moreover, to avoid laser-induced heating and protein degradation the samples were contained in spinning NMR tubes (5 mm outside diameter, WG-5 ECONOMY, Wilmad). The 180° backscattering geometry was used for all measurements and the laser

beam was focused onto the sample using a cylindrical lens. All samples were measured at room temperature. Spectra were calibrated with fenchone (Sigma-Aldrich, WI), toluene-$^2H_6$ and acetone-$^2H_6$ (Cambridge Isotope Laboratories, Inc., MA) and processed with Grams/*32* AI software (Galactic Industries, Salem, NH).

5.3 Results

5.3.1 High Frequency rR of the Ferric States of CYP17A1

The spectrum of substrate-free ND:CYP17A1 (Figure 5.1, trace A) exhibits characteristic features of the ferric state: the ν_4 oxidation state marker is observed at 1372 cm^{-1}. Spin state marker bands ν_3 at 1502 cm^{-1}, the ν_2 at 1581 cm^{-1} and the ν_{10} at 1636 cm^{-1}, are indicative of a pure low spin 6-coordinated state, reflective of the expected coordination of a water molecule to the heme iron.[98,99] The two overlapped features observed at 1621 cm^{-1} and 1629 cm^{-1} are assigned to the ν(C=C) stretching modes of the two peripheral vinyl groups with respective dispositions in and out of the planes of the pyrrole rings to which they are bound, consistent with previously published data.[100]

Figure 5.1, trace B with PROG bound CYP17A1 shows a shift in spin state markers to 1486 cm^{-1} (ν_3), 1565 cm^{-1} (ν_2) and 1627 cm^{-1} (ν_{10}), the last overlapped with vinyl ν(C=C) mode(s). These heme-core mode frequencies are consistent with a pure high spin 5-coordinate state.[100,101] Consistent with UV-Vis spectroscopy reported in Chapter 3.3.1, the binding of 17-OH PROG (Figure 5.1, trace C) results in only a partial spin state conversion, as indicated by the presence of bands characteristic for both low and high spin states. Similar spectral patterns are observed for the PREG and 17-OH PREG substrates, as seen in traces E

and F of Figure 5.1, where only partial spin state conversion is once again seen for the hydroxylated substrate.

Partial spin state conversions upon binding of certain substrates, such as the 17-OH PROG and 17-OH PREG samples above, have been observed previously for other cytochrome P450 enzymes, and is most often attributed to incomplete expulsion of the distal pocket water cluster and coordination of a residual water molecule. However in this case it must be noted that the two substrates producing partial spin state conversions possess 17α-hydroxy substituents. Based on crystal structures of this enzyme in the presence of these substrates, it is expected that this group would be in close proximity to and directed towards the heme iron.[93] Therefore, it is also reasonable to suggest that these R-OH fragments might interact directly with the heme iron. Alternatively, the presence of this R-OH group within the heme pocket might enhance retention of one or more residual water molecules.

Inasmuch as the components in the rR spectra that are associated with the low spin state do not significantly differ among traces A,C and F (i.e., 1636, 1581 and 1502 cm^{-1}), there is no support for arguing that the coordination environment is different for the substrate-free (SF) and the samples bound with the hydroxylated substrates. On the other hand, the high degree of specificity associated with the hydroxylation reactions and the relatively crowded distal side pocket revealed in the crystal structure[92,93] tends to favor the explanation involving direct interaction between the R-OH and heme iron. In either case it is reasonable to suggest that the retention of a significant amount of low spin form for the 17-OH PROG and 17-OH PREG substrates is directly attributable to the juxtaposition of the 17-OH fragment to the heme iron.

Spin state populations for these five samples were estimated using a previously determined relative rR scattering cross-sections of the ν_3 modes for the low spin and high spin forms of cytochrome P450cam (CYP101) as described by Mak *et al.*[102] Using this procedure, the substrate-free enzyme is estimated to be 95% LS, whereas the HS populations of the PROG and PREG bound samples are calculated to be 94% and 95%, respectively. On the other hand, the HS components for the 17-OH PROG- and 17-OH PREG-bound samples are calculated to be 59% and 60%, respectively. These values are in good agreement with UV-Vis data reported in Chapter 3.2.2.

5.3.2 Low Frequency rR of the Ferric States of CYP17A1

The rR spectra in the low frequency region provide useful information not only on the binding of endogenous and exogenous heme axial ligands, but also on the disposition of the heme peripheral groups and out-of-plane distortions of the heme macrocycle as reflected by activation of out-of-plane heme modes. Shown in Figure 5.2, trace A, the spectrum of the substrate-free sample exhibits a single feature associated with the propionate bending mode (at 376 cm^{-1}) and a prominent vinyl bending mode at 424cm^{-1} along with a weak shoulder at 414 cm^{-1}. Significantly, addition of any of the four substrates (Figure 5.2, traces B through E) causes no significant change in the frequencies of the 376 cm^{-1} mode, indicating that hydrogen bonding to the propionate groups is not altered upon binding of any of these substrates. Inspection of the spectra in the vinyl bending mode region indicates that the prominent mode at 424 cm^{-1} is not altered. While there appears to be some difference in the weak lower frequency modes (414 vs 405 cm^{-1}), these bands are of low intensity. Though substrate binding to CYP17A1 causes minimal changes in bending modes of the peripheral

substituents, there is clear indication of activation of out-of-plane (OOP) modes at 318, ~490 cm^{-1} and 816 cm^{-1}, assigned to the γ_7, γ_{12} and γ_{11} modes.

Another type of important information gleaned from the low frequency region of the rR spectra is the status of the axial ligands. In the case of cytochromes P450, the ν(Fe-S) mode is effectively enhanced only in the case of the HS ferric form, using excitation near 350 nm. As shown in Figure 5.3, this mode is observed at 347 cm^{-1} for all substrates used, indicating that substrate structure does not affect the trans-axial linkage with the cysteine thiolate. Note that the apparent diminished intensities of the ν(Fe-S) modes in traces B and D are a result of normalization with the ν_7 mode which contains contributions from the substantial remnants of the LS forms in these two samples. The main point to be made here is that any changes in the modes associated with exogenous axial ligands, such as the CO fragment being studied here, are attributable to distal side interactions.

5.3.3 Ferrous CO adducts of ND:CYP17A1 and its interaction with substrates

The ferrous CO adducts of cytochrome P450 are typically exceptionally stable relative to the oxy-complex. As such, ferrous carbonmonoxy forms are often exploited to probe interactions of exogenous axial ligands with the distal heme pocket residues and substrates. Changes in frequencies and intensities of modes associated with the Fe-C-O fragment reflect the strength of the heme linkage with the proximal endogenous ligand and reliably report the steric and electronic influences presented by the distal pocket environment, such as electrostatic or H-bonding interactions with distal pocket amino acid residues, water molecules or substrates. The key vibrational modes of interest are the ν(Fe-C) stretching modes, usually observed in the region of 460-490 cm^{-1}, and the ν(C-O) stretching modes seen between 1920 and 1970 cm^{-1}. The δ(Fe-C-O) bending modes, very often quite weak and

difficult to detect, are seen in the range from 550-570 cm^{-1}. A well-documented negative linear correlation between the ν(C-O) and ν(Fe-C) stretching frequencies arises from back donation of the Fe(II) d_π electrons to π* orbitals of diatomic ligands, resulting in an increase of the Fe-C bond strength while weakening that of the C-O bond.[103, 104]

In the high frequency rR spectra of the CO-bound ferrous samples the ν_4 oxidation state marker band of all ferrous CO samples is located at 1370 cm^{-1}, while the spin state marker bands, the ν_3 and ν_2 modes, are seen at 1497 cm^{-1} and at 1585 cm^{-1}, respectively. All of these are characteristic for low spin 6-coordinate CO adducts in accordance with previously published data on other cytochromes P450. Figure 5.3.3 shows the low and high frequency rR spectra in the regions where the bands associated with the Fe-C-O fragment are observed. Binding of substrates to the ferrous CO form of Nanodisc-incorporated CYP17A1 has no impact on the heme core modes nor the orientation of vinyl groups, based on invariant frequencies in these regions. Once more in agreement with the data for the substrate-bound ferric forms, the structural differences among the 4 substrates have little or no impact on the heme structure or its interactions with active site residues.

In the spectrum of the substrate-free form (Figure 5.3.3, trace A, left panel) in the region near 450-500 cm^{-1}, there exists a broad envelope with components having maxima near 472 and 485 cm^{-1}. This low frequency spectrum of the substrate free form shows evidence for the presence of two Fe-C-O conformers, an interpretation that is confirmed by the observation of two ν(CO) stretching modes in the high frequency region (Figure 5.3.4, trace A, right panel). Based on relative intensities, the ν(C-O) mode at 1946 cm^{-1} corresponds to the 485 cm^{-1} ν(Fe-CO) mode and the 1957 cm^{-1} feature is correlated with the 472 cm^{-1} ν(Fe-CO) mode. This behavior is consistent with the well-documented inverse frequency

relationship.[103,104] The only remaining point to be noted about the general features of the spectral data is that the weak bands appearing in the 1840-1870 cm^{-1} region are well fit to combination modes involving the ν(Fe-C) and ν_4 modes. Thus, in the case of the substrate-free sample, two combination modes are seen near 1839 and 1852 cm^{-1} corresponding to (472 +1370 cm^{-1} and 485 +1370 cm^{-1}), while the combination modes for the other forms occur at frequencies about 15-25 cm^{-1} higher; e.g., 498 + 1370 cm^{-1} corresponds to 1867 cm^{-1} and 491 + 1370 cm^{-1} corresponds to the broadened combination band centered at 1858 cm^{-1}. It seems important to emphasize the point that the inherent intensities of the ν(C-O) modes are quite weak, being comparable to those of the observed combination bands.

Upon substrate binding substantial shifts in the internal modes of the Fe-C-O fragment occur. The samples with PROG and PREG (traces B and D) exhibit ν(C-O) modes at 1932 and 1940 cm^{-1}, respectively, and an identical frequency of 498 cm^{-1} for the ν(Fe-C) modes. As can be seen by inspection of the inverse-correlation plot shown in Figure 5.6, these points for the PROG and PREG substrates fall along the line generated by the data set for the CYP17A1 samples but at the same time, there is a clear indication that unexpected variations occur inasmuch as these two substrates show identical ν(Fe-C) modes but ν(C-O) frequencies that differ by 8 cm^{-1}. Large shifts of the internal modes of the Fe-C-O fragment upon substrate binding are characteristic for enzymes with relatively small and tightly organized heme pockets. Substrate associated shifts to higher frequency of the ν(Fe-CO) mode of 20-25 cm^{-1} magnitude were previously observed in bacterial cytochrome P450s such as cytochrome P450cam (CYP101).[98] On the other hand, in the case of mammalian drug-metabolizing cytochromes P450, which have larger and relatively flexible heme pockets, addition of substrates typically causes minimal changes in the ν(Fe-CO) frequency (<5 cm^{-}

^{1}).[104] The δ(Fe-C-O) bending modes for substrate-bound samples are upshifted 3 cm^{-1} relative to the bending mode seen in substrate-free sample, consistent with the higher frequencies of the Fe-CO stretching modes.

In the case of the 17α-hydroxy substrates, this alcohol is expected to occupy a position where interaction with the Fe-C-O fragment is possible, Spectral data obtained for the 17-OH PROG bound sample reveals only one ν(Fe-C) and one ν(C-O) mode, appearing at 491 and 1938 cm^{-1}, data that are consistent with a single Fe-C-O conformer. Additionally, the Fe-CO associated modes in the 17-OH PROG bound spectra are relatively narrow; an observation that likely reflects a highly directional H-bonding interaction between the Fe-CO fragment and the 17-OH PROG substrate that restricts the degree of fluctuation of the fragment within the pocket.

In contrast with the relatively straightforward spectral data obtained for 17-OH PROG, the spectra obtained in the presence of 17-OH PREG is extremely complex (Figure 5.4, trace E). In the low frequency region features are seen at 481 and 505 cm^{-1}, with indications of a weak shoulder near 522 cm^{-1}. Carefully conducted rR studies of the region containing the ν(C-O) stretching modes near 1900-1950 cm^{-1} shows only two features attributable to ν(C-O), occurring at 1953 and 1928 cm^{-1}; based on relative intensities the higher frequency mode correlates with the 481 cm^{-1} feature with the other forming the 505/1928 cm^{-1} pair. Given the fact that only two ν(C-O) modes were observed and the relative weakness of the shoulder near 522 cm^{-1}, spectra were also acquired using $^{13}C^{16}O$ in an effort to clarify the three-component envelope.

Figure 5.5, shows rR spectra of the $^{12}C^{16}O$ and $^{13}C^{16}O$ substituted ferrous CO adducts in the low frequency region and their difference pattern. The analysis of the difference trace

is not straightforward because the isotopic shifts are smaller than the bandwidths and as result the peaks seen in difference trace represent frequencies of the bands' wings instead of true frequencies of Fe-C stretches. In order to extract the frequencies of these unresolved Raman bands, the absolute spectra were deconvoluted in the region of 430-610 cm^{-1} with 50/50 % Gaussian/Lorenzian functions. The ν(Fe-C) envelope of $^{12}C^{16}O$ spectrum was best fitted with three bands at 481 cm^{-1}, 505 cm^{-1} and 522 cm^{-1}; attention was given mainly to the ν(Fe-CO) stretching modes, since the region containing the weak δ(Fe-C-O) bending modes, as well as several weak heme modes, was not sufficiently enhanced to properly treat by deconvolution. A similar procedure was applied to the $^{13}C^{16}O$ spectrum, where it was indicated that the Fe-C associated modes were shifted by 4 cm^{-1} to lower frequency (to 477 cm^{-1} and 501 cm^{-1}), while the band at 522 cm^{-1} did not shift. It is noted that a heme mode is observed at this frequency in the spectra obtained for many LS ferric forms and the other CO adducts studied here.

Even though binding of 17-OH PREG to CYP17A1 gives rise to a mixture of two Fe-C-O conformers, these data observed yield a well behaved inverse linear correlation, as shown in Figure 5.6. This figure shows a negative correlation between ν(Fe-C) and ν(CO) for the Nanodisc-incorporated CYP17A1 samples investigated here (red triangles and red line), along with similar plots for other previously reported bacterial and mammalian cytochromes P450 and for mammalian forms of nitric oxide synthase (NOS), another thiolate-ligated heme protein.

It is generally accepted that the slopes of such correlations are mainly determined by distal pocket polarity with positive electrostatic potentials often associated with H-bonding shifting the points to the upper left, reflecting enhanced Fe dπ → π(CO) back-bonding.[97] The

position of such plots along the vertical axis is influenced by the relative strength of the donor ability of the trans-axial heme ligand; e.g., the line for histidine-ligated heme is shifted vertically to higher regions than the lines shown in Figure 5.6

The thiolate in P450cam (CYP101) has three backbone hydrogen bonds from NH groups of nearby amides, yielding an Fe-S bond that exhibits a ν(Fe-S) mode near ~353 cm^{-1}.[51] The point in the lower right of the P450cam line represents the substrate-free state and the points to the higher left side are associated with the substrate-bound states. The CYP101 substrates bind close to the heme iron, expelling water molecules from the heme pocket and allowing the CO ligand to directly interact with H-bond donor groups, which involve the D251 and T252 residues and possibly their associated water molecules. These residues are postulated to play a central role in proton shuttle required for O-O cleavage. The NOS data fall on a separate ν(Fe-C)/ν(CO) line that is much higher than that for cytochrome P450cam, owing to weakening of the Fe-S linkage. The heme-bound thiolate of NOS has only two H-bonds from backbone NH groups, but more importantly, it is involved in one H-bond from a tryptophan sidechain residue. This stronger H-bond was shown to weaken the thiolate donor strength, as reflected in a lower ν(Fe-S) mode (~340 cm^{-1}) relative to CYP101. The result of this weakened trans-axial bond leads to increases in the opposing Fe-C bond strength (and ν(Fe-C) frequency), raising the back-bonding correlation line above that of cytochrome P450cam.

Considering all of the data acquired for CYP17A1, two aspects of the derived correlation need to be addressed. First, it is noted that the points generally fall above those obtained for the CYP101, an observation that is entirely consistent with the weakened Fe-S bond with its ν(Fe-S) mode near 347 cm^{-1} as documented in Figure 5.3.3, versus the value of

353 cm^{-1} reported for CYP101.[51] A secondary observation was that the slope of the derived line obtained for CYP17A1 is significantly greater than those for the other two sets of data. One cause of this might be that the number of data points is insufficient to generate a valid correlation; however, the number of points for the CYP101 and NOS plots is not substantially larger, yet both yield comparable slopes. Alternatively, it seems plausible that the active site structural organization for steroidogenic cytochromes P450 might be relatively more rigid, as reflected by the strict requirements for a high degree of stereospecificity attending the chemical conversions which they orchestrate. Thus, the presence of specific functional groups on the substrate periphery might introduce highly directional steric or electrostatic interactions that lead to a greater slope and/or deviations of some points (substrates) from the typical plots that are determined by more remote or delocalized electrostatic interactions.

Figure 5.5 also shows the dramatically different behavior exhibited for the sample containing 17-OH PREG. Like, 17-OH PROG it introduces into the heme distal pocket the highly polar R-O-H functionality, yet the spectral differences are quite remarkable with the 17-OH PREG substrate giving rise to two Fe-C-O conformers. One conformer (point 9) gives spectral parameters similar to those seen for the two substrate-free forms (points 8 and 10) and is comparably broad, most likely reflecting a conformer that is weakly H-bonded to distal pocket residues or loosely associated water molecules. A second conformer (point 14) is positioned nearer to the points observed for the other three substrates, but apparently experiencing a stronger electropositive field that the other three; i.e., lying higher to the left along the line.

5.4 Conclusions

The rR spectral data acquired here reveal key information regarding the substrate/protein interplay associated with the substrate binding event that can affect the active site structure and reactivity. Careful analysis of the data acquired for the ferric forms show that binding of substrate causes variable degrees of conversion from the low spin to high spin state, with the non-hydroxylated PROG and PREG yielding almost complete high spin form, while the two hydroxylated substrates give only about a 60% conversion to HS. This incomplete conversion is attributable to either a direct interaction of the 17-OH fragment with the heme iron or possibly retention of an active site water molecule that can interact with the heme iron. Another important result from the present study is that the acquired rR spectra of the ferric HS forms as well as the ferrous CO adducts, show that the heme structure and its interactions with the active site protein residues remain constant for all four substrates. The heme group in CYP17A1 is thus held in a relatively fixed orientation with respect to the associated protein, remaining unaffected by any differences in the molecular structure of these four substrates.

An important corollary to the above finding is that any differences encountered in enzymatic processing of these four substrates are most reasonably attributed to subtle alterations in the intermolecular interactions of a given substrate with the associated heme distal axial ligand. Within the natural enzymatic cycle this would include the bound dioxygen ligand, its reduced peroxo- or hydroperoxo- forms, or any species arising from an O-O bond cleavage process, such as the CpdI intermediate. In the present work, the exogenous heme ligand is CO and, the largest changes in the rR spectra acquired for the four different substrates occur for the internal modes of the Fe-C-O fragment. The most intriguing

observation is the appearance of *two* Fe-C-O conformers for the sample containing 17-OH PREG, because it might have been expected that the presence of the 17-OH fragment also would give rise to two conformers for the sample containing 17-OH PROG. The important functional implication of this is that the subtle difference between the –OH and -C=O substituents at the remote 3β-position of the 17-OH PREG and OH PROG, respectively, can significantly alter the interaction of the 17-OH group with the Fe-C-O fragment. While this difference in substrate disposition may lead only to disorder for the weakly H-bonding Fe-C-O fragment, its effects could be enhanced with more strongly H-bonding fragments, including Fe-O-O.

5.5 Tables and Figures

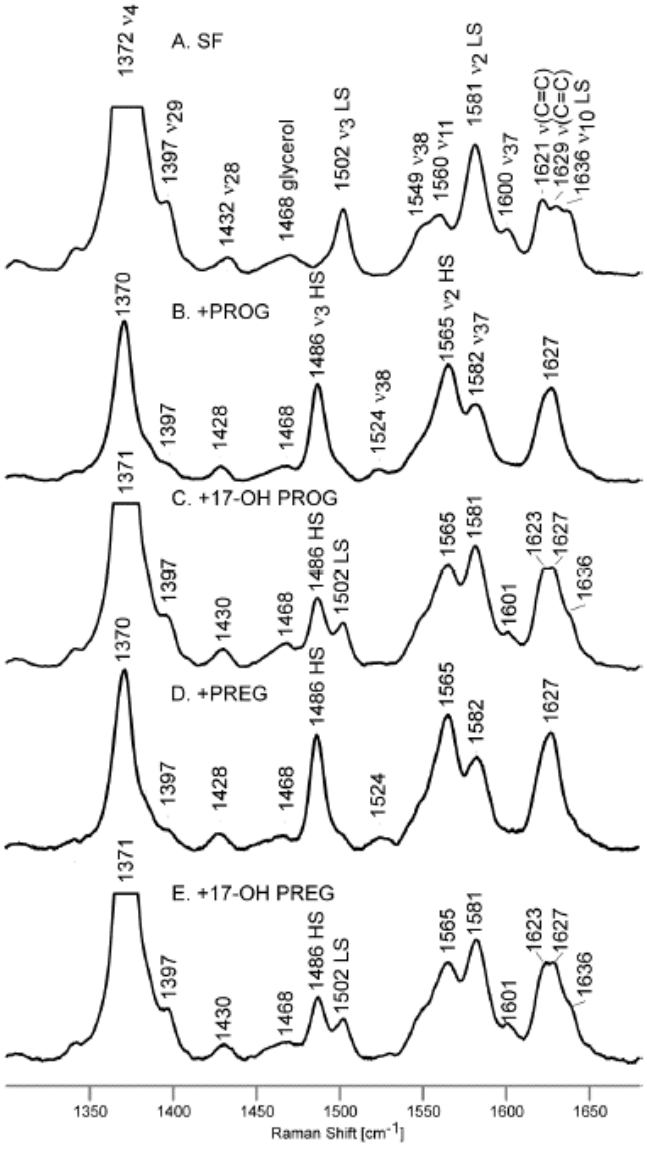

Figure 5.1: High Frequency Spectrum of Ferric CYP17A1

High frequency rR spectrum of ferric CYP17A1 in the substrate free state (A) and with PROG (B), 17-OH PROG (C), PREG (D), and 17-OH PREG (E).

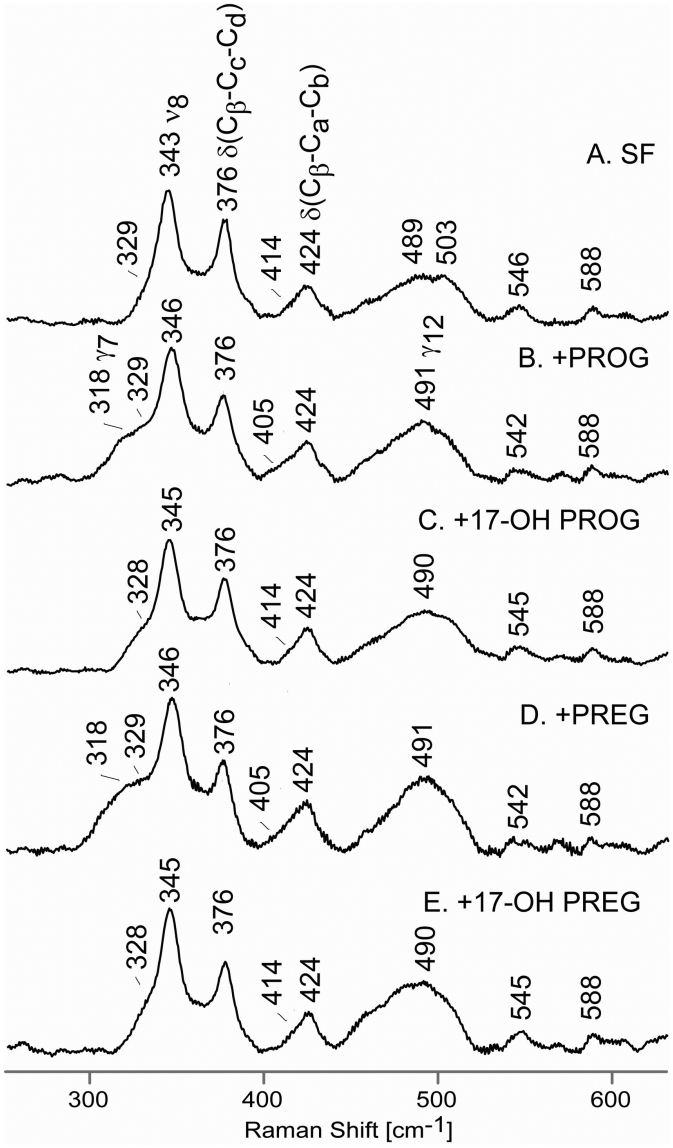

Figure 5.2: Low Frequency Spectra of Ferric CYP17A1

Low frequency rR data of ferric CYP17A1 in substrate free state (A) and with PROG (B), 17-OH PROG (C), PREG (D), and 17-OH PREG (E)

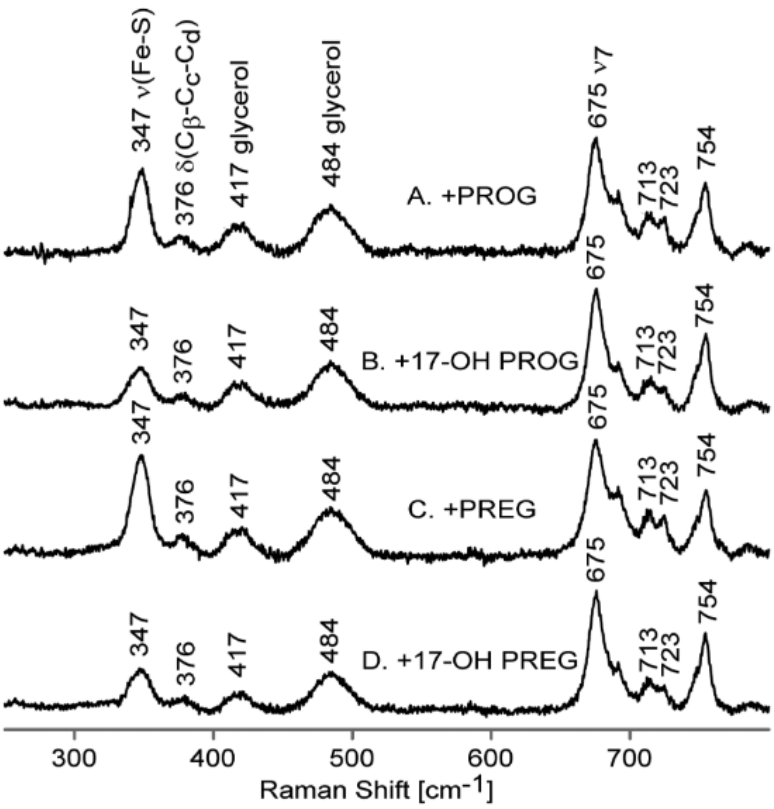

Figure 5.3: Low Frequency Spectra of CYP17A1 (356.7 nm Excitation)

Low frequency rR data of ferric CYP17A1 with PROG (A), 17-OH PROG (B), PREG (C), 17-OH PREG (D). Excitation laser lie was 356.7 nm.

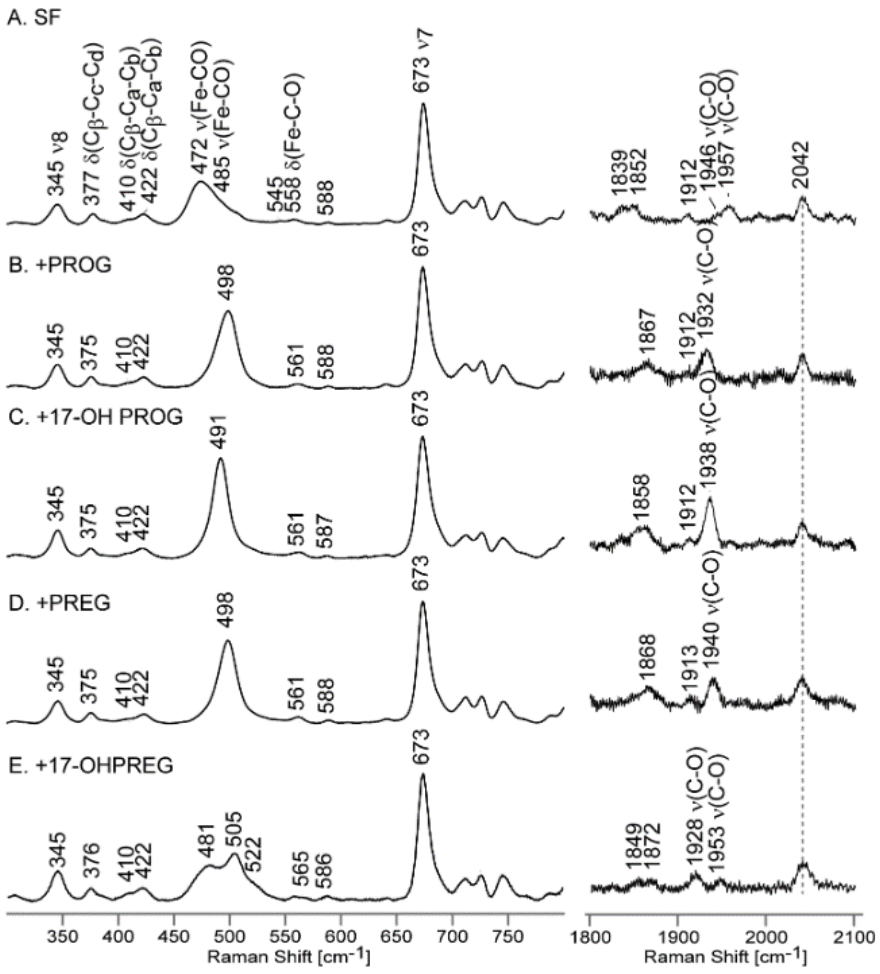

Figure 5.4: rR Spectra of Ferrous:CO States

Low frequency (left panel) and high frequency (right panel) rR data of ferrous CO adducts of substrate free CYP17A1 (A) and with PROG (B), 17-OH PROG (C), PREG (D), 17-OH PREG (E).

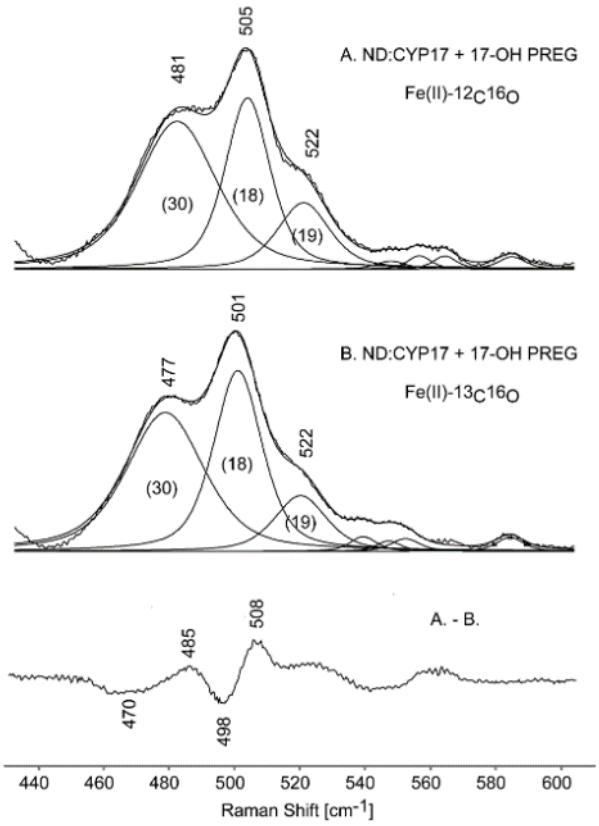

Figure 5.5: Deconvolution of 17-OH PREG Fe-CO Spectra

Experimental spectra of the ferrous 12C16O (A) and the 13C16O adducts of 17-OH PREG bound CYP17A1 (B) and their difference trace. The thin black lines represent fitted 50%/50% Gaussian/Lorenzian functions and their bandwidths are shown in parentheses.

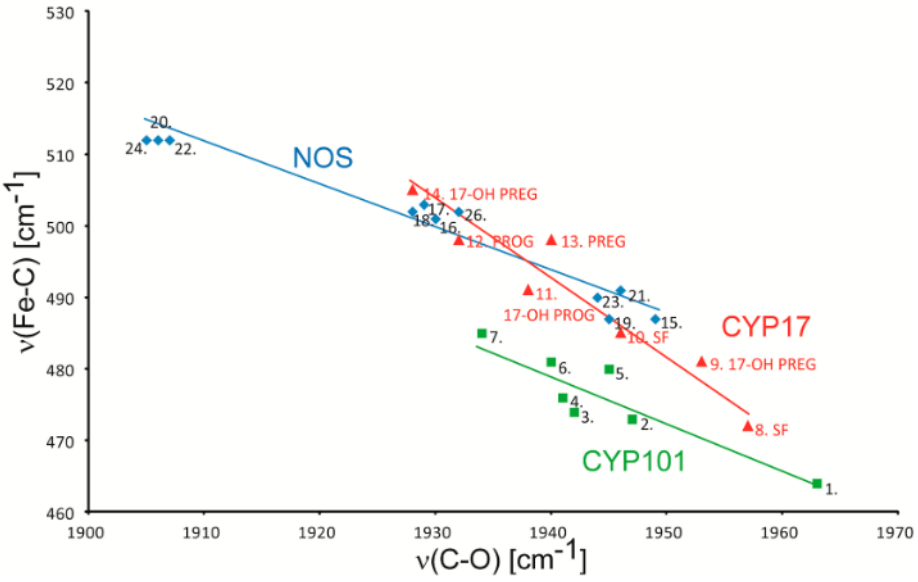

Figure 5.6: Backbonding Correlation Plot

Diagrams showing an inverse correlation for CYPs and NOSs. The numbers represent proteins listed in Supplemantary Table S1. The green squares show points for CYP101 (green line), the red triangles show points for CYP17A1 (red line), and the blue diamonds for mammalian NOS's (blue line).

Chapter 6: Resonance Raman Spectroscopy of the CYP17A1 Oxy Complex[4]

6.1 Introduction

Proceeding "forward" through the P450 catalytic cycle, this chapter documents experiments characterizing the disposition of the oxy-complex in the presence of PREG, PROG, 17-OH PREG, and 17-OH PROG. Formed by binding molecular oxygen to the ferrous heme iron, this is the last quasi-stable intermediate that can be generated with conventional methods and without the use of unnatural oxidants such as m-Chloroperoxybenzoic acid.[24] Interest in the nature of the oxy-complex is multifaceted as the bound dioxygen may be used as a probe of the heme environment in an analogous manner as CO in the preceding chapter. Importantly, while CO adopts a linear arrangement with respect to the heme plane, dioxygen exists in a "bent" orientation that persists following formation of the peroxo- species. Thus it is an easily accessible state expected to reliably report conditions likely to be encountered in later fleeting peroxo and hydroperoxo intermediates. Finally, the amenability of this intermediate to interrogation by rR spectroscopy is well documented in a variety of P450s.[105–109]

[4] Portions of this chapter were reprinted with permission from Gregory, M., Mak, P. J., Sligar, S. G. & Kincaid, J. R. Differential Hydrogen Bonding in Human CYP17A1 Dictates Hydroxylation versus Lyase Chemistry. *Angew. Chemie* **52,** 5342–5345 (2013)

As documented in previous chapters, the minute structural differences between the four native substrates of CYP17A1 substantially vary binding properties, turnover, and positioning of the substrate in the heme environment. In order to determine how these structural elements contribute to the highly regio- and sterospecific reactions catalyzed by CYP17A1 it is essential to evaluate the nature of the later intermediates in the catalytic cycle. Especially intriguing is the roughly 50-fold preference of CYP17A1 for 17-OH PREG versus 17-OH PROG in terms of k_{cat}/K_m that drives human steroidogenic flux almost exclusively through the 17-OH PREG to DHEA pathway.[43,71,110,111]

Clearly, elucidating the factors that control CYP17A1 product formation is crucial for understanding healthy and diseased human physiology. Additionally, particularly intense scrutiny of the C-C lyase activity of this enzyme has led to suggestions that nucleophilic attack on the C-20 carbonyl by the early peroxo-ferric intermediate is utilized in the formation of androgens.[50] Therefore it is important to define structural features of the active site that could control a branch point between O-O bond scission/CpdI formation verses a heme-oxygen intermediate reactive in C-C lyase chemistry.

An important step towards the understanding of androgen formation were the recently reported crystal structures by the Scott laboratory of human CYP17A1 in complex with promising anti-cancer drugs, and in the presence of native substrates.[92,93] These authors used molecular modeling to suggest that interactions of the 3β-alcohol or corresponding ketone fragments of PREG and PROG with active site H-bonding residues position the substrate in correct orientation with respect to the heme prosthetic group. However, they also express that active site topology might be altered by substrates and stressed the pressing need for further experimental work.

The Nanodisc system, which allows functional incorporation of these membrane proteins into homogenous and monodisperse membrane environments, yields exceptionally well-behaved ligand binding properties, as evidenced by clean conversions of spin-state populations, and also enhances stability of their dioxygen adducts.[58,112,113] Combination of this system with the power of resonance Raman (rR) spectroscopy to interrogate active site structure in heme proteins presents an especially effective approach to explore the complex mechanism of CYP17A1. Specifically addressed in this chapter is a particularly intriguing aspect of CYP17A1 structure, wherein the choice of substrate controls hydrogen bonding that defines the catalytic channel for product formation. Here it is shown that rR spectroscopy demonstrates that the single difference at the 3β position of 17-OH PREG and 17-OH PROG leads to unequivocal changes in active site H-bonding interactions with the key Fe-O-O fragment of enzymatic intermediates leading to alterations in electronic structure that then control substrate processing.

6.2 Materials and Methods

6.2.1 Protein Expression, Purification, and Nanodisc Incorporation of CYP17A1

CYP17A1 Nanodisc solutions in 100 mM KPi, pH 7.4 buffer containing 15% ultrapure glycerol were prepared as indicated in Chapter 2.2.3 and Chapter 2.3.

6.2.2 Preparation of Samples for rR Spectroscopy

Samples for rR spectroscopy contained 100 μM CYP17A1:Nanodiscs, 100 mM KPi, pH 7.4, 0.25 M NaCl, and 400 μM of progesterone or 17α-hydroxyprogesterone, pregnenolone, or

17α-hydroxypregnenolone (Sigma) added from ~8mM methanolic stocks. Solutions were prepared in either double distilled 30% (v/v) glycerol in H_2O or 30% (v/v) glycerol-d3 in D_2O, and were de-aerated under argon for 5 minutes. Samples were transferred to 5 mm NMR tubes (WG-5 Economy, Wilmad) and reduced under anaerobic conditions with a 1.5 fold molar excess of sodium dithionite in the presence of 2.5 μM methyl-viologen. Each sample reduced for 10 minutes at room temperature. Complete reduction was verified by UV-Vis spectroscopy. NMR tubes were then sealed and transferred under anaerobic conditions to a dry ice-ethanol bath held at -15 °C where they cooled for 1 minute. Oxy-ferrous complexes were formed by bubbling $^{16}O_2$ or $^{18}O_2$ for 5 seconds, followed by rapid freezing in liquid N_2. Samples were stored at 77K until analysis.

6.2.3 rR Measurements

The resonance Raman spectra of oxy complexes of Nanodisc-incorporated CYP17A1 were acquired using a Spex 1269 spectrometer equipped with a Spec-10 LN-cooled detector having 2048 pixels (Princeton Instruments, NJ). The data were measured with 413.1 nm excitation line from a Kr+ laser (Coherent Innova Sabre Ion Laser) The rR spectra were collected using back scattering (180°) geometry with the laser beam being focused by a cylindrical lens to form a line image on the sample. The laser power was adjusted to 1 mW or less. All measurements were performed at 77 K and total collection time was 4-5 hrs in the high frequency region and 6-7 hrs in the low frequency region. The slit width was set at 150 μm and the 1200 g/mm grating were used; the linear reciprocal dispersion is 0.655 nm/mm near 400nm, corresponding to 0.46 cm-1/pixel. The spectral resolution was determined to be 4.1 cm-1. The frozen samples were contained in 5 mm O.D. NMR tubes (WG-5 ECONOMY, Wilmad). The NMR tubes were positioned into a double-walled quartz low

temperature cell filled with liquid nitrogen. The sample tubes were spun to avoid local heating. Spectra were calibrated with fenchone (Sigma-Aldrich, WI) and processed with Grams/32 AI software (Galactic Industries, Salem, NH).

6.3 Results

Shown in Figure 6.1 are the rR spectra obtained for the $^{16}O_2$ adduct of PROG bound CYP17A1. In addition to structure-sensitive heme modes, including ν_4, ν_3, and ν_2, the key $\nu(^{16}O\text{-}^{16}O)$ mode is observed at 1140 cm^{-1} as confirmed by the uncluttered $^{16}O_2/^{18}O_2$ difference spectrum. The ν(Fe-O) stretching mode appears at 536 cm^{-1}, as documented in the $^{16}O_2/^{18}O_2$ difference trace (Figure 6.1, panel A). These frequencies for the Fe-O-O fragment are similar to those observed for other P450s wherein this fragment is weakly H-bonded to active site protein side chains. Significantly, spectra acquired for this sample in solutions prepared in D_2O (left and right traces in lower section of Figure 6.1, panel A) showed no difference for this non-H-bonding substrate.

Shown in Figure 6.1, panel B, top trace, is the rR spectrum obtained for the $^{16}O_2$ adduct of CYP17A1 harboring 17-OH PROG at its active site. The $\nu(^{16}O\text{-}^{16}O)$ mode now appears ~9 cm^{-1} lower at 1131 cm^{-1}. Expansion of this spectral region, and comparison with the spectrum acquired with $^{18}O_2$, shows that the Fe-O-O fragment exists in two conformations. The minor conformer is apparently identical to the form observed when PROG is bound. As is evidenced by a telltale 2 cm^{-1} shift to higher frequency in solutions prepared in D_2O[114], the dominant form, occurring at 1131 cm^{-1}, is H-bonded. It is most reasonable to attribute the clearly observed H-bonding interaction to the newly introduced C_{17}-OH(D) functionality.

Note that this lowering of the ν(O-O) mode is correlated with a corresponding 6 cm^{-1} *increase* in the frequency of the ν(Fe-O) band relative to its value in the PROG-bound enzyme.

Corresponding spectral data for the PREG and 17-17-OH PREG-bound enzymes are shown in Figure 6.2. As in the case of the PROG-bound enzyme, the ν(O-O) and ν(Fe-O) modes of the PREG-bound enzyme are observed near 1140 and 535 cm^{-1} and show no evidence for H-bonding. As shown in Figure 6.2, panel B, for the 17-OH PREG sample, the ν(O-O) mode is shifted down by only 5 cm^{-1} compared with its value for the PREG-bound form and exhibits a barely detectable upshift in deuterated solvents. However, the ν(Fe-O) is observed at 526 cm^{-1}, exhibiting a 9 cm^{-1} shift to *lower* frequency compared to the value observed for the Fe-O-O fragment present in the sample containing non-H-bonding PREG. The key finding in this case is the rather dramatic differences are observed when comparing the samples bound with 17-OH PROG and 17-OH PREG. Though introduction of the 17-OH group causes downshifts of the ν(O-O) modes for both 17-OH PROG and 17-OH PREG, the corresponding ν(Fe-O) modes shift in <u>opposite</u> directions: the 17-OH PROG yields a 6 cm^{-1} upshift for this mode while the 17-OH PREG shows a 9 cm^{-1} *downshift*. It is emphasized that rR spectra acquired with 356 nm excitation for all four samples showed no evidence for changes in the trans Fe-S bond strength, indicating that the effects on the Fe-O-O fragment arise mainly from distal side interactions, and consistent with results obtained in the ferric and ferrous:CO states in the previous chapter.

6.4 Conclusions

While the acquisition of reference data for the vibrational modes of dioxygen adducts of heme proteins has been hampered by their relative instability towards auto-oxidation, certain fundamental patterns have emerged.[97,114–117] Studies of globin mutants lead to the conclusion that H-bonds to the inner (proximal) O of the Fe-O-O fragment cause a decrease in the ν(Fe-O) mode, with similar but smaller effects on the ν(O-O)--a positive correlation.[118] On the other hand, H-bonding to the outer (terminal) O often leads to significant lowering of the ν(O-O) fragment in P450s and related enzymes.[114–117] Importantly, recent DFT calculations on histidine-ligated oxy complexes indicate that, other factors being held constant, H-bond donation to the proximal oxygen atom (O^P) causes both the ν(Fe-O) and the ν(O-O) modes to shift *in concert* to lower frequency, as a result of weakening of both bonds by withdrawing of electrons into the non-bonding sp^2 orbital on the O^P.[97] In contrast, H-bond donation to the terminal oxygen, O^T, results in a straightforward increase in back-bonding resulting in a *negative* correlation, wherein the ν(O-O) decreases while the ν(Fe-O) shows a corresponding increase in frequency. Therefore, collectively, the rR spectra presented in Figures 6.1 and 6.2 provide convincing evidence that the two hydroxylated substrates interact at *opposite ends* of the Fe-O-O fragment, as depicted in Figure 6.3, leading to crucial implications for CYP17A1 function. It is anticipated that these interactions dictate the preference for the hydroxylation and lyase pathways. Such H-bonding interactions with O^T are expected to promote O-O bond cleavage and CpdI formation, whereas the H---O^P interaction could prolong the lifetime of the ferric peroxo- intermediate that is suggested to be the active fragment in the lyase reaction. Alternatively, proximal hydrogen bonding could promote lyase chemistry by liberating the distal oxygen to initiate a nucleophilic attack on

the C20 carbonyl. Indeed, similar differences in O^T vs O^P H-bonding interactions have been invoked to explain differences in the nitric oxide synthase reaction; in the first cycle the arginine substrate is suggested to provide a H---O^T interaction and facilitate CpdI formation, whereas in the second cycle the hydroxylated substrate (NOHA) is believed to provide a H---O^P interaction and proceed through a peroxo- intermediate.[117,119,120]

In summary, this chapter reports use of Nanodisc incorporated human CYP17A1 to facilitate collection of high resolution rR spectra in order to define the active site hydrogen bonding, where the only significant change being compared is a difference between a 3β-OH group vs a corresponding ketone in natural CYP17A1 substrates. Significantly, this single difference at a relatively remote site is nevertheless sufficient to alter the H-bonding interactions with the critical Fe-O-O fragment in such a way as to dictate its predisposition towards one of two alternative reaction pathways. This conclusion has a structural basis: crystal structures with abiraterone acetate bound have shown that the OH- group on C3 of its pregnene nucleus forms a H-bond to the ketone on the side chain of Asn 202 that projects into the active site cavity. An additional H-bonding interaction with the amino group of this residue is noted with Glu 305 that presumably stabilizes this particular rotomer. Should this structure reflect a persistent state, it would be expected that substrate molecules with H-bond donor at the C3 position (PREG/17-OH PREG) would bind the enzyme in a state more favorable to lyase catalysis.

6.5 Tables and Figures

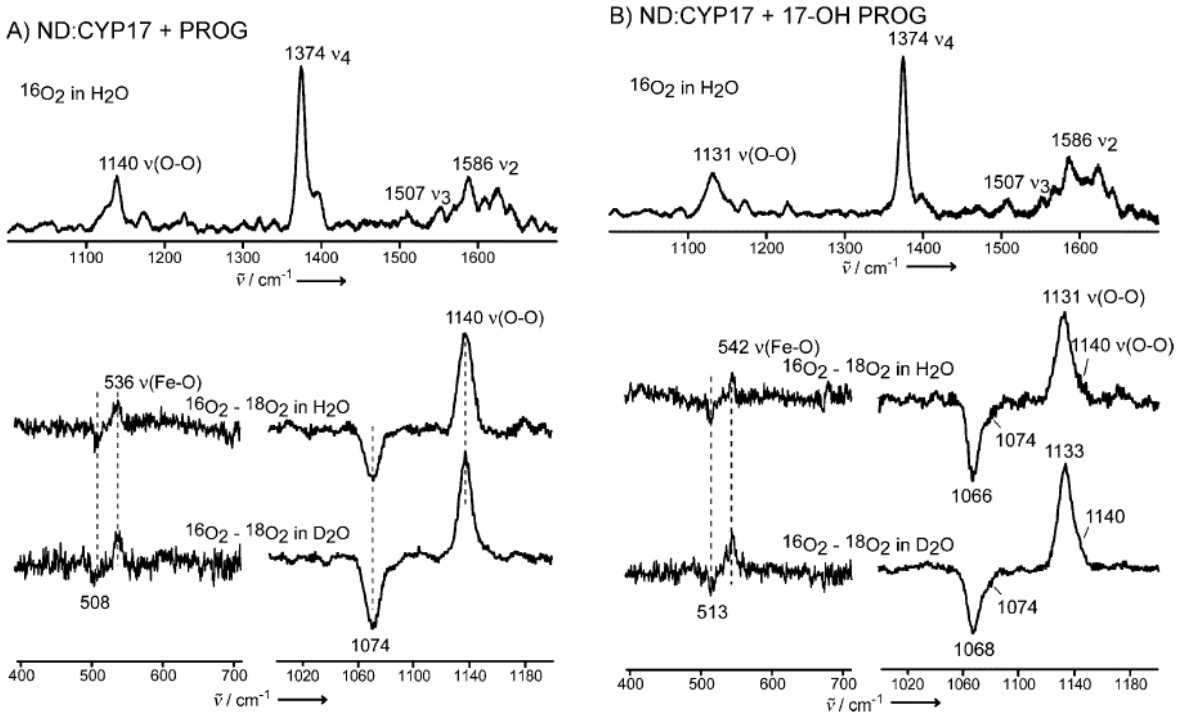

Figure 6.1: rR Spectra of PROG and 17-OH PROG CYP17A1 Oxy-Complex

The rR spectra of PROG (A) and 17-OH PROG (B) bound $^{16}O_2$ adducts (top). The bottom section of each panel shows $^{16}O_2$-$^{18}O_2$ difference plots in H_2O (upper) and D_2O (lower) buffers.

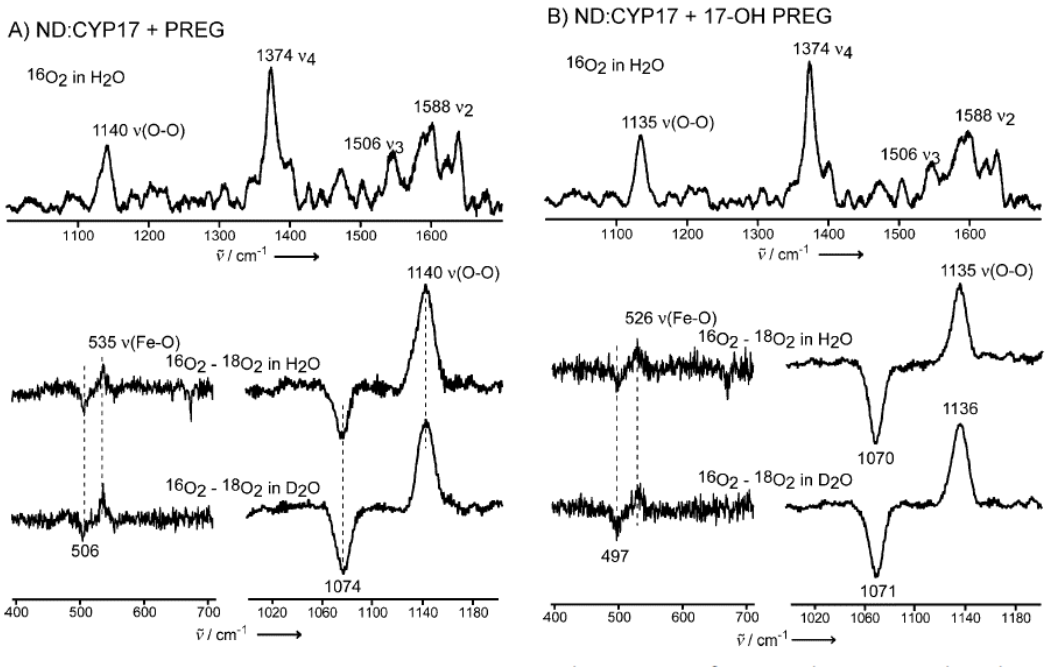

Figure 6.2: rR Spectra of PREG and 17-OH PREG CYP17A1 Oxy-Complex

The rR spectra of PREG and 17-OH PREG bound $^{16}O_2$ adducts of CYP17A1 Nanodiscs in H_2O buffer (panel A and B, respectively). The lower section of each panel shows $^{16}O_2$ – $^{18}O_2$ difference plots in H_2O (upper) and D_2O (lower) buffers.

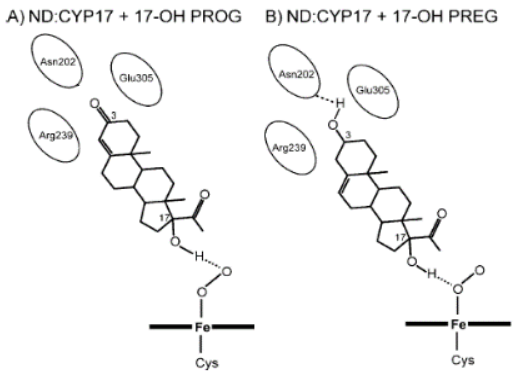

Figure 6.3: Proposed Model of Interaction with the Oxy-Complex

The human CYP17A1 protein-substrate interaction derived from these data, wherein Asn 202 and the C3 substituent dictate H-bonding to either the proximal or distal oxygen.

Chapter 7: Characterizing the Active Intermediate in Androgen Formation[5]

7.1 Introduction

Building on work detailed in the previous chapters, it is clear that investigation of the peroxo- states of CYP17A1 is crucial in defining the nature of the reactive intermediate responsible for carbon-carbon bond scission. This key branching point in human steroidogenesis has been at the center of a protracted debate regarding whether the traditional CpdI, or a peroxoanion is responsible for cleavage of the 17,20 bond, a reaction that is the first committed step in androgen formation. Early work by the Akhtar group first suggested that this reaction could be initiated by a nucleophilic attack on the C20 carbonyl yielding a peroxo-hemiacetal that could decay to androgen product and acetic acid via either homolytic or heterolytic scission of the dioxygen bond therein.[50] However, alternate suggestions of radical mechanisms involving CpdI have also been proposed.[53,121,122] Though strong support is given to the preceding hypothesis by the work documented earlier in this dissertation, characterization of an iron-ligated peroxo-hemiacetal would obviously represent a significant movement towards concluding this decades long debate.

Previously, the highly unstable intermediate species occurring after reduction of the oxy-complex have proved recalcitrant to laboratory analysis due to the inability to generate

---

[5] Portions of this chapter were reprinted with permission from Mak, P. J., Gregory, M. C., Denisov, I. G., Sligar, S. G. & Kincaid, J. R. Unveiling the crucial intermediates in androgen production. *Proc. Natl. Acad. Sci.* **112,** 15856–15861 (2015).

sufficiently large populations to observe experimentally. However, in recent years barriers to interrogating these species have been overcome: the peroxoanion, hydroperoxo-ferric, and CpdI intermediates have all been isolated and characterized in various P450 enzymes.[114,123] To a large extent, these advances have been made through use of cryoradiolytic reduction of oxy-ferrous P450 enzymes. In such a method, the oxy-complex is formed in a solution containing a significant percent of glycerol and subsequently trapped by immersion in liquid N_2. Electron input needed to form the peroxoanion is provided via radiolysis, typically gamma-rays from a ^{60}Co source, at cryogenic temperatures. At 77K, irradiation results in formation of various radiolytic products that are trapped in the frozen solvent matrix, and electrons which are free to reduce the oxy-complex and form the peroxoanion.[124–126]

This method was utilized to trap the peroxoanion using CYP17A1 Nanodiscs in the presence of saturating concentrations of the preferred substrates, PREG and 17-OH PREG. Both optical and resonance raman samples were measured at various temperatures as the resultant peroxoanion was permitted to thermally anneal.

7.2 Materials and Methods

7.2.1 Protein Expression, Purification and Nanodisc Incorporation of CYP17A1.

CYP17A1 Nanodisc solutions in 100 mM KPi, pH 7.4 buffer containing 15% ultrapure glycerol were prepared as indicated in Chapter 2.2.3 and Chapter 2.3.

7.2.2 Preparation of Samples for Raman Spectroscopy

The rR samples contained 280 μM ND/CYP17A1 in 100 mM potassium phosphate (pH 7.4), 250 mM sodium chloride, 30% (vol/vol) distilled glycerol, 6.24 μM methyl viologen, and either 450 μM PREG or 400 μM 17-OH PREG. Deuterated samples were prepared by exhaustive exchange into identical buffer adjusted to pD 7.4 [electrode calibrated by method of Glasoe and Long[85]] prepared with 100% D_2O and distilled glycerol-d_3. Ferric samples were then contained in 5-mm-OD NMR tubes (WG-5 ECONOMY; Wilmad) and de-aerated under argon for 5 min, followed by reduction under anaerobic conditions with a 1.5-fold molar excess of sodium dithionite. Each sample was then transferred to a dry ice-ethanol bath held at −15 °C, where it was cooled for 1 min. Oxy-ferrous complexes were formed by addition of $^{16}O_2$, $^{18}O_2$, or $^{16}O^{18}O$ scrambled oxygen) for 10 s, followed by rapid freezing in liquid N_2. Frozen samples containing oxy-ferrous CYP17A1 were subsequently radiolytically reduced to the peroxo-state by a 4-Mrad dose of gamma-rays in a Gammacell 200 Excel ^{60}Co source while immersed in liquid nitrogen as described previously

7.2.3 rR Measurements

Samples of irradiated oxy-ND/CYP17A1 were excited using a 441.6-nm line provided by a He-Cd laser (IK Series He-Cd laser; Kimmon Koha Co.), whereas the samples annealed to 190 K were measured with 406.7- and 413.1-nm excitation lines from a Kr^+ laser

(Coherent Innova Sabre Ion Laser). The rR spectra of all samples were measured using a Spex 1269 spectrometer equipped with Spec-10 LN-cooled detector (Princeton Instruments). The slit width was set at 150 μm, and the 1,200-g/mm grating was used; with this grating, the resultant spectral dispersion is 0.46 cm^{-1} per pixel. The laser power was kept at ~1 mW or less to minimize photodissociation. Moreover, to avoid laser-induced heating and protein degradation, the samples were contained in spinning NMR tubes (5-mm outside diameter, WG-5 ECONOMY; Wilmad). The 180° backscattering geometry was used for all measurements, and the laser beam was focused onto the sample using a cylindrical lens. The NMR tubes were positioned into a double-walled quartz low-temperature cell filled with liquid nitrogen. All measurements were done at 77 K, and total collection time was around 6 h for the irradiated samples and ~8–9 h for the annealed samples. Spectra were calibrated with fenchone (Sigma–Aldrich) and processed with GRAMS/32 AI software (Galactic Industries).

7.2.4 Preparation of Optical Samples and Collection of Optical Spectra

CYP17A1 Nanodiscs in 100 mM potassium phosphate (pH 7.4), 15% (vol/vol) glycerol, and 400 μM PREG or 17-OH PREG were anaerobically reduced with a 1.5-fold molar excess of sodium dithionite with the aid of methyl viologen at a 1:40 ratio of redox mediator to P450. Oxy-ferrous CYP17A1 was formed by rapid injection of this solution into 100 mM potassium phosphate (pH 7.4) buffer containing 67.5% (vol/vol) glycerol contained in a methacrylate cuvette and chilled to 243 K. After 25 s of vigorous mixing, the sample was rapidly cooled to 210 K, and then to 77 K at a rate of ~4 $K \cdot min^{-1}$. The final concentration of ND/CYP17A1 and glycerol was ~30 μM and 60% (vol/vol), respectively. Samples were irradiated as described in section 7.2.2 and then photobleached for 30 min under a 100-W

tungsten-halogen lamp behind a 450-nm long-pass filter while immersed in liquid nitrogen. Spectra were collected in a home-built optical cryostat[127] aligned within the beam path of a Cary 300 spectrophotometer as the temperature was increased linearly at a rate of ~1 $K \cdot min^{-1}$.

7.3 Results

7.3.1 Thermal Annealing of Optical Peroxo- Samples

Utilizing a home-built optical cryostat, samples were annealed from 77K to 190K at a roughly linear rate of ~1 K per minute. This ramp rate permits collection of a complete spectrum from 350 – 500 nm at 1 K intervals. A strong negative absorption band near 440 nm appeared in the difference spectrum of both PREG and 17-OH PREG, consistent with formation and disappearance of the peroxo-ferric intermediate throughout the course of annealing. In the case of the PREG sample, a steady loss of the peroxo- intermediate was accompanied by an associated increase in absorption at 417 nm, consistent with a transition to the low spin ferric state. Such a transition would be expected should a CpdI mechanism operate in this hydroxylation, as the transition to the hydroperoxo-ferric state is not optically distinguishable from the peroxoanion[128] and the rapid formation and decay of CpdI is unlikely to be observed. Unexpectedly, in an identical experiment conducted in the presence of 17-OH PREG decay of the peroxo-like Soret at 437 nm gave rise to an unidentified species with a Soret at 405 nm (Figure 7.1).

7.3.2 rR Spectra of the Irradiated Oxy Complexes

Next, rR spectroscopy was used to identify the key ν(O-O) and ν(Fe-O) vibrational modes of interest. Figure 7.2, panel A shows spectra obtained at 77K for the sample containing the PREG substrate. Two sets of oxygen isotope-sensitive ($^{16}O_2/^{18}O_2$) modes are clearly seen in the ^{16}O-^{18}O difference traces of the initial cryoreduced samples, signaling the presence of two intermediates. One species exhibited a ν(^{16}O-^{16}O) mode at 802 cm^{-1}, with its corresponding ν(^{18}O-^{18}O) at 764 cm^{-1} (Δ16/18 = 38 cm^{-1}), and a ν(Fe-^{16}O) at 554 cm^{-1}, with its ν(Fe-^{18}O) mode appearing at 527 cm^{-1} (Δ16/18 = 27 cm^{-1}). No observable shift in the difference trace generated for the samples prepared in D_2O was evident (bottom trace in Figure 7.2). The lack of an observable hydrogen/deuterium (H/D) shift is entirely consistent with assignment of this set of bands to a trapped ferric peroxo-intermediate of CYP17A1.

The second species in this sample exhibits a ν(^{16}O-^{16}O) mode at 775 cm^{-1}, which shifts to 738 cm^{-1} for the ^{18}O-analog (Δ16/18 = 37 cm^{-1}), and a corresponding ν(Fe-^{16}O) at 572 cm^{-1}, shifting to 545 cm^{-1} for $^{18}O_2$ (Δ16/18 = 27 cm^{-1}). These observed ^{16}O-^{18}O isotope shifts are consistent with the isotope shifts predicted for Fe-O-O or Fe-O-O-H fragments. Furthermore, the spectra of samples acquired in buffers prepared with D_2O reveal that the 775/572 cm^{-1} modes shift significantly, confirming the identification of this species as the hydroperoxo-derivative. Thus even at 77K a significant fraction of the peroxo-intermediate was converted to the hydroperoxo-intermediate. This finding is particularly important, revealing the fact that when PREG is bound to CYP17A1, the active site architecture is arranged to promote efficient proton transfer thereby facilitating formation of CpdI and the classical hydroxylation reaction required to produce 17-OH PREG.

In the case of the lyase substrate 17-OH PREG, which projects an alcohol into the heme environment that forms an H-bond with the proximal oxygen in the preceding oxy-complex, the initial product of cryoradiolysis at 77 K exhibits a $\nu(^{16}O\text{-}^{16}O)$ mode at 796 cm^{-1} ($\Delta 16/18$ = 38 cm^{-1}), and a corresponding $\nu(Fe\text{-}^{16}O)$ mode occurring at 546 cm^{-1} ($\Delta 16/18$ = 24 cm^{-1}). Furthermore, the observed modes are insensitive to the H/D exchange, confirming the identity of this species as a ferric peroxo-intermediate, but with a slightly different disposition than seen for the PREG-bound sample. In fact, as described in the previous chapter, the lowered $\nu(Fe\text{-}^{16}O)$ frequency of the peroxo-form of the 17-OH PREG sample (546 cm^{-1}), relative to the peroxo-form of the PREG-bound sample (554 cm^{-1}), suggests that an H-bonding interaction occurs between the hydroxyl group of the substrate and the proximal oxygen atom of the $Fe\text{-}O_p\text{-}O_t$ peroxo-fragment.

Next, the samples were subjected to stepwise thermal annealing: samples were immersed in a pentane bath cooled to 165 K where they incubated for one minute before being returned to 77 K. Subsequent rR analysis using 442-nm excitation (Figure 7.2, panel B) show that annealing of the PREG-bound sample resulted in clean conversion of the peroxo-intermediate to more of the hydroperoxo-intermediate involved in the hydroxylation pathway, with the extent of conversion estimated to be a factor of approximately twofold. Interestingly, similar annealing studies of the 17-OH PREG-bound sample provided no evidence for the appearance of any new $^{16}O/^{18}O$-sensitive bands (Figure 7.2, panel D). This outcome was not surprising, given that that the newly arising second intermediate has its Soret maximum near 405 nm, far from resonance with the 442-nm excitation line.

Indeed, rR spectral measurements on annealed samples, using the 406-nm excitation line from an available Krypton ion laser (Figure 7.3), yielded a new set of strongly enhanced bands appearing at 791 cm^{-1} ($^{16}O_2$ sample) and 749 cm^{-1} ($^{18}O_2$ sample). The lack of an observable shift for samples prepared in D_2O-based buffer confirms this species does not possess a bound hydroperoxo-fragment. This rR spectral result is entirely consistent with the increase of the 405-nm electronic absorption band over the same temperature excursion. It is noted that a control experiment conducted on the PREG-bound sample annealed to 190 K, using the same 406-nm excitation line, did not show any evidence for a feature appearing near 790 cm^{-1}, indicating that the peroxo-hemiacetal intermediate is encountered only with the 17-OH PREG substrate, but not with the PREG substrate.

7.4 Conclusions

Although the observation of this feature appearing at 791 cm^{-1} is obviously consistent with an intermediate with "peroxo-like" character, it must be noted that this vibrational frequency and $^{16}O/^{18}O$ isotopic shifts are close to what is expected for the ν(Fe = O) mode of a ferryl heme species. The frequencies of such ferryl species depend on the transaxial ligand and distal pocket interactions, with reported values ranging from 745 cm^{-1} up to about 800 cm^{-1} [129,130]. However, the assignment of this feature to a ferryl species was ruled out by experiments conducted with scrambled oxygen, a (1:2:1) mixture of $^{16}O_2/^{16}O^{18}O/^{18}O_2$. As seen in Figure 7.3, Inset, a distinctive difference pattern emerges when subtracting the spectrum of the $^{16}O_2$ sample from the spectrum of a sample prepared with scrambled dioxygen. If the 791 cm^{-1}/749 cm^{-1} pair arises from a ferryl species (generated through O-O

bond cleavage), a clean two-component difference pattern (Fe-^{16}O and Fe-^{18}O) would be observed in the trace shown. However, we clearly see a third band at 770 cm^{-1}, confirming the fact that the observed intermediate contains an intact O-O bond (i.e., ^{16}O-^{18}O), consistent with the proposed peroxo-hemiacetal species. Finally, it is also noted that the corresponding iron-oxygen ν(Fe-O) modes, expected to be seen for such a peroxo-like intermediate, are indeed seen as weak features appearing at 580 cm^{-1} ($^{16}O_2$) and 553 cm^{-1} ($^{18}O_2$). Collectively, these spectroscopic data establish the nature of the intermediate as the peroxo-hemiacetal.

Further support for this structural interpretation of the species trapped at 190 K is provided from previous studies of other iron-oxygen systems, whose structures are closely related to this intermediate (e.g., acylperoxo-adducts of heme- and nonheme proteins that possess an Fe-O-O peroxo-fragment linked to an oxidized carbon). Unlike the red-shifted Soret band at 435–440 nm characteristic for hydroperoxo-ferric intermediates in P450 enzymes[114,128], a blue-shifted Soret maximum at 405 nm is consistent with the bands seen for an acylperoxo-species derived from metachloroperoxybenzoic acid (mCPBA)[131], as well as other substituted peroxybenzoic acids. In all cases, the Soret maximum varies from 413 nm for the mCPBA adduct down to 409 nm with electron-donating groups, such as the p-methoxy analog. Thus, the 405-nm maximum for the peroxo-hemiacetal intermediate, with its relatively less electrophilic carbon atom compared with the acylperoxo-species, is not unexpected. A more convincing argument for the validity of the assigned structure can be made by noting that Que and coworkers[132] have recently isolated and spectroscopically characterized an acylperoxo-derivative of a nonheme iron protein, reporting a value of 792 cm^{-1} for the frequency of the ν(O-O) mode, a virtually identical value (791 cm^{-1}) to the value we observe for the assigned peroxo-hemiacetal intermediate.

The results presented here, obtained through the combined application of Nanodisc technology, cryoreduction, and rR and optical spectroscopies, reveal that owing to the highly directional H-bonding interaction between the hydroxyl group of 17-OH PREG and the proximal oxygen of the ferric peroxo-anion, this intermediate is poised for attack on the C20 carbon atom of the substrate. Furthermore, methodical application of the structure-sensitive rR technique, using judicious isotopic labeling strategies, provides convincing evidence that the resulting crucial intermediate of this lyase reaction is indeed the previously proposed peroxo-hemiacetal derivative. Therefore, a new view P450 catalytic cycle has emerged when CYP17A1 is employed in C-C bond scission (Figure 7.4).

7.5 Tables and Figures

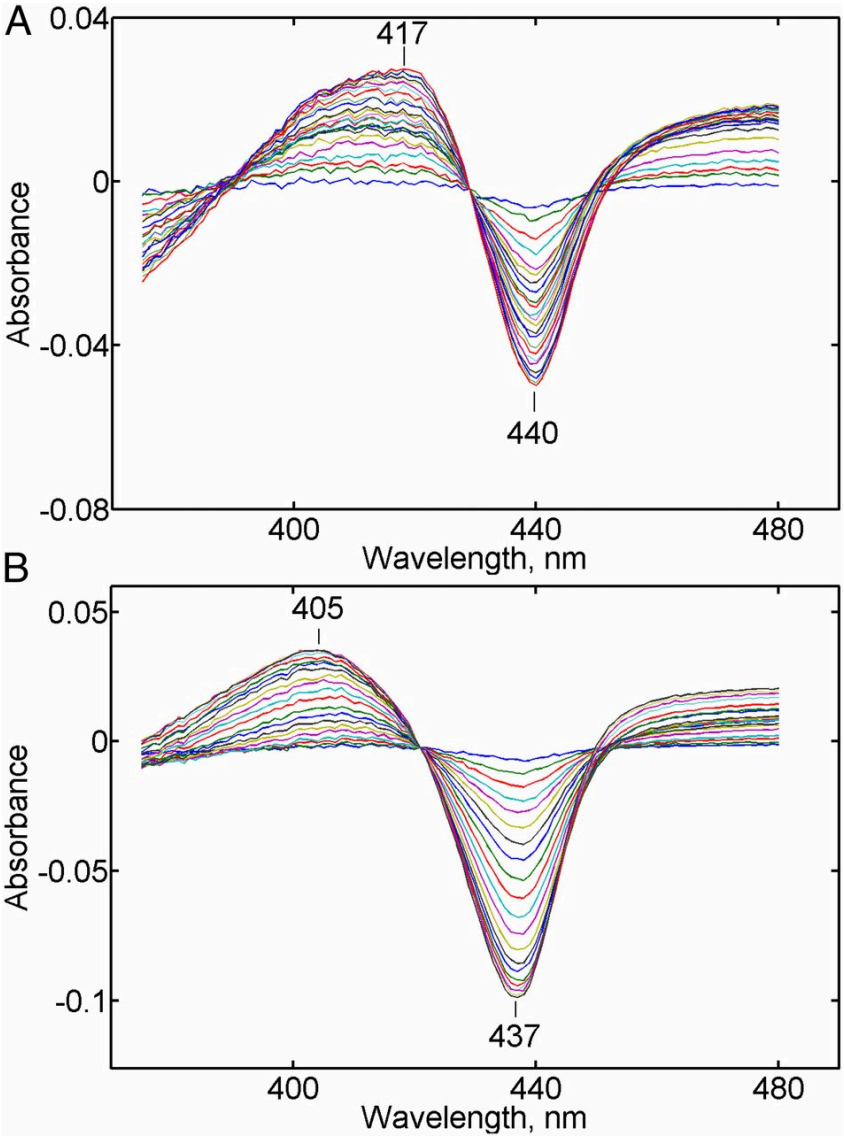

Figure 7.1: Thermal Annealing of Optical Samples

Thermal annealing of peroxo-ferric intermediates monitored by optical absorption spectroscopy in CYP17A1 with PREG (*A*) and 17-OH PREG (*B*).

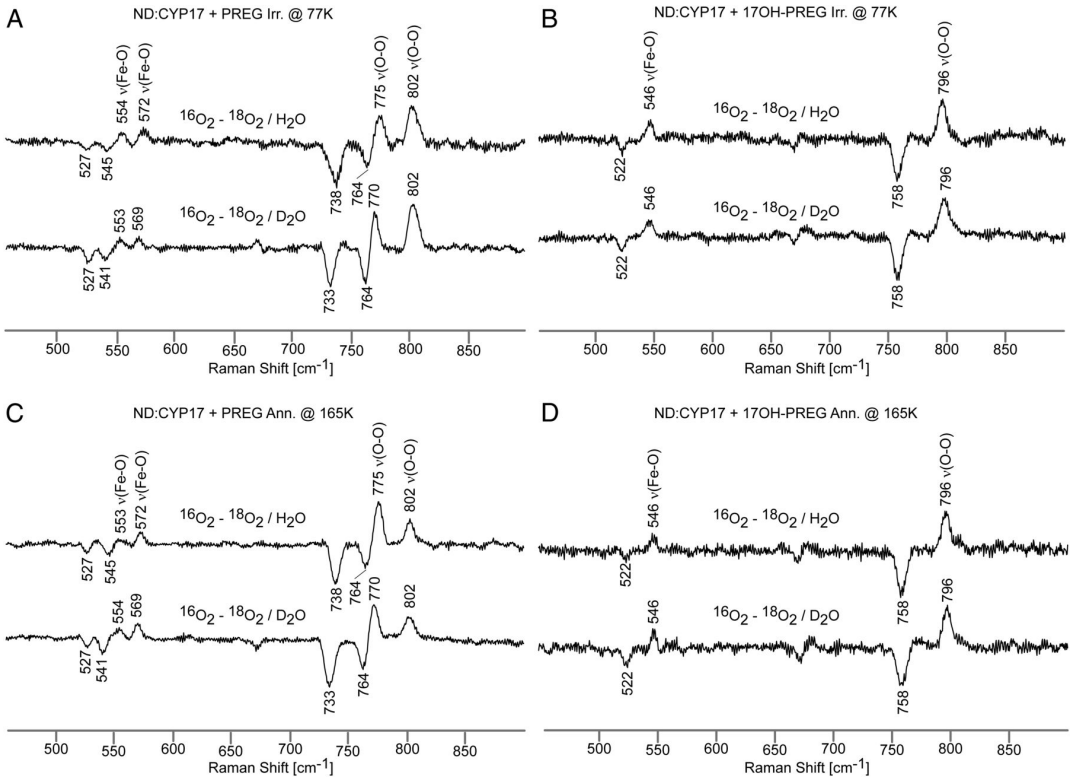

Figure 7.2: rR Spectral Data for Irradiated Dioxygen Adducts

The rR $^{16}O_2$-$^{18}O_2$ difference traces in H_2O and D_2O buffers of irradiated oxy-CYP17A1 samples (before annealing) with PREG (*A*) and 17-OH PREG (*B*) and corresponding samples after annealing to 165 K (*C*) and (*D*) are shown. Excitation was at 442 nm.

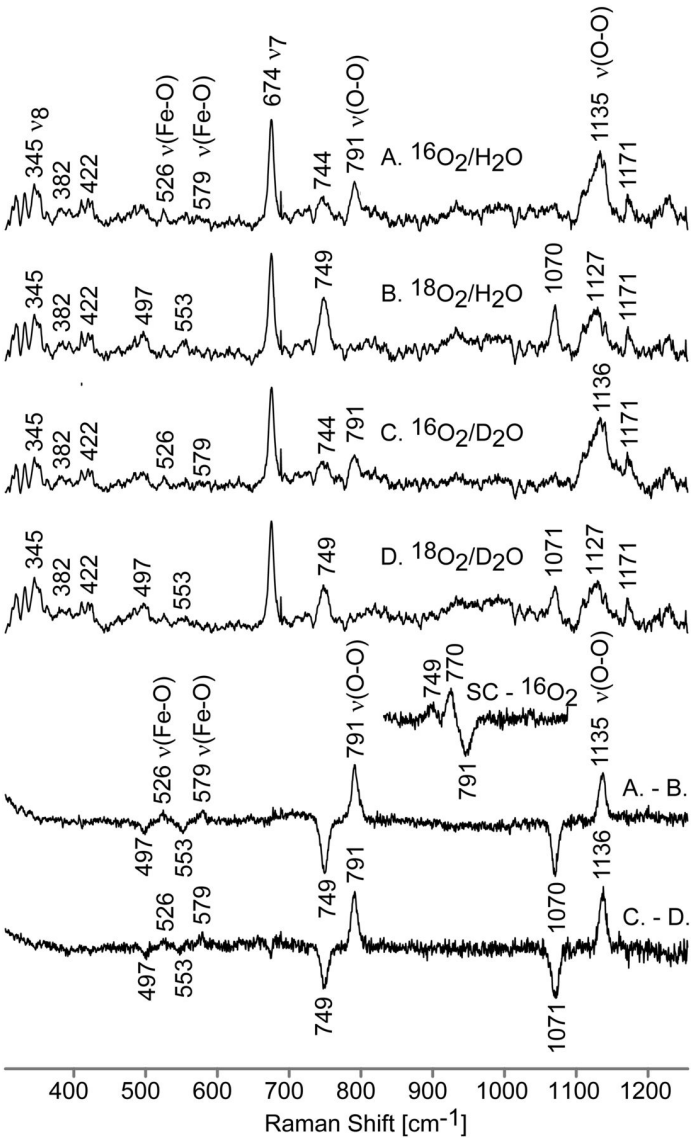

Figure 7.3: rR Spectral Data Annealed to 190K (405nm Excitation)

rR spectral data for irradiated dioxygen adducts of CYP17A1 samples with 17-OH PREG annealed at 190 K. $^{16}O_2/H_2O$ (*A*), $^{18}O_2/H_2O$ (*B*), $^{16}O_2/D_2O$ (*C*), $^{18}O_2/D_2O$ (*D*), and their $^{16}O_2$-$^{18}O_2$ difference traces. (*D*, *Inset*) Difference trace of scrambled oxygen (SC) and the $^{16}O_2$ spectrum. Spectra were measured with a 406-nm excitation line at 77 K,

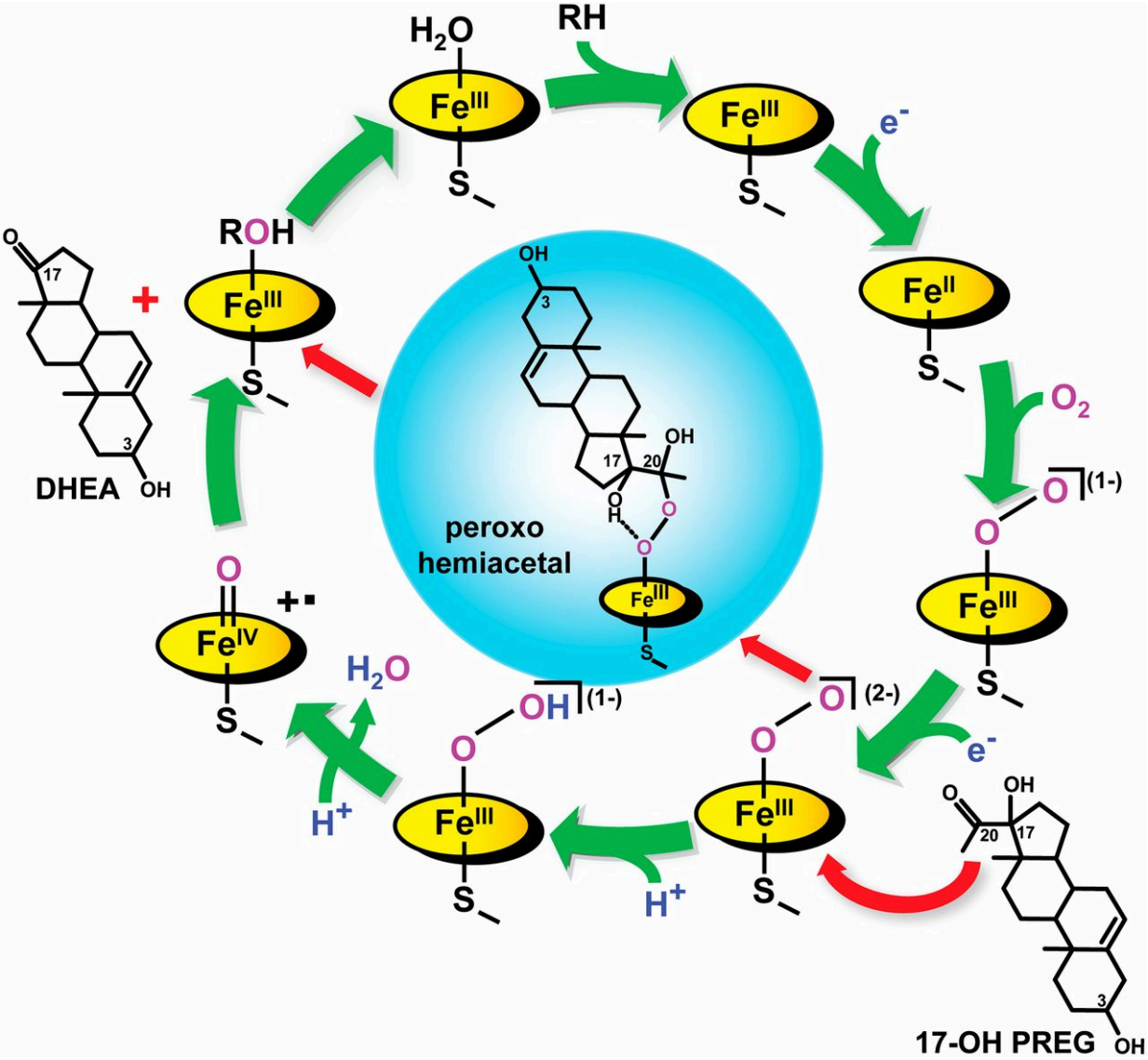

Figure 7.4: P450 Catalytic Cycle Operating in Androgen Formation

Cytochrome P450 enzymatic cycle and formation of a peroxo-hemiacetal intermediate.

Chapter 8: Conclusions

CYP17A1 is a steroidogenic enzyme of critical importance, occupying the "crossroad" that exists at the center of the human steroidogenic pathway. While its 17α-hydroxy products are essential in a variety of biological processes, the latter 17,20 carbon-carbon bond scission catalyzed by this enzyme is particularly intriguing. Though subsequent biological transformations are required to generate the potent androgen receptor agonists testosterone and dihidrotestosterone, the upstream lyase activity of CYP17A1 is rate limiting in their production. The importance of these androgens in the proliferation of prostate cancer coupled with disappointing performance of 5α-reductase inhibitors and androgen receptor antagonists has driven an explosion of interest in this enzyme, most notably resulting in the development and approval of its inhibitor Abiraterone acetate.

Multiple laboratories publicly claim to be engaged in developing lyase-specific or mechanism based inhibitors, but until recently the catalytic processes driving these targeted reactions have remained veiled, representing a significant impediment to the development of next-generation CYP17A1 inhibitors for the treatment of prostate cancer. Recent advances such as the development of the Nanodisc system and cryoradiolytic reduction of P450s have finally permitted removal of the shroud that obfuscated the identity and properties of the key transient intermediates that drive lyase catalysis. This dissertation has described the joint effort of the Sligar and Kincaid laboratories to employ these emerging technologies to define the structural and chemical features of CYP17A1 and its substrates that drive this enzyme's chimeric reactivity.

Beginning with a synthetic gene, expression and purification conditions were devised that were able to yield ~10 mg/L of highly purified, full-length CYP17A1 in a detergent solubilized form. Appropriate parameters for the incorporation of this enzyme into ~10 nm Nanodiscs were identified and a protocol was developed that consistently produced homogeneous CYP17A1:Nanodiscs in high yield. Using the resultant preparation, the substrate binding properties of PREG, PROG, 17-OH PREG, and 17-OH PROG were characterized by both UV-Visible and resonance Raman spectroscopy. Both PREG and PROG bound tightly with < 100 nM spectral dissociation constants and their binding resulted in complete transition to the high spin 5 coordinate state. 17-OH PREG and 17-OH PROG bind the enzyme less tightly, with ~ 1μM K_s values and result in only a 60% transition to the HS form, likely due to interaction of the 17α-OH group with the heme iron atom. Notably, binding of these substrates does not have any significant impact on heme peripheral substituents or the υ(Fe-S) mode, indicating that important structural elements are likely derived from interactions between the substrate and bound exogenous ligands.

Steady state turnover experiments were conducted in the absence and presence of cyt b5, and confirmed previous reports of the stimulatory effect of this protein. Turning towards identification of the reactive intermediate responsible for lyase catalysis, the T306A mutant, with an impaired proton delivery shuttle, was studied. This mutant showed the expected large extent of uncoupling when catalyzing hydroxylation chemistry, but androgen formation from both 17-OH PREG and 17-OH PROG was largely unimpaired, suggesting that lyase chemistry may operate to some extent without the involvement of protons. Next, KSIE data was collected for the steady state turnover of both PREG and 17-OH PREG. PREG hydroxylation exhibited the expected k_H/k_D of 1.3, however in the hase of DHEA formation a

large (0.39) inverse isotope effect was observed, again suggesting involvement of a ferric-peroxoanion.

In another experiment, the oxy-complex of CYP17A1 was probed by rR spectroscopy in the presence of all four native substrates. Both PREG and PROG were found not to interact with the iron-ligated dioxygen adduct, an unsurprising result given the lack of perturbation noted of the ferrous-CO complex in previous studies. On the contrary, 17-OH PREG and 17-OH PROG were found to form hydrogen bonds with the oxy complex. Surprisingly, while 17-OH PROG was found to form a H-bond with the terminal oxygen, the preferred substrate for lyase catalysis, 17-OH PREG, was found to form an H-bond with the proximal oxygen in this intermediate state. Owing to the roughly 50-fold preference of CYP17A1 for this substrate, this result suggests that the directionality of this H-bond may be an important factor in driving peroxoanion mediated androgen formation by properly orienting the substrate C20 carbonyl for a nucleophilic attack.

Finally, the oxy form of CYP17A1 in the presence of PREG and 17-OH PREG was cryoreduced to form the peroxo species. In the case of PREG, even at 77K a significant fraction of the ferric-peroxoanion had already transitioned to the hydroperoxo- state. Conversely, even after annealing to 165K the 17-OH PREG sample still contained only the ferric-peroxoanion. Excitation with a 405 nm laser line after further annealing to 190K permitted observation of a previously unknown, H/D insensitive, mode at 791 cm^{-1} consistent with a bound peroxo-hemiacetal.

CpdI mediated C-C bond scission is wholly incompatible with the presence of an inverse KSIE, the appearance of a peroxo-hemiacetal, and normal catalysis by and enzyme with an impaired proton shuttle. Thus, these results, taken as a whole, clearly define the

peroxoanion as the reactive intermediate in androgen formation when 17-OH PREG is a substrate. Furthermore, these findings highlight the potential for innovation when collaborative endeavors integrate biology, biochemistry, biophysics, and nanotechnology.

Appendix

DNA sequence of CYP17A1 Gene

ATGGCTCTGTTATTAGCAGTTTTCCTGCTGACCTTGGCATACCTGTTCTGGCCGAAACGTCGTTGTCCAGGTGCTAA
GTATCCGAAAAGCCTGCTGAGCTTGCCGCTGGTGGGTAGCTTGCCTTTTCTGCCGCGTCACGGTCACATGCACAACA
ACTTTTTCAAGCTGCAGAAGAAATACGGCCCGATCTATTCCGTGCGTATGGGCACCAAAACCACCGTTATCGTTGGC
CACCATCAACTGGCTAAAGAGGTTCTGATTAAGAAAGGTAAGGACTTCAGCGGTCGTCCGCAAATGGCGACGCTGGA
CATCGCGTCCAACAACCGTAAAGGCATCGCGTTTGCGGACTCGGGTGCGCACTGGCAATTGCATCGTCGTCTGGCTA
TGGCTACCTTCGCCCTGTTTAAGGATGGCGATCAGAAACTGGAGAAAATCATTTGCCAAGAGATTAGCACGCTGTGC
GACATGCTGGCAACCCATAATGGTCAATCTATTGACATTTCGTTCCCGGTCTTTGTGGCGGTCACCAATGTGATCAG
CCTGATTTGCTTTAACACGAGCTATAAGAATGGCGACCCGGAACTGAATGTGATCCAGAATTACAATGAGGGCATCA
TCGACAATTTGAGCAAGGACAGCCTGGTGGACTTGGTCCCGTGGCTGAAGATTTTCCCTAACAAAACGCTGGAAAAG
TTGAAAAGCCATGTCAAAATCCGCAACGATCTGCTGAACAAGATCCTGGAAAACTACAAAGAGAAGTTTCGTTCTGA
CAGCATTACTAACATGCTGGACACGCTGATGCAGGCCAAAATGAATTCCGATAACGGCAATGCAGGTCCGGATCAGG
ACAGCGAGCTGTTGAGCGATAACCATATCCTGACCACGATCGGTGACATCTTTGGTGCCGGTGTGGAAACCACCACC
AGCGTCGTCAAATGGACGCTGGCGTTCCTGCTGCACAATCCGCAGGTGAAAAAGAAGTTGTACGAAGAAATTGATCA
GAACGTTGGCTTCAGCCGCACCCCGACGATTTCCGACCGCAATCGTCTGCTGCTGTTGGAGGCAACGATTCGCGAAG
TTCTGCGCCTGCGTCCGGTTGCGCCAATGCTGATCCCGCACAAAGCCAATGTTGATTCTAGCATCGGTGAGTTCGCA
GTTGACAAAGGTACTGAAGTCATTATCAACTTGTGGGCCCTGCATCACAATGAGAAAGAGTGGCACCAGCCGGACCA
ATTCATGCCGGAACGTTTCCTGAACCCGGCAGGTACTCAACTGATCAGCCCGAGCGTGTCTTACCTGCCGTTCGGTG
CCGGTCCGCGCTCCTGTATTGGTGAGATCCTGGCGCGTCAGGAGCTGTTCCTGATTATGGCGTGGCTGCTGCAACGT
TTTGATCTGGAGGTGCCAGATGATGGCCAGCTGCCTTCCCTGGAAGGCATTCCGAAGGTTGTTTTCCTGATTGATAG
CTTTAAGGTCAAGATTAAGGTGCGCCAAGCGTGGCGCGAGGCACAAGCGGAAGGTAGCACCCACCACCATCACCACT
AA

References

1. Klingenberg, M. Pigments of rat liver microsomes. *Arch. Biochem. Biophys.* **75,** 376–386 (1958).
2. Klingenberg, M. The dragging emergence of the P450 cytochrome. *Arch. Biochem. Biophys.* **412,** 2 (2003).
3. Estabrook, R. W. A passion for P450s (rememberances of the early history of research on cytochrome P450). *Drug Metab. Dispos.* **31,** 1461–1473 (2003).
4. Omura, T. Recollection of the early years of the research on cytochrome P450. *Proc. Jpn. Acad. Ser. B. Phys. Biol. Sci.* **87,** 617–40 (2011).
5. Omura, T. & Sato, R. The Carbon Monoxide-Binding Pigment of Liver Microsomes. I. Evidence for Its Hemoprotein Nature. *J Biol Chem* **239,** 2370–2378 (1964).
6. De Montellano, P. R. O. *Cytochrome P450: Structure, mechanism, and biochemistry: Cytochrome P450: Structure, Mechanism, and Biochemistry: Third edition* (Kluwer Academic, 2005).
7. Katagiri, M., Ganguli, B. N. & Gunsalus, I. C. A soluble cytochrome P-450 functional in methylene hydroxylation. *J. Biol. Chem.* **243,** 3543–3546 (1968).
8. Guengerich, F. P. Common and uncommon cytochrome P450 reactions related to metabolism and chemical toxicity. *Chem. Res. Toxicol.* **14,** 611–650 (2001).
9. Nelson, D. R. *et al.* P450 superfamily: update on new sequences, gene mapping, accession numbers and nomenclature. *Pharmacogenetics* **6,** 1–42 (1996).
10. Werck-reichhart, D. & Feyereisen, R. Protein family review Cytochromes P450 : a success story. *Genome* 1–9 (2000).

11. Vidakovic, M., Sligar, S. G., Li, H. & Poulos, T. L. Understanding the role of the essential Asp251 in cytochrome P450cam using site-directed mutagenesis, crystallography, and kinetic solvent isotope effect. *Biochemistry* **37,** 9211–9219 (1998).

12. Hays, A. M. A. *et al.* Conformational states of cytochrome P450cam revealed by trapping of synthetic molecular wires. *J. Mol. Biol.* **344,** 455–469 (2004).

13. Sakaguchi, M. & Omura, T. in *Medicinal Implications in Cytochrome P-450 Catalyzed Biotransformations* (eds. Ruckpaul, K. & Rein, H.) (1993).

14. De Lemos-Chiarandini, C., Frey, A. B., Sabatini, D. D. & Kreibich, G. Determination of the membrane topology of the phenobarbital-inducible rat liver cytochrome P-450 isoenzyme PB-4 using site-specific antibodies. *J. Cell Biol.* **104,** 209–219 (1987).

15. Williams, P. A., Cosme, J., Sridhar, V., Johnson, E. F. & McRee, D. E. Microsomal cytochrome P450 2C5: Comparison to microbial P450s and unique features. *J. Inorg. Biochem.* **81,** 183–190 (2000).

16. Strushkevich, N. *et al.* Structural basis for pregnenolone biosynthesis by the mitochondrial monooxygenase system. *Proc. Natl. Acad. Sci. U. S. A.* **108,** 10139–43 (2011).

17. Akhtar, M. K., Kelly, S. L. & Kaderbhai, M. A. Cytochrome b(5) modulation of 17{alpha} hydroxylase and 17-20 lyase (CYP17) activities in steroidogenesis. *J Endocrinol* **187,** 267–274 (2005).

18. Das, A. & Sligar, S. G. Modulation of the cytochrome P450 reductase redox potential by the phospholipid bilayer. *Biochemistry* **48,** 12104–12112 (2009).

19. Bayburt, T. H. & Sligar, S. G. Single-molecule height measurements on microsomal cytochrome P450 in nanometer-scale phospholipid bilayer disks. *Proc Natl Acad Sci*

U S A **99,** 6725–6730 (2002).

20. Iyanagi, T. Structure and function of NADPH-cytochrome P450 reductase and nitric oxide synthase reductase domain. *Biochem. Biophys. Res. Commun.* **338,** 520–528 (2005).
21. Iyanagi, T. & Mason, H. S. Properties of hepatic reduced nicotinamide adenine dinucleotide phosphate-cytochrome c reductase. *Biochemistry* **12,** 2297–308 (1973).
22. Iyanagi, T., Makino, N. & Mason, H. S. Redox properties of the reduced nicotinamide adenine dinucleotide phosphate-cytochrome P-450 and reduced nicotinamide adenine dinucleotide-cytochrome b 5 reductases. *Biochemistry* **13,** 1701–1710 (1974).
23. Ewen, K. M., Ringle, M. & Bernhardt, R. Adrenodoxin-A versatile ferredoxin. *IUBMB Life* **64,** 506–512 (2012).
24. Denisov, I. G., Makris, T. M., Sligar, S. G. & Schlichting, I. Structure and chemistry of cytochrome P450. *Chem Rev* **105,** 2253–2277 (2005).
25. Momenteau, M. & Reed, C. a. Synthetic Heme-Dioxygen Complexes. *Chem. Rev.* **94,** 659–698 (1994).
26. Dolphin, D. & Felton, R. H. The Significance of Porphyrin Pi Cation Radicals. **197,** 26–32 (1973).
27. Rittle, J. & Green, M. T. Cytochrome P450 compound I: capture, characterization, and C-H bond activation kinetics. *Science (80-.).* **330,** 933–937 (2010).
28. Groves, J. T., McClusky, G. A., White, R. E. & Coon, M. J. Aliphatic hydroxylation by highly purified liver microsomal cytochrome P-450. Evidence for a carbon radical intermediate. *Biochem. Biophys. Res. Commun.* **81,** 154–160 (1978).

29. Ghayee, H. K. & Auchus, R. J. Basic concepts and recent developments in human steroid hormone biosynthesis. *Rev Endocr Metab Disord* **8,** 289–300 (2007).

30. Miller, W. L. & Auchus, R. J. The Molecular Biology, Biochemistry, and Physiology of Human Steroidogenesis and Its Disorders. *Endocr Rev* **32,** 81–151

31. Gwynne, J. T. & Strauss, J. F. The role of lipoproteins in steroidogenesis and cholesterol metabolism in steroidogenic glands. *Endocr. Rev.* **3,** 299–329 (1982).

32. Soccio, R. E. & Breslow, J. L. StAR-related lipid transfer (START) proteins: Mediators of intracellular lipid metabolism. *J. Biol. Chem.* **278,** 22183–22186 (2003).

33. Mast, N. *et al.* Structural basis for three-step sequential catalysis by the cholesterol side chain cleavage enzyme CYP11A1. *J Biol Chem* **286,** 5607–5613 (2011).

34. Akhtar, M., Wright, J. N. & Lee-Robichaud, P. A review of mechanistic studies on aromatase (CYP19) and 17alpha-hydroxylase-17,20-lyase (CYP17). *J Steroid Biochem Mol Biol* **125,** 2–12 (2011).

35. Lorence, M. C., Murry, B. A., Trantf, J. M. & Mason, I. A. N. Human 3B-Hydroxysteroid Dehydrogenase/Isomerase from Placenta: Expression in Nonsteroidogenic Cells of a Protein that Catalyzes the Dehydrogenation/Isomerization of C21 and C19 Steroids. **126,** 2493–2498 (1990).

36. Kominami, S., Ochi, H., Kobayashi, Y. & Takemori, S. Studies on the Steroid Hydroxylation System in Adrenal Cortex. (1980).

37. Fardella, C. & Miller, W. Molecular Biology of Mineralcorticoid Metabolism. *Annu. Rev. Nutr.* 433–70 (1996).

38. Mornet, E., Dupont, J., Vitek, A. & White, P. C. Characterization of two genes encoding human steroid 11B-hydroxylase (P-450(11B). *J. Biol. Chem.* **264,** 20961–20967

(1989).

39. Luu-The, V., Belanger, A. & Labrie, F. Androgen biosynthetic pathways in the human prostate. *Best Pr. Res Clin Endocrinol Metab* **22,** 207–221 (2008).

40. Kominami, S., Inoue, S., Higuchi, A. & Takemori, S. Steroidogenesis in liposomal system containing adrenal microsomal cytochrome P-450 electron transfer components. *Biochim Biophys Acta* **985,** 293–299 (1989).

41. Chen, Y., Sawyers, C. L. & Scher, H. I. Targeting the androgen receptor pathway in prostate cancer. *Curr Opin Pharmacol* **8,** 440–448 (2008).

42. Huggins, C. & Hodges, C. V. Studies on prostatic cancer I. The effect of castration, of estrogen and of androgen injection on serum phosphatases in metastatic carcinoma of the prostate (Reprinted from Cancer Res, vol 1, pg 293-297, 1941). *J. Urol.* **167,** 948–951 (2002).

43. Lee-Robichaud, P., Wright, J. N., Akhtar, M. E. & Akhtar, M. Modulation of the activity of human 17 alpha-hydroxylase-17,20-lyase (CYP17) by cytochrome b5: endocrinological and mechanistic implications. *Biochem J* **308 (Pt 3,** 901–908 (1995).

44. Miller, W. L. & Auchus, R. J. Role of cytochrome b5 in the 17,20-lyase activity of P450c17. *J Clin Endocrinol Metab* **85,** 1346 (2000).

45. Naffin-Olivos, J. L. & Auchus, R. J. Human cytochrome b5 requires residues E48 and E49 to stimulate the 17,20-lyase activity of cytochrome P450c17. *Biochemistry* **45,** 755–762 (2006).

46. Pandey, A. V & Miller, W. L. Regulation of 17,20 lyase activity by cytochrome b5 and by serine phosphorylation of P450c17. *J Biol Chem* **280,** 13265–13271 (2005).

47. Wang, Y. H., Tee, M. K. & Miller, W. L. Human cytochrome p450c17: single step purification and phosphorylation of serine 258 by protein kinase a. *Endocrinology* **151,** 1677–1684

48. Zhang, L. H., Rodriguez, H., Ohno, S. & Miller, W. L. Serine phosphorylation of human P450c17 increases 17,20-lyase activity: implications for adrenarche and the polycystic ovary syndrome. *Proc Natl Acad Sci U S A* **92,** 10619–10623 (1995).

49. Miller, W. L., Auchus, R. J. & Geller, D. H. The regulation of 17,20 lyase activity. *Steroids* **62,** 133–142 (1997).

50. Akhtar, M., Corina, D. L., Miller, S. L., Shyadehi, A. Z. & Wright, J. N. Incorporation of Label from O-18(2) into Acetate during Side-Chain Cleavage Catalyzed by Cytochrome P-450(17-Alpha) (17-Alpha-Hydroxylase-17,20-Lyase). *J. Chem. Soc. Trans. 1* 263–267 (1994).

51. Lee-Robichaud, P., Shyadehi, A. Z., Wright, J. N., Akhtar, M. E. & Akhtar, M. Mechanistic kinship between hydroxylation and desaturation reactions: acyl-carbon bond cleavage promoted by pig and human CYP17. *Biochemistry* **34,** 14104–14113 (1995).

52. Akhtar, M., Lee-Robichaud, P., Akhtar, M. E. & Wright, J. N. The impact of aromatase mechanism on other P450s. *J Steroid Biochem Mol Biol* **61,** 127–132 (1997).

53. Akhtar, M., Corina, D., Miller, S., Shyadehi, A. Z. & Wright, J. N. Mechanism of the acyl-carbon cleavage and related reactions catalyzed by multifunctional P-450s: studies on cytochrome P-450(17)alpha. *Biochemistry* **33,** 4410–4418 (1994).

54. Yoshimoto, F. K., Gonzalez, E., Auchus, R. J. & Guengerich, F. P. Mechanism of 17α,20-Lyase and New Hydroxylation Reactions of Human Cytochrome P450 17A1. 18O-Labeling and Oxygen Surrogate Evidence for a Role of a Perferryl Oxygen. *J. Biol.*

Chem. jbc.M116.732966 (2016). doi:10.1074/jbc.M116.732966

55. Barnes, H. Maximizing Expression of Eukaryotic Cytochrome P450s in Escherichia coli. *Methods Enzymol.* **272,** 3–14 (1996).

56. Barnes, H., Arlotto, M. & Waterman, M. Expression and enzymatic activity of recombinant cytochrome P450 17α-hydroxylase in Escherichia coli. *Proc. Natl. Acad. Sci.* **88,** 5597–5601 (1991).

57. Imai, T., Globerman, H., Gertner, J., Kagawa, N. & Waterman, M. Expression and Purification of Functional Human 17α-Hydroxylase/17,20-Lyase (P450c17) in Escherichia coli. *J. Biol. Chem.* **268,** 19681–19689 (1993).

58. Mak, P. J., Denisov, I. G., Grinkova, Y. V, Sligar, S. G. & Kincaid, J. R. Defining CYP3A4 structural responses to substrate binding. Raman spectroscopic studies of a nanodisc-incorporated mammalian cytochrome P450. *J Am Chem Soc* **133,** 1357–1366 (2011).

59. Bayburt, T. H. & Sligar, S. G. Membrane protein assembly into Nanodiscs. *Febs Lett.* **584,** 1721–1727 (2010).

60. Ritchie, T. K., Grinkova, Y.V., Bayburt, T.H., Denisov, I.G., Zolnerciks, J.K., Atkins, W.M. & Sligar, S.G. Reconstitution of membrane proteins in phospholipid bilayer nanodiscs. *Methods Enzym.* **464,** 211–231 (2009).

61. Luthra, A., Gregory, M., Grinkova, Y. V, Denisov, I. G. & Sligar, S. G. Nanodiscs in the studies of membrane-bound cytochrome P450 enzymes. *Methods Mol. Biol.* **987,** 115–127 (2013).

62. Luthra, A., Denisov, I. G. & Sligar, S. G. Spectroscopic features of cytochrome P450 reaction intermediates. *Arch Biochem Biophys* **507,** 26–35 (2011).

63. Shen, A. L., Porter, T. D., Wilson, T. E. & Kasper, C. B. Structural analysis of the FMN binding domain of NADPH-cytochrome P-450 oxidoreductase by site-directed mutagenesis. *J Biol Chem* **264,** 7584–7589 (1989).

64. Mulrooney, S. B. & Waskell, L. High-level expression in Escherichia coli and purification of the membrane-bound form of cytochrome b(5). *Protein Expr Purif* **19,** 173–178 (2000).

65. Bayburt, T. H., Grinkova, Y. V. & Sligar, S. G. Self-Assembly of Discoidal Phospholipid Bilayer Nanoparticles with Membrane Scaffold Proteins. *Nano Lett.* **2,** 853–856 (2002).

66. Lin, Z. & Rye, H. S. GroEL-mediated protein folding: making the impossible, possible. *Crit Rev Biochem Mol Biol* **41,** 211–239 (2006).

67. Thain, A., Gaston, K., Jenkins, O. & Clarke, A. R. A method for the separation of GST fusion proteins from co-purifying GroEL. *Trends Genet* **12,** 209–210 (1996).

68. Rohman, M. & Harrison-Lavoie, K. J. Separation of copurifying GroEL from glutathione-S-transferase fusion proteins. *Protein Expr Purif* **20,** 45–47 (2000).

69. Okuda, H. *et al.* Effects of divalent cations on encapsulation and release in the GroEL-assisted folding. *Biometals* **20,** 903–910 (2007).

70. Asby, D. J., Arlt, W. & Hanley, N. A. The adrenal cortex and sexual differentiation during early human development. *Rev Endocr Metab Disord* **10,** 43–49 (2009).

71. Auchus, R. J., Lee, T. C. & Miller, W. L. Cytochrome b5 augments the 17,20-lyase activity of human P450c17 without direct electron transfer. *J Biol Chem* **273,** 3158–3165 (1998).

72. Kuhnvelten, W. N., Bunse, T. & Forster, M. E. C. Enzyme Kinetic and Inhibition

Analyses of Cytochrome-P450xvii, a Protein with a Bifunctional Catalytic Site - Quantification of Effective Substrate Concentrations at the Active-Site and Their Significance for Intrinsic Control of the Hydroxylase Lyase Rea. *J. Biol. Chem.* **266,** 6291–6301 (1991).

73. Raag, R., Martinis, S. a, Sligar, S. G. & Poulos, T. L. Crystal structure of the cytochrome P-450CAM active site mutant Thr252Ala. *Biochemistry* **30,** 11420–11429 (1991).

74. Imai, Y. & Nakamura, M. Point mutations at threonine-301 modify substrate specificity of rabbit liver microsomal cytochromes P-450 (laurate-hydroxylase and testosterone 16 alpha-hydroxylase). *Biochem. Biophys. Res. Commun.* **158,** 717–722 (1989).

75. Nagano, S. & Poulos, T. L. Crystallographic study on the dioxygen complex of wild-type and mutant cytochrome P450cam: Implications for the dioxygen activation mechanism. *J. Biol. Chem.* **280,** 31659–31663 (2005).

76. Schlichting, I. *et al.* The catalytic pathway of cytochrome P450cam at atomic resolution. *Science (80).* **287,** 1615–1622 (2000).

77. Clark, J. P. *et al.* The role of Thr268 and Phe393 in cytochrome P450 BM3. *J. Inorg. Biochem.* **100,** 1075–1090 (2006).

78. Vatsis, K. P. & Coon, M. J. Ipso-substitution by cytochrome P450 with conversion of p-hydroxybenzene derivatives to hydroquinone: evidence for hydroperoxo-iron as the active oxygen species. *Arch. Biochem. Biophys.* **397,** 119–29 (2002).

79. Blobaum, A. L., Kent, U. M., Alworth, W. L. & Hollenberg, P. F. Novel reversible inactivation of cytochrome P450 2E1 T303A by tert-butyl acetylene: the role of threonine 303 in proton delivery to the active site of cytochrome P450 2E1. *J.*

Pharmacol. Exp. Ther. **310,** 281–290 (2004).

80. Keizers, P. H. J. *et al.* Role of the conserved threonine 309 in mechanism of oxidation by cytochrome P450 2D6. *Biochem. Biophys. Res. Commun.* **338,** 1065–1074 (2005).

81. Hiroya, K., Ishigooka, M., Shimizu, T. & Hatano, M. Role of Glu318 and Thr319 in the catalytic effects function of cytochrome P450d (P4501A2): effects of mutations on the methanol hydroxylation. *FASEB J.* **6,** 749–751 (1992).

82. Martinis, S. A., Atkins, W. M., Stayton, P. S. & Sligar, S. G. A Conserved Residue of Cytochrome P-450 Is Involved in Heme-Oxygen Stability and Activation. *J. Am. Chem. Soc.* 9252–9253 (1989).

83. Venkatasubban, K. S. & Schowen, R. L. The Proton Inventory Technique. *Crc Crit. Rev. Biochem.* **17,** 1–44 (1984).

84. Brock, B. J. & Waterman, M. R. Biochemical differences between rat and human cytochrome P450c17 support the different steroidogenic needs of these two species. *Biochemistry* **38,** 1598–1606 (1999).

85. Glasoe, P. K. & Long, F. A. Use of Glass Electrodes to Measure Acidities in Deuterium Oxide. *J. Phys. Chem.* **64,** 188–190 (1960).

86. Liu, Y. Reaction Intermediates and Single Turnover Rate Constants for the Oxidation of Heme by Human Heme Oxygenase-1. *J. Biol. Chem.* **275,** 5297–5307 (2000).

87. Batabyal, D., Li, H. & Poulos, T. L. Synergistic effects of mutations in cytochrome P450cam designed to mimic CYP101D1. *Biochemistry* **52,** 5396–5402 (2013).

88. Aikens, J. & Sligar, S. G. Kinetic Solvent Isotope Effects during Oxygen Activation by Cytochrome P-450cam. *J. Am. Chem. Soc.* **116,** 1143–1144 (1994).

89. Frantom, P. A. & Fitzpatrick, P. F. Uncoupled Forms of Tyrosine Hydroxylase Unmask

Kinetic Isotope Effects on Chemical Steps. *J. Am. Chem. Soc.* **125,** 16190–16191 (2003).

90. Massey, V. Activation of Molecular Oxygen by Flavins and Flavoproteins. *J. Biol. Chem.* **269,** 22459–22462 (1994).

91. Twilfer, H., Sandfort, G. & Bernhardt, F. H. Substrate and solvent isotope effects on the fate of the active oxygen species in substrate-modulated reactions of putidamonooxin. *Eur. J. Biochem.* **267,** 5926–5934 (2000).

92. DeVore, N. M. & Scott, E. E. Structures of cytochrome P450 17A1 with prostate cancer drugs abiraterone and TOK-001. *Nature* **482,** 116–119 (2012).

93. Petrunak, E. M., DeVore, N. M., Porubsky, P. R. & Scott, E. E. Structures of human steroidogenic cytochrome P450 17A1 with substrates. *J. Biol. Chem.* **289,** 32952–32964 (2014).

94. Kitagawa, T. & Mizutani, Y. Resonance Raman spectra of highly oxidized metalloporphyrins and heme proteins. *Coord. Chem. Rev.* **135-136,** 685–735 (1994).

95. Lee, K. B. *et al.* Influence of heme vinyl- and carboxylate-protein contacts on structure and redox properties of bovine cytochrome b5. *J. Am. Chem. Soc.* **113,** 3576–3583 (1991).

96. Reid, L. S., Mauk, M. R. & Mauk, A. G. Role of heme propionate groups in cytochrome b5 electron transfer. *J. Am. Chem. Soc.* **106,** 2182–2185 (1984).

97. Spiro, T., Soldatova, A. & Balakrishnan, G. CO, NO and O2 as Vibrational Probes of Heme Protein Interactions. *Coord. Chem. Rev.* **257,** 511–527 (2013).

98. Wells, A. V, Li, P., Champion, P. M., Martinis, S. A. & Sligar, S. G. Resonance Raman investigations of Escherichia coli-expressed Pseudomonas putida cytochrome P450

and P420. *Biochemistry* **31,** 4384–4393 (1992).

99. Champion, P. M., Gunsalus, I. & Wagnerib, C. Resonance Raman Investigations of Cytochrome P 450cam from Pseudomonas putida. *J. Am. Chem. Soc.* **100,** 3743–3751 (1978).

100. Mak, P. J., Kaluka, D., Manyumwa, M. E., Zhang, H., Deng, T. & Kincaid, J.R. Defining resonance Raman spectral responses to substrate binding by cytochrome P450 from Pseudomonas putida. *Biopolymers* **89,** 1045–53 (2008).

101. Mak, P. J., Im, S. C., Zhang, H., Waskell, L. A. & Kincaid, J. R. Resonance Raman studies of cytochrome P450 2B4 in its interactions with substrates and redox partners. *Biochemistry* **47,** 3950–3963 (2008).

102. Mak, P. J., Zhu, Q. & Kincaid, J. R. Using resonance Raman cross-section data to estimate the spin state populations of Cytochromes P450. *J. Raman Spectrosc.* **44,** 1792–1794 (2013).

103. *The Porphyrin Handbook*. **7,** (Academic Press, 2000).

104. *Biological Applications of Raman Spectroscopy*. (John Wiley & Sons, 1998).

105. Grinkova, Y. V *et al.* The ferrous-oxy complex of human aromatase. *Biochem Biophys Res Commun* **372,** 379–382 (2008).

106. Tosha, T., Kagawa, N., Ohta, T., Yoshioka, S., Waterman, M. R. & Kitagawa, T.. Raman evidence for specific substrate-induced structural changes in the heme pocket of human cytochrome P450 aromatase during the three consecutive oxygen activation steps. *Biochemistry* **45,** 5631–5640 (2006).

107. Denisov, I. G., Grinkova, Y. V, Baas, B. J. & Sligar, S. G. The ferrous-dioxygen intermediate in human cytochrome P450 3A4. Substrate dependence of formation

and decay kinetics. *J. Biol. Chem.* **281,** 23313–23318 (2006).

108. Spiro, T. G., Soldatova, A. V. & Balakrishnan, G. CO, NO and O 2 as vibrational probes of heme protein interactions. *Coord. Chem. Rev.* **257,** 511–527 (2013).

109. Sjodin, T., Christian, J.F., Macdonald, I.D., Davydov, R., Unno, M., Sligar, S.G., Hoffman, B. M. & Champion, P.M.. Resonance Raman and EPR investigations of the D251N oxycytochrome P450cam/putidaredoxin complex. *Biochemistry* **40,** 6852–6859 (2001).

110. Usanov, S. A., Gilep, A. A. & Sushko, T. A. At the crossroads of steroid hormone biosynthesis: The role, substrate specificity and evolutionary development of CYP17. *Biochim. Biophys. Acta-Proteins Proteomics* **1814,** 200–209 (2011).

111. Mathieu, A. P., LeHoux, J. G. & Auchus, R. J. Molecular dynamics of substrate complexes with hamster cytochrome P450c17 (CYP17): mechanistic approach to understanding substrate binding and activities. *Biochim. Biophys. Acta* **1619,** 291–300 (2003).

112. Bayburt, T. H. & Sligar, S. G. Membrane protein assembly into Nanodiscs. *FEBS Lett* (2009).

113. Atkins, W. M., Nath, A., Grinkova, Y. V & Sligar, S. G. Ligand binding to cytochrome P450 3A4 in phospholipid bilayer nanodiscs - The effect of model membranes. *J. Biol. Chem.* **282,** 28309–28320 (2007).

114. Denisov, I. G., Mak, P. J., Makris, T. M., Sligar, S. G. & Kincaid, J. R. Resonance Raman characterization of the peroxo and hydroperoxo intermediates in cytochrome P450. *J Phys Chem A* **112,** 13172–13179 (2008).

115. Chartier, F. J. M. & Couture, M. Substrate-specific interactions with the heme-bound

oxygen molecule of nitric-oxide synthase. *J. Biol. Chem.* **282,** 20877–20886 (2007).

116. Tosha, T., Kagawa, N., Arase, M., Waterman, M. R. & Kitagawa, T. Interaction between substrate and oxygen ligand responsible for effective O-O bond cleavage in bovine cytochrome P450 steroid 21-hydroxylase proved by Raman spectroscopy. *J. Biol. Chem.* **283,** 3708–3717 (2008).

117. Sabat, J. *et al.* Catalytic intermediates of inducible nitric-oxide synthase stabilized by the W188H mutation. *J. Biol. Chem.* **288,** 6095–6106 (2013).

118. Lu, C., Egawa, T., Wainwright, L. M., Poole, R. K. & Yeh, S. R. Structural and functional properties of a truncated hemoglobin from a food-borne pathogen Campylobacter jejuni. *J. Biol. Chem.* **282,** 13627–13636 (2007).

119. Pant, K. & Crane, B. R. Nitrosyl-heme structures of Bacillus subtilis nitric oxide synthase have implications for understanding substrate oxidation. *Biochemistry* **45,** 2537–2544 (2006).

120. Cho, K. B. & Gauld, J. W. Second half-reaction of nitric oxide synthase: computational insights into the initial step and key proposed intermediate. *J. Phys. Chem. B* **109,** 23706–23714 (2005).

121. Pallan, P. S., Nagy, L.D., Gonzalez, E., Kramlinger, V. M., Azumaya, C. M., Wawrzak, Z., Waterman, M. R., Guengerich, P. F. & Egli, M. Structural and kinetic basis of steroid 17,20-lyase activity in Teleost fish cytochrome P450 17A1 and its absence in cytochrome P450 17A2. *J. Biol. Chem.* **290,** 3248–3268 (2015).

122. Westphal Christina, Anne Konkel, and W.-H. S. Monooxygenase, Peroxidase and Peroxygenase Properties and Mechanisms of Cytochrome P450. **851,** 247–297 (2015).

123. Rittle, J., Younker, J. M. & Green, M. T. Cytochrome P450: the active oxidant and its spectrum. *Inorg Chem* **49,** 3610–3617

124. Denisov, I. G., Makris, T. M. & Sligar, S. G. Cryoradiolysis for the study of P450 reaction intermediates. *Methods Enzym.* **357,** 103–115 (2002).

125. Davydov, R., Ledbetter-Rogers, A., Martasek, P., Larukhin, M., Sono, M., Dawson, J. H., Masters, B. & Hoffman, B. M. EPR and ENDOR characterization of intermediates in the cryoreduced oxy-nitric oxide synthase heme domain with bound L-arginine or N-G-hydroxyarginine. *Biochemistry* **41,** 10375–10381 (2002).

126. Davydov, R., Kappl, R., Hettermann, J. & Peterson, J. A. EPR spectroscopy of reduced oxyferrous-P450cam. *FEBS Lett.* **295,** 113–115 (1991).

127. Luthra, A., Denisov, I. G. & Sligar, S. G. Temperature derivative spectroscopy to monitor the autoxidation decay of cytochromes P450. *Anal. Chem.* **83,** 5394–5399 (2011).

128. Denisov, I. G., Makris, T. M. & Sligar, S. G. Cryotrapped Reaction Intermediates of Cytochrome P450 Studied by Radiolytic Reduction with Phosphorus-32. *J. Biol. Chem.* **276,** 11648–11652 (2001).

129. Mak, P. J., Thammawichai, W., Wiedenhoeft, D. & Kincaid, J. R. Resonance Raman spectroscopy reveals ph-dependent active site structural changes of lactoperoxidase compound 0 and its ferryl heme O-O bond cleavage products. *J. Am. Chem. Soc.* **137,** 349–361 (2015).

130. Terner, J. Palaniappan, V., Gold, A., Weiss, R., Fitzgerald, M. M., Sullivan, A. M. & Hosten, C. M. Resonance Raman spectroscopy of oxoiron(IV) porphyrin pi-cation radical and oxoiron(IV) hemes in peroxidase intermediates. *J. Inorg. Biochem.* **100,**

480–501 (2006).

131. Spolitak, T., Funhoff, E. G. & Ballou, D. P. Spectroscopic studies of the oxidation of ferric CYP153A6 by peracids: Insights into P450 higher oxidation states. *Arch. Biochem. Biophys.* **493,** 184–191 (2010).

132. Oloo, W. N., Meier, K. K., Wang, Y., Shaik, S., Munck, E. & Que, L. Identification of a low-spin acylperoxoiron(III) intermediate in bio-inspired non-heme iron-catalysed oxidations. *Nat Commun* **5,** 3046 (2014).